Effects of noise correlations on the performance of quantum error-correcting and -avoiding methods

I n a u g u r a l - D i s s e r t a t i o n

zur

Erlangung des Doktorgrades

der Mathematisch-Naturwissenschaftlichen Fakultät

der Universität zu Köln

vorgelegt von

Stefan Borghoff

aus Köln

Hundt Druck GmbH, Köln

2009

Berichterstatter Dr. Rochus Klesse

Prof. Dr. Claus Kiefer

Tag der mündlichen Prüfung 2009-06-22

Motivation

Once upon a time there was a land of eternal entanglement. Strange qubits lived in that land trying to protect their land of information. But there was a large enemy of them, named decoherence - destroying entanglements and with that the peaceful harmony of the unitary quantum computer. Then this work appeared showing a way out of this misery protected by decoherence-free subspaces and armed with quantum error correcting codes. So the qubits were freed. And if they don't decohere, they are still entangled.

Abstract

In the scope of this work the coherence of quantum information, which is encoded into a qubit register, is analysed. The qubit register is modelled by a spin chain with finite inter-spin distance. In most physically relevant realisations this spin chain irreversibly interacts with a surrounding environment, such that a spin-boson model is used to describe the setting. Due to the interaction decoherence occurs among the qubits register and quantum information gets lost. Mechanisms to slow down this decoherence process are investigated. For that purpose, the techniques of encoding qubits into decoherence-reduced subspaces and quantum error correction are used. In both cases only a linear subspace of the complete available Hilbert space of the spin chain is used as quantum code. The stability of such a code against decoherence has to be evaluated. This evaluation is performed on average over all states within the code by a code fidelity.

Zusammenfassung

Die Kohärenz von quantenmechanischer Information, gespeichert in einem Qubit-Register, wird analysiert. Dieses Register besteht aus einer Spinkette mit endlichem Abstand zwischen den Spins. Zur realistischeren Modellierung wird eine irreversible Wechselwirkung mit einem umgebenden Wärmebad angenommen und das kombinierte System durch ein Spin-Boson-Model beschrieben. Die Wechselwirkung verursacht Dekohärenz, die zu einem Verschwinden der gespeicherten Information führt. Es werden Methoden zur Verlangsamung oder Unterbindung von Dekohärenz untersucht. Dazu zählen sowohl die Codierung in dekohärenzfreie Unterräume, als auch Quantenfehlerkorrektur. In beiden Fällen wird Information in einem Unterraum des zur Spinkette gehörigen Hilbertraums codiert. Die Güte dieser Codes im Schutz vor Dekohärenz wird bewertet. Als Maß dient eine über alle Zustände des Codes gemittelte Fidelity.

Contents

Introduction

During the last decades quantum information theory became an important topic. One of the main subjects within this theory is the question how quantum information can be stored in the state of a corresponding quantum mechanical system. This system is used as quantum memory and a good knowledge about it is needed e.g. to run a quantum computer. In the early 80th the fundamentals for such a quantum computer were developed. This development started with Benioff [Ben80] who recognised that a classical Turing machine could be realised by a quantum mechanical system. Thereby, the quantum mechanical system is a quantum computer which is able to perform the tasks of the conventional Turing machine. Later on, it was observed that a quantum computer provides much more possibilities than only to emulate classical Turing machines. For instance, Feynman [Fey82, Fey86] pointed out that the time evolution of solid state devices could be simulated by a quantum computer in a very efficient way. Then, Deutsch [Deu85] developed the concept of a quantum Turing machine and pointed out its potentiality for faster computations due to quantum parallelism. By taking advantage of this parallelism, the time needed to factorise integers into primes decreases dramatically according to the famous Shor algorithm [Sho94]. Moreover, fast quantum search algorithms could be implemented as it was pointed out by Grover [Gro96].

The advantage of a quantum-bit (qubit) register in comparison to a conventional register relies on the fact that it can be in the superposition of a very large number of classical computational states. Preserving coherence of such a highly superpositional and in general strongly entangled state [Unr94, Joz97] is a challenge for the realisation of a quantum computer which has to be solved. Commonly entanglement gets quickly destroyed in a qubit register which is coupled to a surrounding environment [GJK$^+$96, Zur03]. This process is called decoherence. It unavoidably occurs in a qubit register due to the fact that qubits need to be controlled by external mechanisms, which is in contradiction to a shielding of information within the qubit register against external degrees of freedom. Accordingly, in most physical realisations there is an irreversible interaction between qubits and environment. In many situations due to this interaction the initial state of the qubit system evolves into a classical state. During this process the quantum information, which is stored within the qubit register, gets lost.

Hence, a mechanism has to be invented to maintain as much quantum information as possible. In this field error-correcting and decoherence-avoiding techniques were invented. The first error-correcting schemes were independently derived by Shor [Sho95, CS96] and Steane [Ste96]. They recover a qubit register after distortion by external noise. The existence of these schemes for quantum states has been crucial for the development on this field. The key idea rapidly evolved into a complete theory of quantum error-correcting codes and subsequently to the concept of fault-tolerant

quantum computation [KLZ98]. Independently of quantum error-correcting techniques decoherence-avoiding methods were developed by Palma et al. [PSE97] and enhanced by e.g. Zanardi and Rasetti [ZR97] and Lidar et al. [LCW98]. These mechanisms make use of possible symmetries in the interaction of, say, a quantum register and its surrounding environment. The idea is to encode quantum information into those register states that are protected by symmetry against the decohering interaction. Inasmuch as the symmetry is satisfied, these states span a decoherence-free subspace in the register's Hilbert space. Physical realisations of this concept will have to rely almost necessarily on symmetries that hold only to some approximation. Encoding into subspaces that respect these symmetries can then provides partial protection against decoherence, to an extent that will depend on the actual realisation. In the scope of this work error-correcting and -avoiding methods as well as their combination are analysed. Thereby, a spin-boson model, which was already used by G. M. Palma et al., is used to describe a physical implementation. This model, which showed decoherence-free subspaces due to its symmetry, is transformed according to implementations with distant qubits into a model without symmetry. Then, the former decoherence-free subspaces are analysed. Specifically, subspaces are considered that correspond to encoded quantum registers in which logical qubits are encoded in locally grouped spins. A measure to analyse such subspaces is also developed within this work. In comparison to older approaches on this topic here the correlations between qubits are analytically taken care of. Afterwards, quantum error-correction on the investigated model in combination with the investigated subspaces is considered.

The schedule of this work is presented in the following. An introduction to the phenomenon of decoherence is given in Chapter 1. As already outlined above, decoherence occurs in an open quantum system which is part of a larger closed system. Interactions between the investigated open quantum system and the remaining system lead to decoherence. As fundamental system of this work the n-spin-boson model is analysed. This model is used in literature to describe a single or a couple of spins interacting with a surrounding bosonic environment [BP02]. The spin part of this model is used as qubit register. Accordingly, among the spins decoherence emerges due to interactions with the bosonic environment.

One of the spin-boson model's most important features is that many physical realisations of qubit registers can be mapped onto it as an effective theory. To illuminate this mapping, different physical realisations of qubits are introduced exemplarily. For instance with atoms it is possible to construct spin qubits or qubits formed by the ground and an excited state. A typical candidate for the bosonic environment is given by thermal radiation. Other possibilities to construct qubits are given by Josephson junctions or quantum dots [BVJD98, LD98]. This list is by far not complete but gives an outlook of the basic idea to construct qubits and the mapping onto the spin-boson model.

Afterwards, the dynamics of the spin-boson model is analysed, as it effectively describes all these realisations. For that purpose, in Chapter 2 the time evolution of the n-spin-boson model is investigated. First the complete time evolution of the closed system is determined. Then its reduction to the spin system is calculated by tracing

out environmental degrees of freedom. The resulting time evolution of the spin system is interpreted as a quantum noise process. An analytical solution for this problem is presented for dissipationless couplings between spin part and environment. Within this work the cases of Ohmic and super-Ohmic spectral densities are outlined in full detail. Finally, the noise of a dissipative model is dealt with in Chapter 6. In this case the time evolution is determined by a master equation of Bloch-Redfield type. Detailed knowledge about the decoherence of the considered qubit register is needed to deal with further questions concerning quantum memory.

Chapter 3 deals with the encoding of quantum information into quantum codes. In general, quantum codes are subspaces of the spin part's Hilbert space. Having n spins, it is possible to encode a number of $k \leq n$ logical qubits within a subspace of the desired dimension. As different states of the spin system can be affected in different ways by their interaction to the environment some of them are superior to others. In particular, in the case of spins that are located at one point there are decoherence-free subspaces known which emerge due to symmetry. If the distance between the spins is finite the former symmetry is absent and consequently the codes cease to be decoherence-free. This project deals with the question how these codes can be used in the case of finite inter-spin distance. Accordingly, special codes are presented which are used for further investigation. These codes are called symmetric codes. To decide whether a given code is a good candidate or not, a measure for codes is needed.

This is realised by the code fidelity presented in Chapter 4. By means of this fidelity it is possible to determine the robustness of a given quantum code against the disturbing effects of an acting noise. Starting point to derive the code measure is the channel fidelity. As the channel fidelity itself is only a measure between two quantum states, it is outlined how a useful measure for a complete code is constructed. In this context the average fidelity and entanglement fidelity of a quantum code are derived. The average fidelity is an averaged channel fidelity over all possible states of the code. Thereby, the channel fidelity of each state and its time evolved state is averaged. The entanglement fidelity is a lower bound for the average fidelity which converges to the average fidelity with increasing code size [HHH99, Nie02]. Both of them can be used as a code fidelity. Afterwards, a connection of the entanglement fidelity to experiments is outlined. This connection grounds on the fact that for a dissipationless model the entanglement fidelity and a spin echo measurement [Ram49, Hah50] provide the same information. In case of a dissipative setting this is only approximately correct as long as timescales much lower than the relaxation time of the system are concerned.

Finally, in Chapter 5 the symmetric codes are evaluated using the entanglement fidelity as measure. First, the case of a dissipationless coupling is investigated. This result is compared to the evaluation of a plain qubit register without any encoding. It turns out that there exists a critical time beyond which an encoding into the symmetric codes is superior to plain qubits.

An even greater task than determining the fidelity of a given code is to find the optimal code. This problem is also discussed in Chapter 5. Unfortunately, it is not possible to give a solution to this problem in the scope of this work. Nevertheless, a

simplified problem can be formulated and dealt with. Thereby, the optimal encoding for a single qubit having a dissipationless coupling is determined. Instead of a spin chain, a generalised tetrahedron where all spins have equal distance to each other is analysed first. The optimisation process for this setting leads to the insight that symmetric codes provide the best encoding. In a generalised model of a spin chain this result is confirmed by a numerical method. So far, only dissipationless models were analysed. The missing dissipative couplings are examined in Chapter 6 with the help of the above mentioned master equation. Again, the encoding of a single qubit is investigated and the benefits of the previously introduced symmetric codes in comparison to plain qubits are pointed out.

Quantum error correction applied to the dissipationless model is considered in Chapter 7. In a first step the time evolution of the qubit register is transformed into a Kraus representation [KBDW83, NC00]. This form of noise seems to be best suited to calculate the quantities needed to evaluate quantum codes in combination with quantum error correction. Again, the entanglement fidelity is used as measure to evaluate the codes. In a first step symmetric codes without error correction are compared to locally optimised random codes with quantum error correction. As expected, randomly chosen codes perform better than symmetric codes, except for very weak couplings. In a second step quantum error correction is applied onto the symmetric codes. Surprisingly, it turns out that quantum error correction on randomly chosen codes is more effective than quantum error correction on symmetric codes.

1 The point of interest

In the 80th the idea to use quantum mechanical systems as quantum computers came up. Having such a quantum computer provides the possibilities to handle solid state problems [Fey82, Fey86], search algorithms [Gro96] and many other challenging tasks in a smart way. A main ingredient of each quantum computer is its quantum memory which is used to store quantum information within. Therefore, quantum memory is analysed in this work. Quantum memory consists of several quantum mechanical bits, called qubits. Commonly, qubits occurring in quantum mechanical algorithms like the famous Shor algorithm [Sho94] for factorising integers are in general in highly superpositional and strongly entangled states. For the functionality of a quantum computer the coherence of these states has to be preserved. Accordingly, a good knowledge and control about each involved qubit is very important. To develop this knowledge, the construction of single qubits is focused on in this chapter. Then, having single qubits allows a generalisation to larger qubit registers. Thereby, qubits are not considered independently as they have a shared environment which establishes correlations between them. It turns out that there is a large zoo of possible candidates in nature to form single qubits. In the scope of this work some of the most common candidates are discussed. Namely, atomic spin qubits and qubits build by Josephson junctions [BVJD98] or quantum dots [LD98] are presented. In each case the corresponding fundamental models are examined to outline the physical components of the qubit and its environment. Finally, to represent a qubit, two quantum mechanical states of the describing model have to be chosen. For each model these qubit states are manifested and the interaction to the corresponding environment is pointed out. In a next step an effective model is derived from the qubit states, the environment and the interaction between. To keep the examination as simple as possible in Sec. 1.3 each of the derived effective models is mapped onto a spin-boson model. Accordingly, only this model is discussed in full detail. An introduction to the spin-boson model is presented in Sec. 1.2. The spin part of this model forms the qubit register. A major problem for this qubit register is its sensitivity to the quantum noise occurring due to couplings to the environment. Here, the qubit register is a subsystem of the spin-boson model and accordingly interacts with the bosonic environment. Commonly, due to this interaction between environment and register decoherence might occur which makes it quite challenging to preserve the coherence of such a register. An introduction to decoherence is given in Sec. 1.1. The complete information about the decoherence of a specific system is included in its corresponding quantum noise. This noise is determined by the interaction Hamiltonian of the investigated case. Thereby, the occurring coupling coefficients in combination with the environment play a role.

1.1 Decoherence in an open quantum system

The study of decoherence was initiated in the 70th and 80th with the work on the emergence of classicality in the framework of quantum mechanics by Zeh [Zeh70] and Zurek [Zur81]. To get a feeling for decoherence, this section elaborates on the typical behaviour of a suitable system S interacting in an irreversible manner with a surrounding environment E. An illustration of this setting is given in Fig. 1.1. In the scope of this work the system S is used as quantum memory and the environment is assumed to contain a large number of degrees of freedom. Although the environmental degrees of freedom are treated quantum mechanically, their state is taken unobservable for all practical purpose. The combined system of S and E is considered as a closed quantum mechanical system, labelled SE. Any initial state $\rho_{SE}(0)$ of this joint system evolves

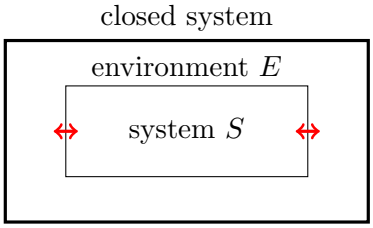

Figure 1.1: The figure shows a schematic picture of the closed system SE with its constituents S (system) and E (environment). Arrows symbolically represent an existing interaction between the two parts as explained above.

unitary in time t according to Schrödinger's equation to a state $\rho_{SE}(t)$. In a physically relevant setting for quantum information theory the initial state $\rho_{SE}(0)$ is taken as a product state of system- and environment part. Thereby, the environment is assumed to start in thermal equilibrium whereas no restrictions are made to the system's initial state $\rho(0)$ as it corresponds to the actual quantum information. In contrast to the time evolution of the joint system, the time evolution of the reduced density operator of the system S, which is obtained by tracing out all environmental degrees of freedom,

$$\rho(t) \;=\; \operatorname*{tr}_{E}\{\rho_{SE}(t)\}\,, \tag{1.1}$$

is not unitary in general. Due to the fact that the stability of quantum information is concerned, this reduced density of the system S at time t has to be compared to its initial state. To illuminate the reduced system's dynamics, the operator $\mathcal{T}_t \;:\; \rho(0) \;\mapsto\; \mathcal{T}_t(\rho(0)) \;\equiv\; \rho(t)$, mapping the reduced density operator $\rho(0)$ on its time evolved density operator $\rho(t)$, is investigated. It can be shown that the operator $\mathcal{T}_t$ is of the form

$$\mathcal{T}_t(\rho) = \mathcal{U}_t \circ \mathcal{N}_t(\rho)\,, \tag{1.2}$$

where $\mathcal{U}_t$ is a purely unitary operator, and $\mathcal{N}_t$ is a non-unitary completely positive map. Various authors in [PSE97, DG98, BLW99, NC00, RQJ02, BP02] have established this form. Dealing with $\mathcal{N}_t$, different behaviours occur depending on the present Hamiltonian. Non trivial effects caused by $\mathcal{N}_t$ are topic of this work. For example, if the intrinsic energy of the eigenbasis of the system S is preserved by the Hamiltonian, occurring non-trivial effects caused by the operator $\mathcal{N}_t$ are called decoherence if they lead to a loss of coherence. In this case the non-diagonal terms in the reduced density operator vanish. In general due to decoherence an entangled state $\rho(0)$ continuously evolves into a classical state [GJK$^+$96, Zur03]. For a non-energy preserving Hamiltonian also dissipative effects might occur and would also be contained in $\mathcal{N}_t$. Here, an energy exchange with the environment leads to thermalisation of the initial state. Often such a dissipative setting is accompanied by decoherence. Concluding, the chosen form of the interaction between system and environment determines if decoherence and dissipation occurs.

1.2 The n-spin-boson model

For the purpose of this work, a special spin-boson model is used to represent a finite number of qubits coupled to an environment. As usual, the spin-boson model is a combined model, consisting of two parts. The first part of the model, labelled S, is a lattice of spin-1/2 carrying objects. This lattice is considered to be one- or more-dimensional, having an equidistant inter-spin distance a and a finite quantity of n lattice sites. Each spin itself has the functionality of a single qubit. The second part of the model is a shared environment E which is a bosonic bath locally interacting with all spins. As no other external interactions are taken into account, the combined model of these two parts, labelled SE, is a closed system.

1.2.1 The Hamiltonian of the effective model

The full Hamiltonian, describing a lattice of spins coupled to an external bath, is divided into a free and an interacting part, $\hat{H} = \hat{H}_0 + \hat{H}_I$. Here, the free Hamiltonian $\hat{H}_0$ must not contain terms that include any interaction between the spin system and the environment. According to this condition the free Hamiltonian divides into a spin and an environment part,

$$\hat{H}_0 = \hat{H}_S + \hat{H}_E \,. \tag{1.3}$$

The first term $\hat{H}_S$ describes the spin system. Its explicit form, introducing the energy splitting ϵ, reads

$$\hat{H}_S = \frac{\epsilon}{2} \sum_{\mathbf{m}} Z_{\mathbf{m}} \otimes \mathbb{1}_E \,. \tag{1.4}$$

The index $\mathbf{m}$ is a tuple of positive integers with the dimension of the spin system and labels different lattice-sites. $Z_{\mathbf{m}} \equiv \sigma_{z,\mathbf{m}}$ is a Pauli spin matrix acting on the spin on the lattice site $\mathbf{m}$. For simplification only the one-dimensional case of a spin chain with $\mathbf{m} \in \mathbb{N}_0\, \mathbf{e}_3$ is investigated. According to this notation the spin-carriers are arranged along the $\mathbf{e}_3$-axis. The energy splitting of each spin is taken to arise along the $\mathbf{e}_1$-axis as

shown in Fig. 1.2. In the spin-boson model the spins are surrounded by an environment,

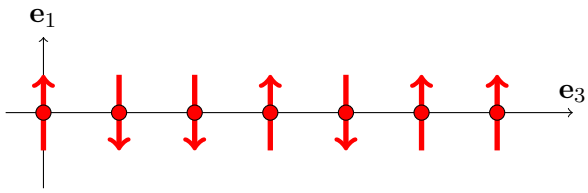

Figure 1.2: The qubits are arranged in a chain along the $\mathbf{e}_3$-axis with equidistant inter-spin distance.

often called bath. This environment is modeled by bosonic excitations. The Hamiltonian of this bath, being the second term in Eq. (1.3), is given by

$$\hat{H}_E = \mathbb{1}_S \otimes \sum_{\mathbf{k}} \hbar\omega_{\mathbf{k}} b_{\mathbf{k}}^\dagger b_{\mathbf{k}} \,. \tag{1.5}$$

This Hamiltonian consists of bosonic annihilation operators $b_{\mathbf{k}}$ and creation operators $b_{\mathbf{k}}^\dagger$. A set of these operators belongs to the $\mathbf{k}^{\text{th}}$ bath mode with energy $\hbar\omega_{\mathbf{k}}$. Thermal radiation as a typical candidate would lead to a three-dimensional bath, but corresponding to a different setting also another dimension of the bath would be possible. The interaction Hamiltonian $\hat{H}_I$ of the spin-boson model describes the interplay between spin system and bath. $\hat{H}_I$ is given in the form of

$$\hat{H}_I = \cos\eta \hat{H}_Z + \sin\eta \hat{H}_X, \tag{1.6}$$

with a dimensionless control parameter η. The first term of the interaction Hamiltonian describes a dissipationless coupling via

$$\hat{H}_Z = \sum_{\mathbf{m}} Z_{\mathbf{m}} \otimes B(a\mathbf{m}) \,. \tag{1.7}$$

Here, $Z_{\mathbf{m}}$ is the Pauli spin matrix that already occurred in Eq. (1.4). The other term of the interaction Hamiltonian leads to a dissipative coupling by

$$\hat{H}_X = \sum_{\mathbf{m}} X_{\mathbf{m}} \otimes B(a\mathbf{m}) \,. \tag{1.8}$$

The operator $X_{\mathbf{m}}$ is a Pauli spin matrix corresponding to the above mentioned $Z_{\mathbf{m}}$. In both cases bosonic field operators

$$B(\mathbf{r}) = \sum_{\mathbf{k}} g_{|\mathbf{k}|} e^{-i\mathbf{k}\cdot\mathbf{r}} b_{\mathbf{k}}^\dagger + H.c. \tag{1.9}$$

with coupling coefficients $g_{|\mathbf{k}|}$ occur. Each of these coupling coefficients acquires a phase $e^{-i\mathbf{k}\cdot\mathbf{r}}$, reflecting the wavelike character of the bosonic modes. Except for this phase the coupling is isotropic and identical for all spins. The coupling coefficients carry information about the spin-environment coupling and are specified in form of a spectral density

$$J(\omega) = \alpha\omega^s e^{-\omega/\Omega} = 4\sum_{\mathbf{k}} \delta(\omega - \omega_{\mathbf{k}})|g_{|\mathbf{k}|}|^2\,, \tag{1.10}$$

with linear energy-momentum relation $\omega_{\mathbf{k}} = c|\mathbf{k}|$, high-energy cut-off Ω and the speed of the bosons c. The parameter s is called spectral parameter. This parameter has to respect the dimension of the bath. In case of a three-dimensional bath s has a two-times larger exponent as in comparison to an one-dimensional bath according to the Jacobi determinant of a coordinate transformation from Cartesian coordinates to spherical ones. The coefficient α is ω-independent and can be read off in each $|g_{\mathbf{k}}|^2$ by respecting the ω-independent part of the Jacobi determinant and an integration over occurring angles. With this definition of a spectral density it is possible to replace the sum over discrete modes $\sum_{\mathbf{k}} |g_{\mathbf{k}}|^2$ by the integral $\int_0^\infty \mathrm{d}\omega\, J(\omega)$ over a continuum.

This work mainly deals with two different regimes of the spectral density. One of them is the Ohmic setting having a spectral parameter s being equal to one. The discussion of this case is of further interest as many dissipative models can effectively be described by a dissipationless model having an Ohmic coupling. This happens in particular if the bath acts one-dimensional. The other setting is e.g. needed to describe atomic absorption and emission processes and is given for a spectral parameter s being equal to three. Dealing with other couplings requires the same tools as the are presented for the settings of $s = 1, 3$.

1.3 Physical realisations of qubits

Starting from a microscopic view, this section elaborates on some physical realisations of qubits. Each of these realisations finally is given by an effective Hamiltonian. In the scope of this work only effective Hamiltonians which can be mapped onto a spin-boson model are observed. The first part, Sec. 1.3.1, deals with the usual matter-radiation interaction of atoms. Here, different physical implementations are considered. For example, the model of an atomic spin coupled to a magnetic field is discussed. Afterwards common photon absorption and emission processes are analysed, which will play a role, if qubits are constructed via different states of an atom. The rest of this section deals with Josephson junctions in Sec. 1.3.2 and quantum dots in Sec. 1.3.3.

There are two aims for the rest of this chapter. The first aim is to give insight to the fundamental models and a taste of the different mechanisms which are used to construct qubits. A concrete mapping for each of the presented systems on a spin-boson model is given in detail. The second aim of this section is to determine the spectral parameter s for different models as the behaviour of decoherence varies with s. This difference is further investigated in Chapter 2.

1.3.1 Atom-field interaction Hamiltonian

To describe the coupling of a single atom to an electromagnetic field, the minimal coupling Hamiltonian is investigated. Starting with this Hamiltonian the qubit states have to be selected. Possible candidates are given by the states of an atom's electron of charge e and mass m. In the given setting this electron interacts with an external electromagnetic field, given by a vector potential $\mathbf{A}$ and scalar potential Φ. Therefore, the model is described by the minimal coupling Hamiltonian which is given by

$$\hat{H} = \frac{\left(\hat{\mathbf{p}} - e\mathbf{A}(\mathbf{r},t)\right)^2}{2m} + e\Phi(\mathbf{r},t) + V(\mathbf{r}) - \underline{\mu}_j \cdot \left(\nabla \times \mathbf{A}(\mathbf{r},t)\right). \tag{1.11}$$

Here, the free Hamiltonian (without interaction to the electromagnetic field) of the electron itself is identified as

$$\hat{H}_S = \frac{\mathbf{p}^2}{2m} + V(\mathbf{r}). \tag{1.12}$$

At this point the explicit structure of the qubit has to be chosen. In the following, two different possibilities are outlined. During the next part a spin qubit is presented. In this case the level splitting of the electron ground state due to a static magnetic field gives the two needed qubit states. Afterwards another possibility is presented. Thereby, the ground and first exited state of the electron in the absence of a magnetic field form the qubit.

Construction of a spin qubit. Calculations in the following paragraph are performed in hydrogen approximation. Accordingly, only the state of the outer electron of an atom is described by this method, such that this approximation is good for most alkali metals. As mentioned above, the quantum-mechanical degree of freedom used for the qubit is the spin of the outer electron. This kind of qubit can be realised with cold Caesium atoms e.g., which is referred to in [GWO00, SDK$^+$04]. In the scope of the cited work a dipole trap is used to arrange the atoms along the desired lattice, as shown in Fig. 1.2. This arrangement is performed by a focused laser beam, such that the induced electric dipole moment together with the occurring dipole force keeps the atom in the centre of the trapping beam. Additionally, a static magnetic field causes the energy splitting of the spin systems Hamiltonian (cf. Eq. (1.4)) and keeps the magnetic axis of each atom fixed. To construct a qubit with full functionality it has to be possible to apply operations on them. In the present case all kind of needed operations can be performed by applying further external fields on the qubit lattice.

To continue, the interaction of the introduced spin qubit to an environment is pointed out. In the scope of this work an interaction due to the magnetic field of thermal radiation is investigated. The corresponding Hamiltonian is read off by the last term of the minimal coupling Hamiltonian in Eq. (1.11). Accordingly, the interaction Hamiltonian has Zeeman shape

$$\hat{H}_I = -\underline{\mu}_j \cdot \mathbf{B}, \tag{1.13}$$

where $\mathbf{B} = \nabla \times \mathbf{A}$ is the external magnetic field due to thermal radiation. The vector

$\underline{\mu}_j$ is connected to the total momentum operator $\mathbf{j}$ of the electron. The total momentum operator is given by the sum of spin operator $\mathbf{s}$ and orbital momentum operator $\mathbf{l}$ as $\mathbf{j} = \mathbf{l} + \mathbf{s}$. The related vector $\underline{\mu}_j$ is given by

$$\underline{\mu}_j = \underline{\mu}_s + \underline{\mu}_l = -\mu_B \frac{2\mathbf{s} + \mathbf{l}}{\hbar} \,. \tag{1.14}$$

In the declared setting of an outer electron in an alkali metal, the orbit with $\mathbf{l} = 0$ is occupied by the electron. Therefore, only the spin contributes to the interaction Hamiltonian. At this point the quantised version of the magnetic field is inserted into the Hamiltonian. For a derivation of the quantised magnetic field see e.g. the references [Lou73, SZ97]. To announce notation a short presentation of this derivation is delivered in Appendix C. There it becomes clear that the quantised magnetic field is optimal adapted to the problem if it is presented in the interaction picture. Following the presented instruction delivers the interaction Hamiltonian in the interaction picture,

$$\tilde{H}_I(t) = \mu_B \sum_{\mathbf{m}} \underline{\sigma}_{\mathbf{m}} \cdot \frac{1}{c} \frac{i}{\sqrt{\nu}} \sum_{\mathbf{k},\lambda} \sqrt{\frac{\hbar\omega_k}{2\epsilon_0}} a_{\mathbf{k}\lambda} e^{i(\mathbf{k}\mathbf{r}_\mathbf{m} - \omega_k t)} \frac{\mathbf{k}}{|\mathbf{k}|} \times \underline{\epsilon}_{\mathbf{k}\lambda} + H.c. \tag{1.15}$$

Here, $\underline{\sigma}$ is the vector of Pauli matrices and ν the quantisation volume. The vectors $\underline{\epsilon}_{\mathbf{k}\lambda}$ are polarisation vectors belonging to wave vector $\mathbf{k}$ and polarisations $\lambda = 1, 2$, such that $\{\hat{\mathbf{k}}, \underline{\epsilon}_{\mathbf{k}1}, \underline{\epsilon}_{\mathbf{k}2}\}$ forms an orthonormal basis. These polarisation vectors for a given wave vector $\mathbf{k}$ are illustrated in Fig. 1.3.

Following the concept that was presented at the beginning of this chapter, the spectral parameter s, which was introduced in Eq. (1.10), is determined. For that purpose, the coupling coefficients $g_\mathbf{k}$ have to be identified in the presented form of the interaction Hamiltonian in Eq. (1.15). Taking the absolute square of these coefficients and neglecting its ω-dependence produces the coupling coefficient α up to a dimensionless constant. Here, this coupling constant of the spectral density is proportional to

$$\alpha \sim \mu_B^2 \frac{1}{c^2} \frac{1}{(2\pi)^3} \frac{\hbar}{2\epsilon_0} = \frac{\mu_B^2}{2\pi^3 c^2 \hbar \epsilon_0} \,. \tag{1.16}$$

The dimension of the bath enters into the calculation of the spectral parameter. A short analysis of the occurring $|g_\mathbf{k}|^2$ shows that this expression growths linearly with ω. According to Eq. (1.10) the spectral parameter turns out to be $s = 3$.

Now some further illumination on the given interaction Hamiltonian is performed. as it is illustrated in Fig. 1.2. In principle the interaction Hamiltonian in Eq. (1.15) contains couplings via all Pauli spin matrices due to $\underline{\sigma}$. For simplification a restriction to the coupling via the Pauli spin matrix Z by $Z \otimes B_z$ is performed. The coupling in this case is dissipationless. It should be mentioned that the couplings via X and Y can be handled analogously. Just to remember, the homogeneous magnetic field, which leads to the Zeeman splitting of the spins, is applied along $\mathbf{e}_1$-direction, Hence, the z-component of the magnetic field in the chosen basis is $B_z = \mathbf{B} \cdot \mathbf{e}_1$. According to the derivation of

the magnetic field it is given as a sum over all photonic modes with wave vectors $\mathbf{k}$ (cf. Eq. (C.24) in Appendix C). At this point the continuum limit of these photonic modes is performed. Conveniently, spherical coordinates with radial distance k, azimuth angle φ and zenith angle θ are introduced. For a qubit, which is arranged along the $\mathbf{e}_3$-axis at

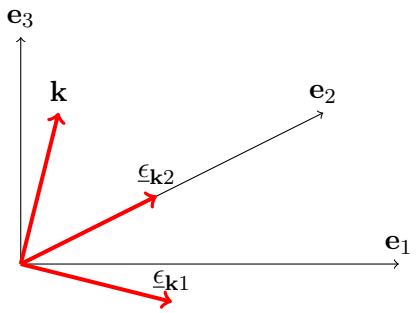

Figure 1.3: Picture, showing the vector $\mathbf{k}$ and associated polarisation vectors for $\varphi = 0$ and $\theta = \sphericalangle(\mathbf{e}_3, \mathbf{k})$.

position $\mathbf{r}$, the projection of the magnetic field on the selected z-direction is given by

$$B_z(\mathbf{r}) = \sum_{\mathbf{k}} g_{|\mathbf{k}|} \left(\mathbf{e}_1 \cdot \sum_{\lambda} \hat{\mathbf{k}} \times \underline{\epsilon}_{\mathbf{k}\lambda} a_{\mathbf{k}\lambda} \right) e^{i(\mathbf{k}\cdot\mathbf{r} - \omega_k t)} + H.c. \tag{1.17}$$

$$= \sum_{k,\varphi_{\mathbf{k}},\theta_{\mathbf{k}}} g_{|\mathbf{k}|} (\cos\theta_{\mathbf{k}} \cos\varphi_{\mathbf{k}} a_{\mathbf{k}2} - \sin\varphi_{\mathbf{k}} a_{\mathbf{k}1}) e^{i(kr\cos\theta_{\mathbf{k}} - \omega_k t)} + H.c. \tag{1.18}$$

The complex coupling constants $g_{|\mathbf{k}|}$ can be read off e.g. in Eq. (1.15). The given form of the magnetic field is easy to verify using the proper polarisation vectors, having Fig. 1.3 in mind. By the selected choice of coordinates it turns out that only the length of $\mathbf{r}$ occurs in the equation, such that $B_z(\mathbf{r}) \equiv B_z(r)$. Furthermore it can be established that for each $\mathbf{k}$ the expectation value of two of these magnetic fields at positions $\mathbf{r}_a$ and $\mathbf{r}_b$ is given by $\left\langle B_z(\mathbf{r}_a) B_z^\dagger(\mathbf{r}_b) \right\rangle = |g_{|\mathbf{k}|}|^2 (\cos\theta_{\mathbf{k}} \cos\varphi_{\mathbf{k}} - \sin\varphi_{\mathbf{k}}) e^{ik|\mathbf{r}_a - \mathbf{r}_b|\cos\theta_k} \left\langle 2a_{\mathbf{k}}^\dagger a_{\mathbf{k}} + 1 \right\rangle$. Note that only the distance r between the two qubits at position $\mathbf{r}_a$ and $\mathbf{r}_b$ comes into play. An important class of functions consiting of this expectation value are the spectral correlations, which are used later on to describe the time evolution of qubits. Anticipatory, the continuum limit of the bath modes is closer investigated. Occurring integrals have the form

$$I[f(k,\varphi,\theta), r] = \int_0^\infty \mathrm{d}k \int_0^{2\pi} \mathrm{d}\varphi \int_0^\pi \mathrm{d}\theta \, k^2 \sin\theta e^{ikr\cos\theta} f(k,\varphi,\theta)\,, \tag{1.19}$$

where f is a function depending on the two involved magnetic fields. In the present case

f turns out to be $f(k,\varphi,\theta) = (\cos\theta\cos\varphi - \sin\varphi)^2 \left\langle 2a_k^\dagger a_k + 1 \right\rangle$. To calculate the desired expectation value of $B_z(\mathbf{r}_a)$ and $B_z(\mathbf{r}_b)$ the following integrals are important:

$$I_0[f(k),r] := I[f(k),r] = 4\pi \int_0^\infty \mathrm{d}k\, k^2 \frac{\sin(kr)}{kr} f(k)\,, \tag{1.20a}$$

$$I_1[f(k),r] := I[f(k)\sin^2\theta, r] = 8\pi \int_0^\infty \mathrm{d}k\, k^2 \frac{\sin(kr) - kr\cos(kr)}{k^3 r^3} f(k) \tag{1.20b}$$

$$\text{and} I[f(k)\cos^2\varphi\cos^2\theta, r] = I_0[f(k),r]/2 - I_1[f(k),r]/2\,. \tag{1.20c}$$

Obviously $I[f(k)\sin^2\varphi, r] = I_0[f(k),r]/2$ holds. Finally the desired integral over expectation values of the magnetic fields is given by

$$\int_{\mathbb{R}^3} \mathrm{d}\mathbf{k} \left\langle B_z(\mathbf{r}_a) B_z^\dagger(\mathbf{r}_b) \right\rangle = I_0\left[\tilde{f}(k), r\right] - I_1\left[\tilde{f}(k), r\right]/2 \tag{1.21}$$

with $r = |\mathbf{r}_a - \mathbf{r}_b|$ and $\tilde{f}(k) = |g_{|\mathbf{k}|}|^2 \left\langle 2a_k^\dagger a_k + 1 \right\rangle$. In the following calculations the term $I_1[|\tilde{f}(k), r]/2$ is neglected for the sake of simplicity. In principle all methods that are needed to handle this term are shown later on.

Qubit construction using the ground and first excited state. In this paragraph the minimal coupling Hamiltonian (cf. Eq. (1.11)) without Zeeman energy,

$$\hat{H} = \frac{(\hat{\mathbf{p}} - e\mathbf{A}(\mathbf{r},t))^2}{2m} + e\Phi(\mathbf{r},t) + V(\mathbf{r})\,, \tag{1.22}$$

is used, neglecting the spin of the electron. This setting is motivated in the absence of a static magnetic field. Here, an electron bound by a potential $V(\mathbf{r})$ to a force centre located at $\mathbf{r}_0$ is investigated. In the scope of this work the qubit's two level system is determined by the ground state $|g\rangle \equiv |1\rangle$ and the first exited state $|e\rangle \equiv |0\rangle$ of the electron. To arrange the atomic lattice a magnetic trap might be used. This trap holds each atom due to its magnetic dipole momentum in position. A possible candidate for interactions is again given by thermal radiation. Accordingly the vector potential $\mathbf{A}$ and scalar potential Φ of the thermal radiation determine the environment. The vector potential (cf. Eq. (C.22) in Appendix C) of a plane electromagnetic wave is given by $\mathbf{A}(\mathbf{r}_0+\mathbf{r},t) = \sum_{\mathbf{k}} g_{\mathbf{k}}(t) e^{i\mathbf{k}\cdot(\mathbf{r}_0+\mathbf{r})}$. This potential may be written in dipole approximation as

$$\mathbf{A}(\mathbf{r}_0+\mathbf{r},t) = \sum_{\mathbf{k}} \left(g_{\mathbf{k}}(t) e^{i\mathbf{k}\cdot\mathbf{r}_0} + \mathcal{O}(\mathbf{k}\cdot\mathbf{r}) \right)\,. \tag{1.23}$$

A good justification for the dipole approximation is given if each wave only varies a little on the length of the atom. This is formally achieved for $\mathbf{k}\cdot\mathbf{r} \ll 1$. Here, the high energy cutoff Ω introduced in Eq. (1.10) can be used to ensure this condition. A local

gauge transformation is applied on the minimal coupling Hamiltonian in Eq. (1.22). The gauge field for this transformation is given by $\chi(\mathbf{r},t) = -e\mathbf{A}(\mathbf{r}_0,t)\cdot\mathbf{r}$. The corresponding transformation of the wavefunction ψ, vector potential $\mathbf{A}$ and scalar potential Φ is given by

$$\psi \mapsto \psi e^{i\chi}, \quad \mathbf{A} \mapsto \mathbf{A} + \frac{1}{e}\nabla\chi \quad \text{and} \quad \Phi \mapsto \Phi - \frac{1}{e}\partial_t\chi\,. \tag{1.24}$$

After this gauge transformation the approximated minimal coupling Hamiltonian reads

$$\hat{H} = \frac{\mathbf{p}^2}{2m} + e\dot{\mathbf{A}}(\mathbf{r}_0,t)\cdot\mathbf{r} + V(\mathbf{r})\,. \tag{1.25}$$

Within this Hamiltonian the free part of the electron is identified to be $\hat{H}_S = \frac{\mathbf{p}^2}{2m} + V(\mathbf{r})$. The remaining term provides the interaction Hamiltonian. The vector potential fulfils $\dot{\mathbf{A}} = -\mathbf{E}$, such that the interaction Hamiltonian in this setting is identified to be

$$\hat{H}_I = -\mathbf{E}(\mathbf{r}_0,t)\cdot\underline{\mathcal{D}}\,, \tag{1.26}$$

where $\underline{\mathcal{D}} = e\mathbf{r}$ is the dipole operator.

Now the interaction Hamiltonian for a concrete setting is investigated. Again the question for the spectral parameter s (cf. Eq. (1.10)) arises. Further progress is achieved under some assumptions. A single atom at position $\mathbf{r}_0$ is investigated. For simplification the dipole momentum of the atom is assumed to point in Cartesian $\mathbf{e}_1$ direction. In this case the scalar product between electric field and dipole is $\mathbf{E}\cdot\underline{\mathcal{D}} = |\mathbf{E}(\mathbf{r}_0,t)|(\cos\theta\cos\varphi - \sin\varphi)\wp_{eg}$, as $\mathbf{e}_1\cdot\sum_\lambda \underline{\epsilon}_{\mathbf{k}\lambda} = \cos\theta\cos\varphi - \sin\varphi$. The occurring scalar dipole momentum $\wp_{eg}$ is defined as $\wp_{eg} = |\langle 0|\underline{\mathcal{D}}|1\rangle|$. Accordingly, the interaction Hamiltonian of a complete chain of qubits is given by

$$\hat{H}_I = -\sum_{\mathbf{m}} \mathbf{X}_{\mathbf{m}} \otimes B(\mathbf{r}_{\mathbf{m}}) \quad \text{with} \quad B(\mathbf{r}_{\mathbf{m}}) = \mathbf{E}(\mathbf{r}_{\mathbf{m}})\cdot\mathbf{e}_1\wp_{eg}\,. \tag{1.27}$$

Comparing the derived formula with Eq. (1.9) yields the coupling coefficient of the bath operators $B(\mathbf{r})$ as

$$g_{\mathbf{k}} = \frac{i}{\sqrt{\nu}}\sqrt{\frac{\hbar\omega_{|\mathbf{k}|}}{2\epsilon_0}}(\cos\theta\cos\varphi - \sin\varphi)\wp_{eg}\,. \tag{1.28}$$

The absolute square of these coefficients is taken to calculate the coupling constant of the spectral density, cf. Eq. (1.10). It turns out that the coupling constant is proportional to

$$\alpha \sim \frac{1}{(2\pi)^3}|\wp_{eg}|^2\frac{\hbar}{2\epsilon_0} = \frac{\hbar|\wp_{eg}|^2}{8\pi^3\epsilon_0}\,. \tag{1.29}$$

Analysing the ω-dependence of the $|g_{\mathbf{k}}|^2$ together with the dimension of the bath immediately reveals that the spectral parameter s for the examined setting is given by $s = 3$. Note that a three-dimensional bath is used.

1.3.2 Qubits with Josephson junctions

In this section the construction of qubits with the help of Josephson junctions is outlined. First, these junctions are illuminated to understand the working mechanisms. Afterwards, a charge qubit as it was presented by Bouchiat et al. [BVJD98] is discussed. This kind of qubit is constructed by a Josephson junction and some basic elements of an electric circuit. The fundamental Hamiltonian of such a charge qubit is derived. Afterwards this Hamiltonian is mapped on a spin-boson model. In this framework the corresponding spectral parameter is calculated.

The physics inside Josephson junctions. In this context the famous Josephson relations are derived. Starting point is the composition of a Josephson junction. Such a junction consists of two generic superconducting electrodes that are connected by a small tunnelling barrier. This device is illustrated in Fig. 1.4, where the cross represents the barrier and the upper and lower part symbolise the superconductors. This composition has a capacitance C_J, which is also visualised in the figure.

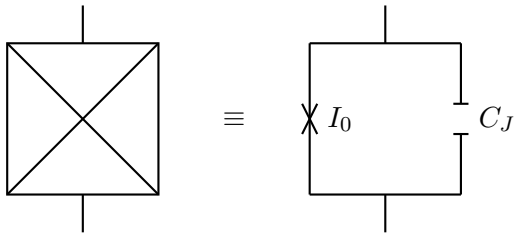

Figure 1.4: Josephson junction with critical current I_0 and junction capacitance C_J.

Following the theory of Feynman [FLS65], the system is considered as a two-level quantum mechanical system, describing Cooper pairs. Now the voltage U is applied to the junction, such that the energy-levels of a given Cooper pair are separated by $2eU$. The fundamental dynamics of the system is described by Schrödinger's equation $i\hbar\partial_t |\psi(t)\rangle = \hat{H} |\psi(t)\rangle$ with a specific Hamilton operator $\hat{H}$. As only discrete states, labelled $|\psi_k\rangle$ with $k = 1, 2$, are allowed in the model, the wavefunction of the system is expanded into a series $|\psi(t)\rangle = \sum_k c_k(t) |\psi_k\rangle$ with complex and time depending coefficients $c_k(t)$. Inserting this ansatz into the Schrödinger equation leads to differential equations for all coefficients $c_k(t)$,

$$i\hbar \frac{\mathrm{d}}{\mathrm{d}t} c_k(t) = \sum_l H_{kl} c_l(t)\,, \tag{1.30}$$

with matrix elements $H_{lk} = \langle \psi_l | \hat{H} | \psi_k \rangle$. The energy scale of the system is chosen in a way, such that the diagonal elements of the matrix H are $H_{11} = eU$ and $H_{22} = -eU$. The tunnelling coefficient in this model is given by $H_{12} = K$. Using this notation, the

two differential equations in Eq. (1.30) are

$$i\hbar\frac{\mathrm{d}}{\mathrm{d}t}c_1(t) = eUc_1(t) + Kc_2(t) \quad \text{and} \quad i\hbar\frac{\mathrm{d}}{\mathrm{d}t}c_2(t) = Kc_1(t) - eUc_2(t)\,. \tag{1.31}$$

The absolute square $|c_k(t)|^2$ is normalised in a way, such that $|c_k(t)|^2 \equiv n_s(t)$ is the superconducting electron density in the junction. As the amplitude of a coefficient $c_k(t)$ is fixed by this condition, each coefficient can only acquire an additional phasefactor $\theta_k(t)$, leading to

$$c_k(t) = \sqrt{n_s(t)}e^{i\theta_k(t)}\,. \tag{1.32}$$

Inserting this ansatz in the differential equation above reveals a set of three differential equations for $n_s(t)$, $\theta_1(t)$ and $\theta_2(t)$ given by

$$\frac{\mathrm{d}}{\mathrm{d}t}n_s(t) = \frac{2Kn_s(t)}{\hbar}\sin\phi(t), \tag{1.33a}$$

$$\frac{\mathrm{d}}{\mathrm{d}t}\theta_1(t) = -\frac{K}{\hbar}\cos\phi(t) - \frac{eU}{\hbar}, \tag{1.33b}$$

$$\frac{\mathrm{d}}{\mathrm{d}t}\theta_2(t) = -\frac{K}{\hbar}\cos\phi(t) + \frac{eU}{\hbar}\,. \tag{1.33c}$$

Here, the phase difference $\phi(t) = \theta_1(t) - \theta_2(t)$ is introduced. Remember that the superconducting electron density is given by $n_s(t)$. Obviously, the current through the tunnel junction is proportional to the time derivative of this density,

$$I(t) = \frac{\mathrm{d}}{\mathrm{d}t}n_s(t)\,. \tag{1.34}$$

Accordingly, Cooper pairs start to leave one of the superconducting electrodes. This effect is immediately compensated by the arrival of new electrons from an external source, as the junction is part of a closed electric circuit. Consequently, the density $n_s(t)$ remains constant due to electroneutrality of the system as a whole. In this way the first fundamental Josephson relation,

$$I(t) = I_0\sin\phi(t), \tag{1.35}$$

is derived. It describes the time dependence of the current through the junction. Now the phase difference $\phi(t)$ is investigated. The second fundamental Josephson relation,

$$\partial_t\phi(t) = \frac{2eU}{\hbar}\,, \tag{1.36}$$

can easily be derived from Eq. (1.33b) and Eq. (1.33c). Finally, the Josephson energy is given as

$$E(t) = \int_{-\infty}^{t}\mathrm{d}\tau\, I(\tau)U = -E_J\cos\phi(t) \tag{1.37}$$

with $E_J = \hbar I_0/2e$.

There are two common ways of creating qubits by the use of Josephson junctions. In the following paragraph the construction of a charge qubit corresponding to the work of Bouchiat [BVJD98] is explained. An alternative implementation is given by flux qubits, which are found e.g. in reference [CNHM03].

Construction of a charge qubit. Construct a circuit with an applied gate voltage U_g and implement a Josephson junction and an additional capacitor with capacity C_g, as illustrated in Fig. 1.5. There is a part of the circuit which is isolated by the capacitor on

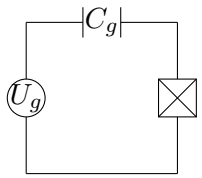

Figure 1.5: Charge qubit with gate voltage U_g, a capacitor having capacity C_g and a Josephson junction.

the one and the junction on the other side. A certain number of Cooper pairs is within this island. This number can be controlled by changing the gate voltage.

The first step is the derivation of the model's Hamiltonian. One contribution to the Hamiltonian is the charging energy $E_c = e^2/2(C_g+C_J)$, which is needed to transport electrons into the qubit area. The gate charge number is given as $n_g = C_g U_g/2e$. Together with the Josephson energy, derived in Eq. (1.37), the system's Hamiltonian is

$$\hat{H} = 4E_c(n - n_g)^2 - E_J \cos\phi\,, \tag{1.38}$$

where n is the particle-number operator of the isolated area. As particle-number operator and phase operator are conjugated variables, according to the Susskind-Glogower formalism [Lyn95], the commutator is $[\phi, n] = i$. For the phase it is known that $e^{\pm i\phi}\,|\,n\,\rangle = |\,n \pm 1\,\rangle$. Now the Hamiltonian is given by

$$\hat{H} = \sum_n \left[4E_c(n - n_g)^2\,|\,n\rangle\langle\,n\,| - \frac{E_J}{2}(|\,n\rangle\langle\,n+1\,| + |\,n+1\rangle\langle\,n\,|) \right]. \tag{1.39}$$

This Hamiltonian determines the complete physics of the specified device.

In the following an explicit construction of a qubit within this model is outlined. A qubit consists of two states. For this purpose the ground and first excited state are selected. The corresponding particle-number operator is given by

$$n = \begin{pmatrix} 0 & 0 \\ 0 & 1 \end{pmatrix} = \frac{1 - Z}{2}\,. \tag{1.40}$$

This operator is inserted into the Hamiltonian above. Within the given sum all terms that include other states than the ground and first exited state are neglected. Finally, after rescaling, the Hamiltonian has the form

$$\hat{H} = -2E_c(1-2n_g)Z - \frac{E_J}{2}X\,. \tag{1.41}$$

In a physical implementation of a charge qubit, noise occurs up to the fact that the gate voltage U_g fluctuates. Building a lattice, with an index m that labels different sites, the free Hamiltonian of the system is

$$\hat{H}_0 = -\sum_m 2E_c(1-2n_{g,m})Z_m\,. \tag{1.42}$$

Let δU_m be the difference of the voltage to the original gate voltage. Than, the interaction Hamiltonian is given by

$$\hat{H}_I = -\sum_m \frac{E_J}{2}X_m - 2\frac{C_g\delta U_m}{e}Z_m\,. \tag{1.43}$$

Now an explicit choice for the noise is taken and the corresponding spectral parameter s of the spectral density is calculated. Assuming δU_m occurs by a change of the flux through the circuit caused by thermal photons. Then, the voltage is given by

$$\delta U_m = \dot{\Phi}_m = -\int_0^{2\pi} \mathrm{d}s\, \dot{\underline{\gamma}}_m(s)\cdot\mathbf{E}(\underline{\gamma}_m(s),t) \tag{1.44}$$

with flux Φ, electric field $\mathbf{E}$ and circuit parametrisation $\underline{\gamma}$. Taking a circuit in form of a circle of radius L, one possible parametrisation is

$$\underline{\gamma}_m(s) = am\mathbf{e}_3 + L(\cos(s)\mathbf{e}_1 + \sin(s)\mathbf{e}_2)\,. \tag{1.45}$$

If a kind of dipole approximation is applied to this setting such that the electromagnetic field is assumed to be constant over the area of each circuit, the spectral parameter of the spectral density, cf. Eq. (1.10), is $s = 5$.

Note that there are other kinds of noise in these junctions and their influence seems to be even more disturbing than the effects which occur due to the above mentioned coupling. As these charge qubits are normally part of a larger solid crystal there are impurities around, which interact with the qubit. Each of these fluctuators causes a telegraph noise, resulting in a $1/f$-noise. A description to this phenomenon is given in [MSS03] and references therein. This setting cannot be mapped to a spin-boson model such that it is not further discussed within the scope of this work.

1.3.3 Qubits with quantum dots

Quantum dots are systems of some to a few hundred electrons which are spatially confined in a region of nanometre scale. One possible realisation of a quantum dot is due to semiconductors. By the choice of different material layers an effective two-dimensional electron gas is formed in these devices. With additional gates on the device a potential is created to isolate the electrons in a certain area, the quantum dot. The energy levels of such dots are quantised due to the confinement of the electrons. In the following consideration a quantum dot with a single confined electron is investigated. The ground-state $|g\rangle \equiv |1\rangle$ and the first excited state $|e\rangle \equiv |0\rangle$ of such an electron form the qubit. This concept of quantum computation with quantum dots was introduced by Loss and DiVincenzo [LD98].

Introduction to electron-phonon interactions. Starting point is a slightly generalised setting with a finite amount of electrons in the quantum dot and not just a single one. A typical kind of interaction with an environment of these electrons is due to phonons, as it is pointed out in this section. For reference see the book of Mahan [Mah81]. Starting point is the Hamiltonian

$$\hat{H} = \hat{H}_p + \hat{H}_e + \hat{H}_{ei}\,, \tag{1.46}$$

where electrons interact via phonons with their lattice ions. Thereby, the free Hamiltonian of a phononic environment is

$$\hat{H}_p = \sum_{\mathbf{k},\lambda} \omega_{\mathbf{k},\lambda} \left(a^\dagger_{\mathbf{k}\lambda} a_{\mathbf{k}\lambda} + \frac{1}{2} \right) . \tag{1.47}$$

Here, $a^\dagger_{\mathbf{k}\lambda}$ and $a_{\mathbf{k}\lambda}$ are bosonic creation and annihilation operators of the $\mathbf{k}^{\text{th}}$ mode with polarisation λ. The energy of a mode $\mathbf{k}$ is given by $\hbar\omega_{\mathbf{k}}$. Another contribution to $\hat{H}$ is due to electrons. Their free Hamiltonian is given by the sum of their kinetic energy and coulomb repulsion potential as

$$\hat{H}_e = \sum_i \frac{p_i^2}{2m} + \frac{e^2}{2} \sum_{i \neq j} \frac{1}{r_{ij}}\,. \tag{1.48}$$

In this equation, m is the mass of a electron and r_{ij} is the distance between the i^{th} and j^{th} electron. The remaining part of $\hat{H}$ is the interaction Hamiltonian. This interaction of the confined electrons with their lattice ions is given by

$$\hat{H}_{ei} = \sum_i \tilde{V}(\mathbf{r}_i)\,. \tag{1.49}$$

Here, $\mathbf{r}_i$ is the position of the i^{th} electron and $\tilde{V}$ is the effective potential which is produced by all lattice ions. Now these effective potentials are investigated. The i^{th} electron at position $\mathbf{r}_i$ and its interaction with the j^{th} lattice ion is observed. Let $\mathbf{R}_j$ be

the position of the j^{th} lattice ion. Consequently, the interaction between electron and ion is given by a potential $V_{ei}(\mathbf{r}_i - \mathbf{R}_j)$. As the effective potential $\tilde{V}$ for the i^{th} electron is given by the interaction with all lattice ions it reads

$$\tilde{V}(\mathbf{r}_i) = \sum_j V_{ei}(\mathbf{r}_i - \mathbf{R}_j)\,. \tag{1.50}$$

Now the position of the j^{th} ion is given by its equilibrium value $\mathbf{R}_j^{\text{eq}}$ and the displacement from its origin $\mathbf{Q}_j$ as $\mathbf{R}_j = \mathbf{R}_j^{\text{eq}} + \mathbf{Q}_j$. The above introduced potential V_{ei} is, assuming a small displacement, expanded into a Taylor series,

$$V_{ei}(\mathbf{r}_i - \mathbf{R}_j^{\text{eq}} - \mathbf{Q}_j) = V_{ei}(\mathbf{r}_i - \mathbf{R}_j^{\text{eq}}) + \mathbf{Q}_j \cdot \nabla V_{ei}(\mathbf{r}_i - \mathbf{R}_j^{\text{eq}}) + \mathcal{O}\left(Q^2\right). \tag{1.51}$$

The first contributing term is the one linear in Q, as the constant term $\sum_j V_{ei}(\mathbf{r}_i - \mathbf{R}_j^{\text{eq}})$ can be neglected. This neglection of the constant term is formally achieved by a rescaling of the Hamiltonian. A rescaling is possible as the constant term corresponds to the potential energy of the electrons if the ions are at their equilibrium position. Concluding, the effective potential for a electron-phonon interaction is given by

$$\tilde{V}(\mathbf{r}) = \sum_j \mathbf{Q}_j \cdot \nabla V_{ei}(\mathbf{r} - \mathbf{R}_j^{\text{eq}})\,, \tag{1.52}$$

where higher orders of the expansion are neglected. Now the potential $V_{ei}(\mathbf{r})$ is expanded into a Fourier series over phononic modes $\mathbf{k}$ given by $V_{ei}(\mathbf{r}) = \frac{1}{N}\sum_{\mathbf{k}} V_{ei}(\mathbf{k}) e^{i\mathbf{k}\cdot\mathbf{r}}$, where N is the number of interacting ions. Its gradient in the Fourier transformed form is easily calculated to be $\nabla V_{ei}(\mathbf{r}) = \frac{i}{N}\sum_{\mathbf{k}} \mathbf{k} V_{ei}(\mathbf{k}) e^{i\mathbf{k}\cdot\mathbf{r}}$. Inserting this result into Eq. (1.52) gives

$$\tilde{V}(\mathbf{r}) = \left(\frac{i}{N}\sum_{\mathbf{k}} \mathbf{k} V_{ei}(\mathbf{k}) e^{i\mathbf{k}\cdot\mathbf{r}}\right) \cdot \left(\sum_j \mathbf{Q}_j e^{-i\mathbf{k}\cdot\mathbf{R}_j^{\text{eq}}}\right). \tag{1.53}$$

The summation over all modes $\mathbf{k}$ is replaced by two summations over $\mathbf{q}$ and $\mathbf{G}$ with $\mathbf{k} = \mathbf{q} + \mathbf{G}$. Here, $\mathbf{G}$ is a reciprocal lattice vector and $\mathbf{q}$ lies within the first Brillouin zone. Therefore, $\mathbf{G} \cdot \mathbf{R}_j^{\text{eq}}$ is a multiple of 2π and accordingly the effective potential is given by

$$\tilde{V}(\mathbf{r}) = \left(\frac{i}{\sqrt{N}}\sum_{\mathbf{q},\mathbf{G}} \mathbf{k} V_{ei}(\mathbf{k}) e^{i\mathbf{k}\cdot\mathbf{r}}\right) \cdot \left(\frac{1}{\sqrt{N}}\sum_j \mathbf{Q}_j e^{-i\mathbf{q}\cdot\mathbf{R}_j^{\text{eq}}}\right). \tag{1.54}$$

The last part is identified to be the Fourier transformed of $\mathbf{Q}_{\mathbf{q}}$, given by $\mathbf{Q}_{\mathbf{q}} = \frac{1}{\sqrt{N}}\sum_j \mathbf{Q}_j e^{-i\mathbf{q}\cdot\mathbf{R}_j^{\text{eq}}}$. At this point an ansatz for the coefficients $\mathbf{Q}_{\mathbf{q}}$, in the form of

$$\mathbf{Q}_{\mathbf{q}} = -i\sqrt{\frac{\hbar}{2M\omega_{\mathbf{q}}}}\xi_{\mathbf{q}}(a_{\mathbf{q}} + a_{-\mathbf{q}}^{\dagger})\,, \tag{1.55}$$

is inserted. Here, M is the mass of an ion and $\xi_{\mathbf{q}}$ is the polarisations of the mode $\mathbf{q}$. Volume ν and the density of the solid ρ are introduced by $MN = \rho\nu$ such that the effective potential reads

$$\tilde{V}(\mathbf{r}) = -\sum_{\mathbf{q},\mathbf{G}} \sqrt{\frac{\hbar}{2\rho\nu\omega_{\mathbf{q}}}} (\mathbf{q}+\mathbf{G}) V_{ei}(\mathbf{q}+\mathbf{G}) \hat{\xi}_{\mathbf{q}} (a_{\mathbf{q}} + a^{\dagger}_{-\mathbf{q}}) e^{i(\mathbf{q}+\mathbf{G})\cdot\mathbf{r}} \,. \tag{1.56}$$

Having the effective potential provides full information about the interaction Hamiltonian in Eq. (1.49).

Two different regimes are discussed in the following. First the deformation potential, occurring due to the coupling to acoustical phonons is presented. Afterwards the piezoelectric interaction is outlined.

The deformation potential. The deformation potential is a coupling to acoustical phonons in the long-wavelength limit of Eq. (1.56). This limit corresponds to small norms of $\mathbf{q}+\mathbf{G}$. Hence, only the part with $\mathbf{G} = 0$ remains, as other terms are obviously of shorter wavelengths. The potential is replaced by the deformation constant D, as $V_{ei}(\mathbf{q}) \to D$ in the considered limit of long wavelength. Assuming a nondegenerated band at long wavelength only longitudinal phonons are important, such that $\hat{\xi}_{\mathbf{q}} \to \hat{\mathbf{q}}$. In this limit the interaction Hamiltonian is

$$\hat{H}_{ei} = \sum_{l} D \sum_{\mathbf{q}} \sqrt{\frac{\hbar}{2\rho\nu\omega_{\mathbf{q}}}} |\mathbf{q}| (a_{\mathbf{q}} + a^{\dagger}_{-\mathbf{q}}) e^{i\mathbf{q}\cdot\mathbf{r}_l} \,. \tag{1.57}$$

Piezoelectric interactions. Piezoelectric interactions are the interactions of a solid to an electric field. The microscopic effect of this interaction is that a crystal is squeezed if an electric field is applied and vice versa. The analysis of this piezoelectric interaction is adduced by a short excursion to the stress of a solid. The stress $\mathbf{S}$ is defined as the symmetric derivative of the displacement field $\mathbf{Q}$,

$$\mathbf{S}_{ij} = \frac{1}{2}\left(\frac{\partial \mathbf{Q}_i}{\partial r_j} + \frac{\partial \mathbf{Q}_j}{\partial r_i}\right) = \frac{1}{2} \sum_{\mathbf{q}} \sqrt{\frac{\hbar}{2\rho\nu\omega_{\mathbf{q}}}} (\xi_i q_j + \xi_j q_i)(a_{\mathbf{q}} + a^{\dagger}_{-\mathbf{q}}) e^{i\mathbf{q}\cdot\mathbf{r}} \,. \tag{1.58}$$

Note that $\mathbf{Q}_i$ in this case is the i^{th} component of the field $\mathbf{Q} \equiv \mathbf{Q}(\mathbf{r})$ and not the displacement $\mathbf{Q}$ at the position of the i^{th} ion. The Fourier transformed displacement $\mathbf{Q}(\mathbf{r}) = \frac{1}{\sqrt{N}} \sum_{\mathbf{q}} \mathbf{Q}_{\mathbf{q}} e^{i\mathbf{q}\cdot\mathbf{r}}$ is inserted, having Fourier coefficients $\mathbf{Q}_{\mathbf{q}}$ within the sum that were already introduced in Eq. (1.55). For a given stress S_{ij} on the crystal the electric field is proportional to the stress,

$$E_l = \sum_{i,j} \mathbf{M}_{ijl} \mathbf{S}_{ij} \,, \tag{1.59}$$

where the matrix $\mathbf{M}_{ijl}$ is constant. This electric field is longitudinal and points into the direction of the phonons. On the other side, the electric field is proportional to the gradient of a potential $\phi(\mathbf{r})$. Now these two insights are combined. Therefore, replacing the potential by its Fourier transformed expression leads to

$$E_l = -\frac{\partial\phi(\mathbf{r})}{\partial r_l} = -\frac{1}{\sqrt{\nu}}\sum_{\mathbf{q}} i\mathbf{q}_l\phi_{\mathbf{q}}e^{i\mathbf{q}\cdot\mathbf{r}}\,. \tag{1.60}$$

Concluding, it is to mention that the potential is proportional to the displacement. As the matrix $\mathbf{M}$ does not depend on the magnitude of $\mathbf{k}$, but on its direction and polarisation λ, the potential is given by

$$\phi(\mathbf{r}) = i\sum_{\mathbf{q},\lambda}\sqrt{\frac{\hbar}{2\rho\nu\omega_{\mathbf{q},\lambda}}}M_\lambda(\hat{\mathbf{q}})(a_{\mathbf{q},\lambda} + a^\dagger_{-\mathbf{q},\lambda})e^{i\mathbf{q}\cdot\mathbf{r}}\,. \tag{1.61}$$

Consequently, for a piezoelectric interaction the corresponding interaction Hamiltonian is obtained to be

$$\hat{H}_{ei} = \sum_l i\sum_{\mathbf{q},\lambda}\sqrt{\frac{\hbar}{2\rho\nu\omega_{\mathbf{q},\lambda}}}M_\lambda(\hat{\mathbf{q}})(a_{\mathbf{q},\lambda} + a^\dagger_{-\mathbf{q},\lambda})e^{i\mathbf{q}\cdot\mathbf{r}_l}\,. \tag{1.62}$$

Construction of a quantum dot qubit. Piezoelectric interaction are assumed to dominate the physics within a given quantum dot. For simplicity only a single qubit is investigated, using one confined electron within this quantum dot. For this electron the level structure of a three-dimensional harmonic oscillator (cf. Appendix C) with mass m and circular frequency ω_0 in each direction is assumed. To construct a qubit two states of the system have to be selected, e.g.

$$|1\rangle = |g\rangle = \varphi_{000}(x,y,z) \quad \text{and} \quad |0\rangle = |e\rangle = \varphi_{100}(x,y,z)\,. \tag{1.63}$$

According to the notation introduced in Appendix C, these two states are given with $\mathbf{r} = (x,y,z)$ and $\beta = m\omega_0/\hbar$ by $\varphi_{000}(x,y,z) = (\beta/\pi)^{3/4}e^{-\beta\mathbf{r}^2/2}$ and $\varphi_{100}(x,y,z) = (\beta/\pi)^{3/4}e^{-\beta\mathbf{r}^2/2}\sqrt{2\beta}x$. The corresponding dissipative interaction Hamiltonian is

$$\hat{H}_I = \sum_{i,j\in\mathbb{Z}_2;i\neq j}\left\langle i\right|\hat{H}_{ei}\left|j\right\rangle\left|i\right\rangle\!\left\langle j\right|\,. \tag{1.64}$$

For the chosen qubit states the matrix element is given as

$$\left\langle 0\right|\hat{H}_{ei}\left|1\right\rangle = -\sum_{\mathbf{q},\lambda}\sqrt{\frac{\hbar}{2\rho\nu\omega_{\mathbf{q},\lambda}}}M_\lambda(\hat{\mathbf{q}})(a_{\mathbf{q},\lambda} + a^\dagger_{-\mathbf{q},\lambda})\left(e^{-\mathbf{q}^2/4\beta}\sqrt{\frac{\hbar}{2m\omega_0}}\mathbf{q}_x\right)\,. \tag{1.65}$$

By analysing the coupling coefficients $g_{\mathbf{k}}$ in this case it turns out that the spectral density of this model has a spectral parameter of $s = 3$.

Note that in principle there are other ways of building a qubit using quantum dots. Instead of using the ground and first excited state of the isolated electron within the dot as a two level system it is also possible to access the spin of this electron as it is done by Vandersypen et al. [VHvB$^+$02]. Here, via Zeeman splitting the ground state becomes a usable two-level system. Another two level system can be constructed using two quantum dots with a fixed number of electrons on each of them and one electron which can tunnel between the two dots.

Conclusion

This chapter dealt with different constructions of qubits. An explicit derivation for a spin qubit was given first. Spin qubits and their interaction to thermal radiation could be derived starting from the minimal coupling Hamiltonian in the presence of a static magnetic field. Then, again the minimal coupling Hamiltonian was investigated, but in the absence of a static magnetic field. In this case the ground and first exited state of an atom could be used to form a qubit. The corresponding interaction to thermal radiation was pointed out. Other qubit constructions with Josephson junctions or quantum dots were also included. The fundamental models in each case was mapped onto a spin-boson model. For that purpose, the spin-boson model was introduced. The coupling between qubits and environment was described by a spectral density. This density was analysed for the different types of qubits. Thereby, all investigated settings showed a super-Ohmic coupling according to their three-dimensional environment. An Ohmic coupling would be expected for an one-dimensional environment. Due to the interaction between environment and qubits decoherence occurred. Obligatory, a general introduction to decoherence was shown. To outline the explicit form of decoherence for one of the introduced qubits their corresponding time evolution has to be discussed. Accordingly, the time evolution of the spin-boson model is analysed in the next chapter. In particular the spin part and its dynamics of the model which corresponds to the qubit register is examined.

2 Decoherence of an n-qubit register

In this chapter the time evolution of a qubit register is determined. This register is given by the spin part of the previously introduced spin-boson model. Quantum information is stored in this spin part in form of an initially prepared state $\rho(0)$. Due to the interaction of the spins with the environment an effective noise $\mathcal{N}_t$ acts on the qubit register during the time t and evolves the initial state to $\mathcal{N}_t(\rho(0)) = \rho(t)$. In principle, this noise can be used to decide whether the analysed system is a good candidate for the realisation of a qubit register or not. This analysis is performed in the later chapters, whereas exact expressions for $\mathcal{N}_t$ are calculated in this chapter. Various authors have already discussed this phenomenon for different settings, e.g. [PSE97, BP02, RQJ02, DWHK07], but a final satisfying result is still missing. Actually, there is no known universal analytical solution of the time evolution of the spin-boson model. Many different methods exist to deal with this problem. Some of them, in particular those dealing with dissipative couplings involve master equations. In the scope of this work a dissipative spin-boson model is solved using this technique with some approximations in Chapter 6. In the present chapter an analytical method is introduced, which does not require any approximation and does not involve a master equation. The price for being without any approximation is that this attempt is only correct for a dissipationless coupling between spin part and environment and does not hold for a dissipative setting. Nevertheless a dissipationless model is chosen for further progress. Accordingly, the time evolution of the dissipationless spin-boson model is calculated first. Then, the noise which acts on the qubit register is read off in this time evolution. In this case the noise can be brought into a special form given by decoherence coefficients. With the help of these decoherence coefficients it is possible to describe the time evolution for each entry of the reduced density operator of the qubit register on its own. It is remarkable by itself that entries of this reduced density operator evolve independently of each other. The corresponding calculations are performed in Sec. 2.2. An analysis of the decoherence coefficient shows that it is possible to decouple them into two parts. The first part depends on the entries of the register only, and the second part consists of a decoherence function which just depends on time and distance. In Sec. 2.2 these decoherence functions are calculated. For an Ohmic spectral density and the super-Ohmic case exact results are presented within this chapter. Having knowledge about the time evolution provides the opportunity to further investigate the qubit register.

2.1 Decoherence coefficients

The decoherence of a qubit register is illuminated in this section. In the scope of this work the qubit register is part of a closed system. This closed system includes an environment having interactions to the qubit register, such that the combined system is described by a spin-boson model. The dynamics of the spin part, which is used as the qubit register, is analysed. Decoherence within this spin part appears in the time evolution of its reduced density operator. Here, the time evolution of the qubit register cannot be calculated without taking the environment into account. Hence, in a first step the time evolution of the complete system is calculated. This time evolution is unitary as the system is closed and follows the prediction of quantum mechanics accordingly. Then the time evolution of the qubit register is distilled out of the time evolved density operator of the complete system. For each time the environmental degrees of freedom of the closed system's density operator are traced out. The remaining state is the reduced density operator of the qubit register at the given time. Here, the environment is taken to be initially in thermal equilibrium and the complete system is taken to be initially in a product state of environment and qubit register. At the end of this procedure a mapping from the initial state of the qubit to its time evolved state is obtained.

First, the time evolution of the closed system is determined. The interaction picture turns out to be a good choice for calculations to decouple effects of the free Hamiltonian from those of the interaction Hamiltonian. As a result, in the interaction picture states and operators are time depended. The operators evolve in time according to the free Hamiltonian of the system, whereas the states evolve according to the interaction Hamiltonian. As the interaction Hamiltonian itself is an operator, its expression in the interaction picture has to be calculated. It is given by

$$\tilde{H}_I(t) = \sum_{\mathbf{m}} Z_{\mathbf{m}} \otimes B(a\mathbf{m}, t)\,. \tag{2.1}$$

The index $\mathbf{m}$ is a tuple of positive integers with the dimension of the spin system and labels different lattice-sites. $Z_{\mathbf{m}} \equiv \sigma_{z,\mathbf{m}}$ is a Pauli spin matrix acting on the spin on the lattice site $\mathbf{m}$. The above mentioned time dependency of the operators also affects the occurring bath operators. The bath operators $B(a\mathbf{m}, t)$ in the interaction picture are calculated, starting from the operators $B(\mathbf{r})$ in Eq. (1.9). The time evolution of the free Hamiltonian, $B(\mathbf{r}, t) = e^{i\hat{H}_0 t} B(\mathbf{r}) e^{-i\hat{H}_0 t}$, is applied, such that they are given by

$$B(\mathbf{r}, t) = \sum_{\mathbf{k}} g_{|\mathbf{k}|} e^{-i(\mathbf{k}\cdot\mathbf{r} - \omega_{\mathbf{k}} t)} b_{\mathbf{k}}^{\dagger} + H.c. \tag{2.2}$$

In this way the interaction Hamiltonian in the interaction picture is determined. With the help of this Hamiltonian it is possible to calculate the time evolution of states within this picture. All calculations presented in the scope of this work have well defined starting conditions. Here, initially the closed system of spin part and environment is

assumed to be in a product state

$$\rho_{SE}(0) = \rho(0) \otimes \rho_E, \tag{2.3}$$

where $\rho(0)$ is the initial state of the qubit register and ρ_E is the initial state of the environment. The latter is taken to be in thermal equilibrium at temperature T. The spin part

$$\rho(0) = \sum_{\mu,\nu \in \mathbb{Z}_2^n} \rho_{\nu\mu}(0) \, |\nu\rangle\langle\mu| \tag{2.4}$$

is expressed in the computational basis. The unitary time evolution of states in the closed system is determined by a time evolution operator $U_I(t)$. This time evolution operator is given by

$$U_I(t) \;=\; T_{\leftarrow} \exp\left(-i\hbar^{-1} \int_0^t \mathrm{d}s \, \tilde{H}_I(s) \right) , \tag{2.5}$$

having the above calculated interaction Hamiltonian as component. Here, the operator $T_{\leftarrow}$ denotes chronological order from right to the left. Finally, the time evolution of an initial density operator $\rho_{SE}(0)$ of the closed system is given by $\rho_{SE}(t) \;=\; U_I(t)\rho_{SE}(0)U_I^\dagger(t)$.

Having the time evolution of the complete system's density operator the reduced density operator of the qubit register is determined. Therefore, all degrees of the environment have to be traced out in the complete system's density operator, such that the time evolution of the reduced density operator is given by

$$\rho(0) \mapsto \rho(t) = \operatorname*{tr}_E \left\{ U_I(t)\rho_{SE}(0)U_I^\dagger(t) \right\} . \tag{2.6}$$

It is established by various authors (see [PSE97, DG98, BLW99, RQJ02, BP02, NC00, Zur03] for reference) that this time evolution can be written with the help of a unitary operator $\mathcal{U}_t$ and noise $\mathcal{N}_t$ (cf. Eq. (1.2)) as

$$\rho(t) = \mathcal{U}_t \circ \mathcal{N}_t(\rho(0)) \, . \tag{2.7}$$

The unitary part $\mathcal{U}_t$ originates from the register's own dynamics but also includes the Lamb-shift caused by the bosonic bath. As $\mathcal{U}_t$ is a unitary operator, the effects caused by this operator are in principle reversible and are neglected accordingly. Thus, to extend the knowledge about decoherence the noise operator $\mathcal{N}_t$ is investigated in the scope of this work.

In a dissipationless model it is possible to rewrite the noise operator $\mathcal{N}_t$ in an effective way. This is possible as each element of the reduced density operator evolves independently in time and is not influenced by others. Decoherence coefficients $\mathrm{D}_{\nu\mu}(t)$ are introduced for the reformulation. With the help of these coefficients it is possible to rewrite the noise operator $\mathcal{N}_t$, such that it acts on the reduced density operator of the

spin system by

$$\mathcal{N}_t(\rho(0)) = \sum_{\mu,\nu\in\mathbb{Z}_2^n} e^{-\mathrm{D}_{\nu\mu}(t)} \left|\nu\right\rangle\!\left\langle\nu\right| \rho(0) \left|\mu\right\rangle\!\left\langle\mu\right| . \tag{2.8}$$

This double summation extends over all computational states $|\nu\rangle$, which are labelled by $\nu \in \{0,1\}^n \equiv \mathbb{Z}_2^n$. Here, it is important that the considered system has no dissipation, as otherwise the time evolution could not be written in this form. To have full knowledge about the complete time evolution of the qubit register all decoherence coefficients have to be calculated. For each set of states ν and μ the decoherence coefficient is determined by

$$e^{-\mathrm{D}_{\nu\mu}(t)+i\phi} = \operatorname*{tr}_E \left\{ \left\langle \nu \right| U_I(t) \left| \nu \right\rangle \rho_E \left\langle \mu \right| U_I^\dagger(t) \left| \mu \right\rangle \right\} , \tag{2.9}$$

where ϕ is a phase, which also depends on time and the involved states. In principle it is possible to obtain the phases ϕ; the corresponding calculation is presented in Appendix A. In the scope of this work these phases are neglected as they only contribute to $\mathcal{U}_t$. Now Eq. (2.9) is analysed. The matrix elements occurring in this equation are given by

$$\left\langle \nu \right| U_I(t) \left| \nu \right\rangle = T_{\leftarrow} \exp\left(-i\hbar^{-1} \int_0^t \mathrm{d}\tau \sum_{\mathbf{m}} (-1)^{\nu_{\mathbf{m}}} B(a\mathbf{m},\tau) \right) . \tag{2.10}$$

The chronological order performed by $T_{\leftarrow}$ is neglected in the following, as it only contributes to the phase ϕ and in this way to $\mathcal{U}_t$. The remaining integral is dealt with in the following. To proceed and conclude, Eq. (2.10) without time order is inserted into Eq. (2.9) and phases are neglected. In the presented Eq. (2.10) matrix elements permute under the trace. For that purpose, they are written into the same exponential function. Additionally $(-1)^{\nu_{\mathbf{m}}} - (-1)^{\mu_{\mathbf{m}}} = 2(\mu_{\mathbf{m}} - \nu_{\mathbf{m}})$ is replaced. The remaining formula has the form of a thermal expectation value, such that it can be written as

$$e^{-\mathrm{D}_{\nu\mu}(t)} = \left\langle \exp\left(-2i\hbar^{-1} \int_0^t \mathrm{d}\tau \sum_{\mathbf{m}} (\mu_{\mathbf{m}} - \nu_{\mathbf{m}}) B(a\mathbf{m},\tau) \right) \right\rangle_T , \tag{2.11}$$

where T is the temperature of the bath. Now the Wick theorem is applied to this expectation value. Each decoherence coefficient is expressed as a summation over expectation values of a product of two bath operators. Afterwards the relation $\langle B(a\mathbf{m},\tau)B(a\mathbf{l},\tau')\rangle_T = \langle B(a(\mathbf{m}-\mathbf{l}),|\tau-\tau'|)B(\mathbf{0},0)\rangle_T$ for these bath operators is used. This relation can be easily seen by direct calculation. At this point an integral substitution is applied, which reads $\int_0^t \mathrm{d}\tau' \int_0^t \mathrm{d}\tau \, \langle B(\mathbf{r},|\tau-\tau'|)B(\mathbf{0},0)\rangle_T = 2\int_0^t \mathrm{d}\tau' \int_0^{\tau'} \mathrm{d}\tau \, \langle B(\mathbf{r},\tau)B(\mathbf{0},0)\rangle_T$. Finally the decoherence coefficients are given by

$$\mathrm{D}_{\nu\mu}(t) = \sum_{\mathbf{m},\mathbf{l}} (\mu_{\mathbf{m}} - \nu_{\mathbf{m}})(\mu_{\mathbf{l}} - \nu_{\mathbf{l}}) \, \mathrm{K}(a(\mathbf{m}-\mathbf{l}),t) . \tag{2.12}$$

Here, decoherence functions $\mathrm{K}(\mathbf{r},t)$ depending on distance $\mathbf{r}$ and time t occur. These decoherence functions are given by

$$\mathrm{K}(\mathbf{r},t) = 4\int_0^t \mathrm{d}\tau'\, \Re[\mathrm{C}(\mathbf{r},\tau')]\,, \tag{2.13}$$

where space and time dependent functions

$$\mathrm{C}(\mathbf{r},t) = \hbar^{-2}\int_0^t \mathrm{d}\tau\ \langle B(\mathbf{r},\tau)B(\mathbf{0},0)\rangle_T \tag{2.14}$$

are introduced. The functions $\mathrm{C}(\mathbf{r},t)$ are called correlation functions. They include the thermal average of two bath operators, such that they do not depend on any state. In total, the decoherence coefficients together with the decoherence functions determine the time evolution of states within the non dissipative spin-boson model.

Note that Eq. (2.12) reveals the constancy of the populations of the reduced density operator as $\mathrm{D}_{\nu\nu}(t) \equiv 0$. This constancy is a well known behaviour of a dissipationless coupling. Further on, the rate $\mathrm{K}(0,t)$ itself describes the decoherence of a single spin in the absence of other spins.

2.2 Decoherence functions

In the remaining part of this chapter decoherence functions $\mathrm{K}(\mathbf{r},t)$ (cf. Eq. (2.13)) for different settings are calculated. These decoherence functions are the last ingredients to achieve full knowledge about the time evolution of the qubit register. Decoherence functions are defined by Eq. (2.13) and Eq. (2.14) together with the bath operators of Eq. (2.2). Starting with a correlation function given by Eq. (2.14) the occurring thermal expectation value is resolved. The corresponding bath is assumed to be in thermal equilibrium at temperature T. Accordingly the initial state of the bath is given as

$$\rho_E = \bigotimes_{\mathbf{k}} e^{-\beta\omega_{\mathbf{k}} n_{\mathbf{k}}}(1-e^{-\beta\omega_{\mathbf{k}}}) \tag{2.15}$$

with temperature $\beta^{-1} = k_{\mathrm{B}}T$, Boltzmann constant k_{B} and particle number operator $n_{\mathbf{k}} = b_{\mathbf{k}}^{\dagger}b_{\mathbf{k}}$. Analysing the expectation value of a product of two bath operators in Fock space reveals that for each mode $\mathbf{k}$ the operator $2n_{\mathbf{k}}+1$ occurs. A short calculation shows that for each mode $\mathbf{k}$ the corresponding expectation value is proportional to

$$\langle 2n_{\mathbf{k}}+1\rangle_T = \coth\frac{\omega_{\mathbf{k}}}{2k_{\mathrm{B}}T}\,. \tag{2.16}$$

Now the two remaining integrals over time are solved. Afterwards, the decoherence function turns out to be.

$$\mathrm{K}(\mathbf{r},t) = 4\hbar^{-2}\sum_{\mathbf{k}}|g_{|\mathbf{k}|}|^2\frac{1-\cos(\omega_{\mathbf{k}}t)}{\omega_{\mathbf{k}}^2}\coth\frac{\omega_{\mathbf{k}}}{2k_{\mathrm{B}}T}e^{i\mathbf{k}\cdot\mathbf{r}}\,. \tag{2.17}$$

This is the exact result for the decoherence function for a discrete set of bath modes $\mathbf{k}$.

For an explicit calculation of the decoherence function the continuum limit of the bath modes has to be performed. This continuum limit is performed with the help of the spectral density. According to Eq. (1.10) the spectral density with spectral parameter s and high energy cutoff Ω is given by

$$J(\omega) = \alpha\omega^s e^{-\omega/\Omega} = 4f_E(\omega)\sum_{\mathbf{k}}\delta(\omega-\omega_{\mathbf{k}})|g_{|\mathbf{k}|}|^2\,. \tag{2.18}$$

At this point it is helpful to introduce spherical coordinates for each bath mode $\mathbf{k}$. Then, an additional integration with integration variable ω is performed to get rid of the summation. Thereby, due to the delta function the right terms are selected. Now the contribution of the $e^{i\mathbf{k}\cdot\mathbf{r}}$-part of the decoherence function is investigated. It turns out that for the distance dependent decoherence functions this contribution is given by $\frac{\sin(\omega r)}{\omega r}$, according to

$$\begin{aligned}\int\limits_{\mathbb{R}^3}\mathrm{d}\mathbf{k}\,e^{i\mathbf{k}\cdot\mathbf{r}}f(k) &= \int\limits_0^\infty\mathrm{d}k\int\limits_0^{2\pi}\mathrm{d}\varphi\int\limits_0^{\pi}\mathrm{d}\theta\,k^2\sin\theta e^{ikr\cos\theta}f(k)\\ &= 4\pi\int\limits_0^\infty\mathrm{d}k\,k^2\frac{\sin(kr)}{kr}f(k)\,,\end{aligned} \tag{2.19}$$

which is valid for any k-depending function f. Note that the Jacobi determinant $4\pi k^2$ does not contribute as only the difference between $\int_{\mathbb{R}^3}\mathrm{d}\mathbf{k}\,e^{i\mathbf{k}\cdot\mathbf{r}}f(k)$ and $\int_{\mathbb{R}^3}\mathrm{d}\mathbf{k}\,f(k)$ is investigated. The Jacobi determinant itself is included in the spectral density. With the help of this consideration the decoherence function in the continuum limit is obtained to be

$$\mathrm{K}_s(\mathbf{r},t) = \alpha\hbar^{-2}\int\limits_0^\infty\mathrm{d}\omega\,J(\omega)\frac{1-\cos(\omega t)}{\omega^2}\coth\left(\frac{\omega}{2k_{\mathrm{B}}T}\right)\begin{cases}1 & ,\mathbf{r}=0\\ \frac{\sin(\omega r)}{\omega r} & ,\mathbf{r}\neq 0\end{cases}\,. \tag{2.20}$$

Now the integrals which occur in this decoherence functions are classified. Afterwards the physically relevant ones are calculated. In this context all decoherence functions are expressed by bath correlation functions. These bath correlation functions are introduced in the following. For a real variable $q\in\mathbb{R}$ and complex variables $z,w\in\mathbb{C}$ a bath

correlation function $\mathrm{C}_q(z,w)$ is defined as

$$\mathrm{C}_q(w,z) = \int_0^\infty \mathrm{d}x\, x^q e^{iwx}(1-\cos(xz))\coth\frac{x}{2}\,. \tag{2.21}$$

It has to be ensured that this is a well defined expression, e.g. the integral should not diverge. On the one hand a possible divergence at the upper bound has to be avoided. At the upper bound the integral converges for a positive imaginary part of w as this leads to a damped integrand for large values of x. A divergence at the lower boundary of the integral is avoided by the following conditions to q. The real part $\Re[\mathrm{C}_q(z,w)]$ is defined for $q > -2$ and the imaginary part $\Im[\mathrm{C}_q(z,w)]$ is defined for $q > -3$.

Now the decoherence functions can be formally expressed by bath correlation functions. In this way, comparing Eq. (2.20) and Eq. (2.21), the decoherence functions are given by

$$\mathrm{K}_s(\mathbf{r},t) = \alpha\beta^{-(s-1)} \begin{cases} \mathrm{C}_{s-2}\big(iT\Omega^{-1}, Tt\big) & ,\mathbf{r}=0 \\ \frac{1}{T|\mathbf{r}|}\Im\left[\mathrm{C}_{s-3}\big(T(|\mathbf{r}|+i\Omega^{-1}), Tt\big)\right] & ,\mathbf{r}\neq 0 \end{cases}. \tag{2.22}$$

Note that for a wide range of the parameter s the bath correlation function can be expressed by combinations of Hurwitz zeta and gamma functions. Dealing with a positive parameter $q > 0$ (or the limit $q \to 0$) the bath correlation function is given by

$$\begin{aligned}\mathrm{C}_q(w,z) =& \Gamma(q+1)\,\{2\zeta_{q+1}(-iw) - \zeta_{q+1}(-i(w+z)) - \zeta_{q+1}(-i(w-z)) \\ &-\frac{(-1)^{q+1}}{2}\left(\frac{2}{(iw)^{q+1}} - \frac{1}{(i(w+z))^{q+1}} - \frac{1}{(i(w-z))^{q+1}}\right)\Big\}\,,\end{aligned} \tag{2.23}$$

where $\zeta_q(\nu) = \sum_{n=0}^\infty (n+\nu)^{-q}$ is the Hurwitz zeta function. This identity is easily derived using the definition of the Hurwitz zeta function together with the definition of the gamma function and the relations between both of them.

2.2.1 Ohmic coupling (spectral parameter s=1)

The topic of this section is Ohmic coupling. An Ohmic spectral density, as defined in Eq. (1.10), has a spectral parameter $s \equiv 1$ and hence looks like

$$J(\omega) = \alpha\omega e^{-\omega/\Omega}\,. \tag{2.24}$$

Decoherence functions are determined for this Ohmic setting. According to Eq. (2.22) decoherence functions for vanishing and finite distance have to be calculated separately.

First the decoherence functions for vanishing distance $r = 0$ are calculated. The corresponding bath correlation function has a parameter $q = -1$. With some effort,

outlined in Appendix A, the bath correlation function for $q = -1$ is obtained to be

$$\mathrm{C}_{-1}(w,z) = \frac{1}{2}\ln\left(\frac{\Gamma^4(-iw)}{\Gamma^2(-i(w-z))\Gamma^2(-i(w+z))}\frac{w^2}{(w^2-z^2)}\right). \tag{2.25}$$

Now this bath correlation function is inserted into Eq. (2.22), having $w = iT\Omega^{-1}$ and $z = Tt$. Using transformation rules of the logarithm and the property that the gamma function is analytical immediately leads to

$$\mathrm{K}_1(0,t) = 2\alpha\ln\left|\frac{\Gamma(T/\Omega)}{\Gamma(T/\Omega+iTt)}\right| - \frac{\alpha}{2}\ln(1+t^2\Omega^2)\,. \tag{2.26}$$

This result is illuminated in the following. For this purpose, different time regimes are investigated. In the case of times lower than the inverse temperature, $t \ll \frac{1}{T}$, an approximation for the gamma function with small arguments is applied (cf. Lemma 15 in Appendix B) and leads to the result below. For times larger than the inverse temperature, $t \gg \frac{1}{T}$, Binet's expression for the logarithm of the gamma function is used. With an expansion of the resulting formula in T/Ω, the result is calculated up to first order. These calculations show that in good approximation the decoherence function has the form of

$$\mathrm{K}_1(0,t) = \alpha\begin{cases} \ln(1+t^2\Omega^2)/2 & ,t \ll \frac{1}{T} \\ \pi Tt + \ln\frac{\Omega}{2\pi T} & ,t \gg \frac{1}{T} \end{cases}. \tag{2.27}$$

This function itself describes the decoherence of a single spin ($n = 1$). The density operator of a single qubit register $\rho(0)$ would evolve in time to $\rho(t)$ according to

$$\rho(0) = \begin{pmatrix}\rho_{00} & \rho_{01}\\ \rho_{10} & \rho_{11}\end{pmatrix} \mapsto \rho(t) = \begin{pmatrix}\rho_{00} & \rho_{01}e^{-\mathrm{K}_1(0,t)}\\ \rho_{10}e^{-\mathrm{K}_1(0,t)} & \rho_{11}\end{pmatrix}. \tag{2.28}$$

The mapping shows that populations of the density operator stay constant and off diagonal entries shrink according to the rate $\mathrm{K}_1(0,t)$. This is the expected result for a single spin which is coupled without dissipation to a surrounding environment.

Now the case of a finite distance $r > 0$ is investigated. In the scope of this work the speed of the bath bosons is set to $c = 1$. Accordingly times and distances have the same dimension. The calculation for decoherence functions with $r > 0$ is divided into two parts. The first part is given for times lower than the distance and the second part is given for times that are greater than the distance. The corresponding calculation is presented in full length in the Appendix A and only a sketch of it is shown in the following. The first regime is given for short times $t \leq r$. The decoherence function is calculated via a contour integral, such that it reads

$$\mathrm{K}_1(r,t) = \alpha\left(\frac{\pi Tt^2}{2r} + \frac{\mathrm{Li}_2\left(e^{-2\pi T(r-t)}\right) + \mathrm{Li}_2\left(e^{-2\pi T(r+t)}\right) - 2\mathrm{Li}_2\left(e^{-2\pi Tr}\right)}{4\pi Tr}\right). \tag{2.29}$$

Here, $\mathrm{Li}_2(x)$ denotes a polylogarithm. For the regime of times $t > r$ the calculation is a

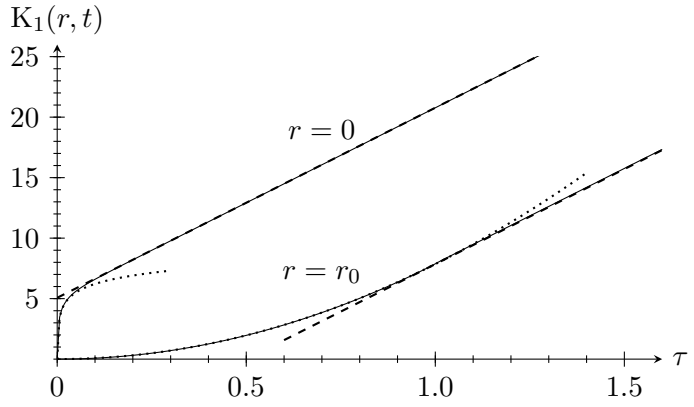

Figure 2.1: Decoherence functions $\mathrm{K}_1(0,t)$ and $\mathrm{K}_1(r_0,t)$ as a function of dimensionless time $\tau = t/r_0$ at temperature $T = 5/r_0$. The cut-off energy is $\Omega = 10^3 T$. The dotted and dashed curves are short- and long-time approximation, respectively.

bit more complicated as an additional integration is involved. Starting point to calculate the decoherence function in this case is the result at time $t = r$, which was derived before. Afterwards the derivative of the function with respect to time is integrated over the time interval from r to t and then added to the previous result. The integral occurring in this step is solved by a contour integration again. At the end of this procedure the decoherence function for $t > r$ is

$$\mathrm{K}_1(r,t) = \alpha\left(\pi T\left(t-\frac{r}{2}\right) + \frac{\pi}{12Tr} + \frac{\mathrm{Li}_2\left(e^{-2\pi T(t+r)}\right) - \mathrm{Li}_2\left(e^{-2\pi T(t-r)}\right) - 2\mathrm{Li}_2\left(e^{-2\pi Tr}\right)}{4\pi Tr}\right). \tag{2.30}$$

For times much larger than the distance r the terms including polylogarithms only lead to an exponentially small contribution.

The decoherence functions $\mathrm{K}_1(0,t)$ and $\mathrm{K}_1(r,t)$ together with their approximations are shown in Fig. 2.1. Having these decoherence functions a complete knowledge about the time evolution of a qubit register with an Ohmic coupling is achieved.

2.2.2 Super-Ohmic coupling (spectral parameter s=3)

A super-Ohmic coupling between qubit register and environment is examined in this section. Decoherence functions for this coupling are derived. These decoherence functions occur e.g. for a quantum-mechanical spin coupled to an external magnetic field.

Starting point for calculations are decoherence functions as they are given in Eq. (2.22) with a spectral parameter $s = 3$. Using the integral representation and recurrence relations for the digamma and polygamma function (cf. Lemma 9 and Lemma 13 in

Appendix B) these decoherence functions can be calculated with some effort. Similar to the case of Ohmic coupling it is necessary to divide the calculation into two parts. In the first part functions with finite distances are dealt with and in the second part function with distance zero are considered. The distance depending decoherence function with distance $r > 0$ turns out to be

$$\begin{aligned}\mathrm{K}_3(r,t) =& \frac{\alpha T}{\hbar^2 r}\left(\Im\left[2\psi(T/\Omega + iTr) - \psi(T/\Omega + iT(r-t)) - \psi(T/\Omega + iT(r+t))\right]\right) \\ &- \frac{\alpha}{2\hbar^2 r}\left(\frac{2r}{1/\Omega^2 + r^2} - \frac{r-t}{1/\Omega^2 + (r-t)^2} - \frac{r+t}{1/\Omega^2 + (r+t)^2}\right). \end{aligned} \tag{2.31}$$

The occurring $\psi(z)$ denotes the digamma function with complex argument $z \in \mathbb{C}$. The decoherence function with distance zero, which describes the decoherence of a single qubit e.g., is given by

$$\mathrm{K}_3(0,t) = \frac{2\alpha T^2}{\hbar^2}\left(\psi^{(1)}(T/\Omega) - \Re\left[\psi^{(1)}(T/\Omega + iTt)\right]\right) - \frac{\alpha}{\hbar^2}\left(\Omega^2 + \frac{t^2 - 1/\Omega^2}{(t^2 + 1/\Omega^2)^2}\right). \tag{2.32}$$

Here, $\psi^{(1)}(z)$ is a polygamma function with complex argument $z \in \mathbb{C}$. Having the decoherence functions for all times and distances gives full knowledge about the time evolution of the qubit register for the given super-Ohmic setting.

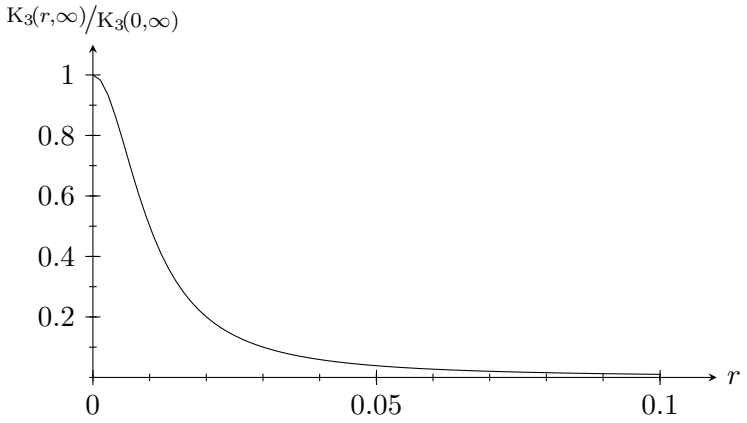

Figure 2.2: Long time limit of the fraction $\mathrm{K}_3(r,t) \,/\, \mathrm{K}_3(0,t)$.

Finally, the derived decoherence functions for a super-Ohmic setting are analysed. The decoherence functions have to fulfil the relation $\lim_{r\to 0} \mathrm{K}_3(r,t) = \mathrm{K}_3(0,t)$ as a consequence of their definition in Eq. (2.17). It turns out that $\mathrm{K}_3(r,t)$ is a decreasing function in r, which is illustrated in Fig. 2.2. Another remarkable point is that the rate

$\mathrm{K}_3(r,t)$ saturates with time to

$$\lim_{t\to\infty} \mathrm{K}_3(r,t) = \frac{\alpha}{\hbar^2} \begin{cases} 2T^2\psi^{(1)}(T/\Omega) - \Omega^2 & , r = 0 \\ \frac{2T}{r}\Im\left[\psi(T/\Omega + iTr)\right] - \frac{1}{(1/\Omega^2+r^2)} & , r > 0 \end{cases} . \tag{2.33}$$

Saturation occurs for all decoherence functions in the super-Ohmic regime, as long as the spectral parameter is larger than two ($s > 2$).

Conclusion

The time evolution of the dissipationless spin-boson model was derived. Especially the spin part of this model was studied, as this part was used to store quantum information. In the scope of this work only contributions of the time evolution which led to decoherence were studied. Phases that contributed unitarily to the time evolution were neglected. The hole problem was best solved in a computational basis of the spins. The remaining time evolution of the spin system was described by decoherence coefficients and decoherence functions. Each entry of the spin system's reduced density operator evolved according to a corresponding decoherence coefficient. Thereby, the decoherence coefficient were formally given as a summation over decoherence functions with coefficients that depend only on the index of the reduced density operator. Hence, the structure of these decoherence coefficients did not directly depend on the coupling, whereas the structure of the decoherence function was influenced by the spectral parameter of the corresponding spectral density. The calculations for the decoherence functions in the cases of an Ohmic ($s = 1$) and a super-Ohmic spectral density with parameter $s = 3$ were presented in full detail.

3 Quantum codes

In this chapter the storage of quantum information in a physical model is dealt with. For an introduction to quantum codes see the book of Nielsen and Chuang [NC00] and references therein. Commonly, quantum information is stored in states of an accessible Hilbert space $\mathcal{H}_n$. Here, the n-spin-boson model is investigated and its spin part is used as a qubit register. It was pointed out in the previous chapters that states in this qubit register decohere. As not all states are affected by the same strength of decoherence it seems to be a solution to store quantum information only within a restricted part of the available Hilbert space to ensure its stability. The assignment of a quantum code clarifies which part of the Hilbert space is used. Evaluating the dimension of a physical system with n spins reveals that it is possible to store a qubit register consisting of $k \leq n$ logical qubits. In general, there are many possibilities to encode k logical qubits, but the only relevant property of the encoding is the linear subspace $\mathcal{C} \subset \mathcal{H}_n$, which is used for the embedding. This implies that formally a code is a subspace of the spin system's Hilbert space. Technically it might be an advantage to work in a basis of the code $\mathcal{C}$ to derive some formulae. Then, the basis states of such a basis are called codewords. Obviously, it is sufficient to declare a set of codewords to describe a specific quantum code. In the following some special codes, called symmetric subspaces, are introduced and analysed. These symmetric subspaces respect a certain symmetry of the interaction Hamiltonian which is present if all spins are are located at one point. In this case those symmetric codes are decoherence-free, as it is pointed out in the work of Palma et al. [PSE97] or Zanardi and Rasetti [ZR97]. In this work these symmetric codes are analysed in a dissipationless n-spin-boson model with finite inter-spin distance [BK08]. Due to the finite inter-spin distance the former symmetry is absent and the investigated codes cease to be decoherence-free. To analyse these codes nevertheless an effective noise is derived which is again given by decoherence coefficients. In comparison to the previously examined plain qubits it turns out that the structure of the decoherence coefficient remains the same but new effective decoherence functions replace the former ones. These effective decoherence functions are calculated in the scope of this chapter.

Having a code, its robustness against decoherence has to be evaluated. First, it is helpful to chose a reference code, such that constructed codes can be compared to it. A natural way of assigning a reference code is to use the full Hilbert space $\mathcal{H}_n$ itself as quantum memory. This code is implemented by identifying every physical qubit with a logical one, corresponding to the common notation of $|0\rangle = |\uparrow\rangle$ and $|1\rangle = |\downarrow\rangle$. Second, it has to be decided which measure is taken to determine the preservation of entanglement in a given quantum code. Possible candidates are the average code fidelity or the entanglement fidelity, as it is pointed out in Chapter 4. On the other hand a first rough estimate for the robustness can be performed on the basis of the present

decoherence functions. The effective decoherence functions of the symmetric subspaces are compared to those of a plain qubit register. Thereby, it turns out that a single logical qubit within the symmetric subspaces shows much less decoherence than a plain one.

3.1 Introduction to symmetric subspaces

First the dissipationless spin-boson model with vanishing lattice constant a is examined. In this case the locations of all spins of the quantum register fall onto a single point $\mathbf{r}_0$. This implies a highly symmetric spin-boson interaction

$$\hat{H}_I = \sum_m Z_m B(\mathbf{r}_0)\,. \tag{3.1}$$

Hence, this Hamiltonian annihilates all states with vanishing total spin z component. As a consequence, any code $\mathcal{C}$ that is spanned by such states is not affected by the bosonic bath at all. It represents a decoherence-free subspace [PSE97, ZR97, LCW98, BK08]. At a finite lattice constant a the former symmetry is absent and consequently $\mathcal{C}$ ceases to be decoherence-free. However, by reasons of continuity the decoherence of states in $\mathcal{C}$ is much lower than for arbitrary states as long as the lattice constant a is not to large. In this case the code $\mathcal{C}$ is called decoherence-reduced code.

Of course, the decoherence reduction at a finite lattice constant a strongly varies for different choices of the code $\mathcal{C}$. In this work codes are investigated that result from an encoding of (logical) qubits in local groups of physical qubits. This is supposed to be done in a regular manner, such that the resulting structure forms a regular encoded quantum register, as illustrated in Fig. 3.1. Within the scope of this work the resulting codes are called symmetric subspaces. A new code $\mathcal{C}_Z \equiv \mathcal{C}_Z^1$ is constructed using a

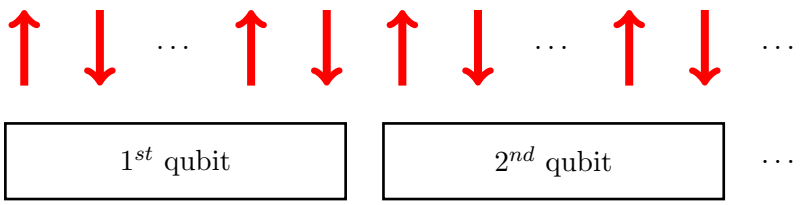

Figure 3.1: Sketch of the assignment of qubits.

subspace of the plain qubit code $\mathcal{H}_n$ by the following instruction. In a first step new logical qubits are formed using neighbouring pairs of qubits along the spin array. In this way two qubits carry the information of a single logical one, such that in comparison to the plain qubit code $\mathcal{H}_n$ the number of logical qubits is halved. According to this choice of encoding the code space factorises into sectors, one for each logical qubit. An additional restriction for each of these new logical qubits is that it has to be invariant under the symmetric interaction Hamiltonian in Eq. (3.1). Accordingly, the logical zero

$|0\rangle_Z$ state as well as the logical one state $|1\rangle_Z$ have to be annihilated by this Hamiltonian, $\sum_m Z_m |0\rangle_Z = 0 = \sum_m Z_m |1\rangle_Z$. Finally, the sector of each logical qubit is given by $\mathrm{Span}\{|01\rangle, |10\rangle\}$. The complete code $\mathcal{C}_Z$ is the direct product over this sectors. This method is illustrated in Fig. 3.2.

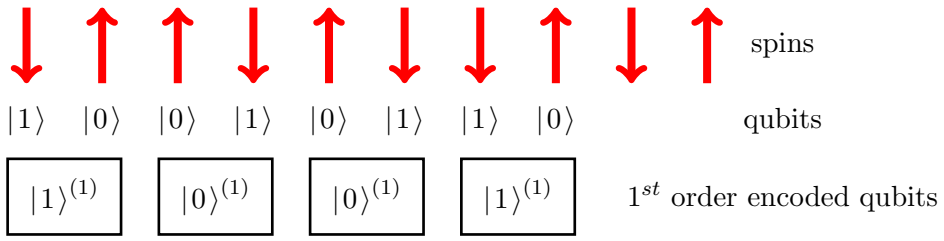

Figure 3.2: Spin array representing qubits taken out of the code $\mathcal{H}_n$ and encoded logical qubits out of the code $\mathcal{C}_Z^1$.

The construction of the code $\mathcal{C}_Z$ gives insight into a mechanism to build new codes iteratively. This iteration process is outlined in the following. Assuming that the codes $\mathcal{C}_Z^1, \ldots, \mathcal{C}_Z^{\chi-1}$ are already constructed. Note that an anchor is already given by the code $\mathcal{C}_Z^1$. The next order χ of codes $\mathcal{C}_Z^\chi$ is constructed by the declaration of its logical qubits. To construct them pairs of neighboring logical qubits out of $\mathcal{C}_Z^{\chi-1}$ are formally connected to create the next iteration, illustrated for a single logical qubit by

$$|0\rangle^{(\chi)} = |0\rangle^{(\chi-1)} \otimes |1\rangle^{(\chi-1)} \quad \text{and} \quad |1\rangle^{(\chi)} = |1\rangle^{(\chi-1)} \otimes |0\rangle^{(\chi-1)} . \tag{3.2}$$

These two states span the subspace of a single logical qubit. The complete code space is again formed by the direct product over these single qubit subspaces. In this manner the complete code $\mathcal{C}_Z^\chi$ is determined. In comparison to the former code $\mathcal{C}_Z^{\chi-1}$ the number of logical qubits is halved again. Starting with n spins this procedure finally leads to $n/2^\chi$ logical qubits.

Now a dissipative coupling between spin register and environment is investigated. For this purpose, the dissipative interaction Hamiltonian $\hat{H}_X$ (cf. Eq. (1.8)) is considered. Due to symmetry, there also exist decoherence-free subspaces for this Hamiltonian in the case where all spins are located at one point. A related strategy to the one above is followed. The logical states

$$|0\rangle = |+\rangle \equiv (|\uparrow\rangle + |\downarrow\rangle)/\sqrt{2} \quad \text{and} \quad |1\rangle = |-\rangle \equiv (|\uparrow\rangle - |\downarrow\rangle)/\sqrt{2} \tag{3.3}$$

are defined in a way, such that $\sum_m X_m |0\rangle |1\rangle = 0 = \sum_m X_m |1\rangle |0\rangle$. Accordingly, the symmetric subspace of a single qubit is given by $|0\rangle_X = |0\rangle |1\rangle$ and $|1\rangle_X = |1\rangle |0\rangle$. This is formally identical to the case of Z coupling with the replacement $Z \to X$. Hence, new codes $\mathcal{C}_X^\chi$ are created similarly to the iterative codes in the previous setting. Pairings of these plain qubits have to be performed to build new logical qubits. As

above, these logical qubits have to be invariant under the operator $\hat{H}_X$ with inter-spin distance formally set to zero.

Following the same strategy a code for a model with interaction via X and Z can be constructed. The starting conditions for each codeword $|\psi\rangle$ within this code are given by $\sum_m X_m |\psi\rangle = 0$ and $\sum_m Z_m |\psi\rangle = 0$. To build a logical qubit there need to be two linearly independent states to form the logical zero and one states. In a system with four physical qubits the states

$$|0\rangle_{XZ} = \frac{1}{2}(|1010\rangle - |1001\rangle - |0110\rangle + |0101\rangle) \tag{3.4}$$

and

$$|1\rangle_{XZ} = \frac{1}{\sqrt{3}}(|1100\rangle + |0011\rangle) - \frac{1}{2\sqrt{3}}(|1010\rangle + |0101\rangle) - \frac{1}{2\sqrt{3}}(|1001\rangle + |0110\rangle) \tag{3.5}$$

fulfil the requirements. The corresponding code is $\mathcal{C}_{XZ} = \mathrm{Span}\{|0\rangle_{XZ}, |1\rangle_{XZ}\}$. For spins that are located at one point this code is also free of decoherence.

3.2 Symmetric subspaces in the spin-boson model

In this section qubit registers formed by the previously introduced symmetric subspaces $\mathcal{C}_Z^\chi$ are analysed. Therefore, the time evolution of these effective qubit registers has to be determined. In Chapter 2 the complete time evolution (up to unitary transformations) of qubit registers in the dissipationless spin-boson model was derived. The time evolution has a representation that uses decoherence coefficients which were introduced in Eq. (2.12). Of course, this result also includes the present codes but turns out to be quite unhandy. For symmetric subspaces given by the codes $\mathcal{C}_Z^\chi$ the expression of the decoherence coefficients can be further simplified. Here, the case of an Ohmic spectral density (with spectral parameter $s = 1$) is exemplarily investigated. The case of a super-Ohmic spectral density is dealt with in a later chapter. Also the codes $\mathcal{C}_X$ and $\mathcal{C}_{XZ}$ are not discussed as no time evolution for a dissipative spin-boson model was derived so far. Note that it is impossible to express the time evolution of a dissipative model by decoherence coefficients. Consequently, the method presented in the following does not hold for such a setting.

Now a specific code $\mathcal{C}_Z^\chi$ with a fixed χ is analysed for a dissipationless model. For further progress an explicit form of the investigated code has to be selected. To proceed, a basis that spans the code is chosen. As already mentioned, in Sec. 3.1 a code (in this case $\mathcal{C}_Z^\chi$) can be described by a set of computational basis states $\nu, \mu \in \mathcal{C}_Z^\chi$. Taking a state ν, the entry ν_m denotes the m^{th} logical qubit. With the help of this notation new effective decoherence coefficients $\mathrm{D}_{\nu\mu}(t)$ are defined. These effective decoherence coefficient determine the time evolution of the qubit register in complete analogy to the previous decoherence coefficients. Accordingly, each effective decoherence coefficient describes the decoherence of an element of the qubit registers density operator by $\rho_{\nu\mu}(t) = \rho_{\nu\mu}(0)e^{-\mathrm{D}_{\nu\mu}(t)}$. A short calculation shows that these effective coefficients only

depend on the new logical qubits, such that they are given by

$$\mathrm{D}_{\nu\mu}(t) = \sum_{m,l=1}^{n} (\mu_m - \nu_m)(\mu_l - \nu_l)\, \mathrm{K}^{(\chi)}(|m-l|, a, t) \ . \tag{3.6}$$

Here, effective decoherence functions $\mathrm{K}^{(\chi)}(m, a, t)$ occur. These functions are given as a combination of decoherence functions of the previous code $\mathcal{C}_Z^{\chi-1}$. The new iteration of effective decoherence functions is given by

$$\mathrm{K}^{(\chi)}(m, a, t) = 2\,\mathrm{K}^{(\chi-1)}(2m, a, t) - \mathrm{K}^{(\chi-1)}(|2m-1|, a, t) - \mathrm{K}^{(\chi-1)}(|2m+1|, a, t) \ . \tag{3.7}$$

The initial condition for these functions, according to the first code, is given for $\chi = 0$ with $\mathrm{K}^{(0)}(m, a, t) = \mathrm{K}_1(ma, t)$. Initial decoherence functions $\mathrm{K}_1(ma, t)$ can be looked up in Sec. 2.2.1.

Now the code $\mathcal{C}_Z^{(1)}$ is investigated more closely. In this code $\mathrm{K}^{(1)}(0, a, t)$ describes the decoherence of a single encoded qubit, according to Eq. (3.7) it is given by

$$\mathrm{K}^{(1)}(0, a, t) = 2\,(\mathrm{K}_1(0, t) - \mathrm{K}_1(a, t)) \ . \tag{3.8}$$

This function is consecutively studied in different temperature regimes. In the high-

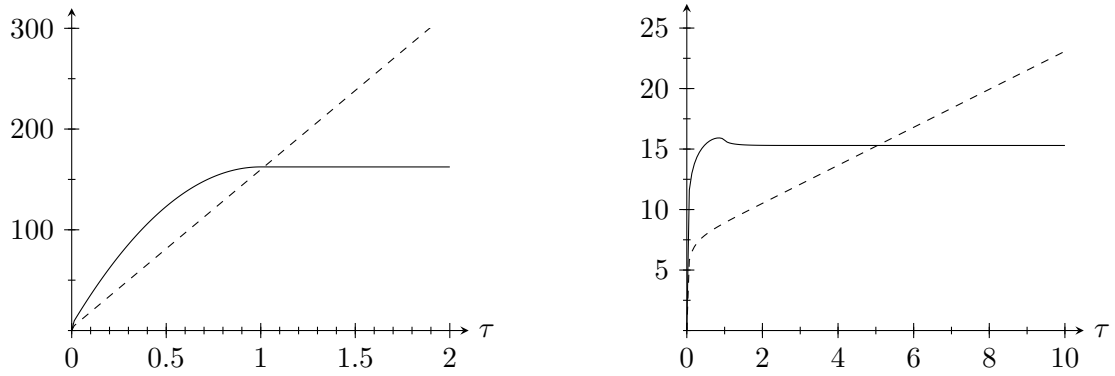

(a) (b)

Figure 3.3: Decoherence functions $\mathrm{K}_1(0, t)$ (dashed line) and $\mathrm{K}^{(1)}(0, a, t)$ (solid line) as function of dimensionless time $\tau = t/a$ at high (a) and low (b) temperatures with cut-off $\Omega = 10^3/a$, and $T = 10/a$ in (a) and $T = 0.1/a$ in (b).

temperature regime $t, a \gg 1/T$ it turns out that the effective decoherence function is

$$\mathrm{K}^{(1)}(0, a, t) = 2\alpha \ln \frac{\Omega}{2\pi T} + \begin{cases} \alpha\pi T a & , t > a \\ \alpha\pi T \left(2t - t^2/a\right) & , t \le a \end{cases} \ . \tag{3.9}$$

This function increases twice as fast in time as $\mathrm{K}_1(0, t)$, but quickly saturates to a

constant value at time $t \approx a$ (cf. Fig. 3.3a). Qualitatively, this remains to be also true at lower temperatures. For $a \ll 1/T \ll t$ it turns out that

$$\mathrm{K}^{(1)}(0,a,t) = \alpha \left(\ln \frac{\Omega a}{e} + \mathcal{O}\left((aT)^3\right) \right) , \tag{3.10}$$

which is reached again at $T \approx a$ (cf. Fig. 3.3b). In this way it is shown that for any finite distance a the effective decoherence function of a single encoded qubit approaches a finite asymptotic value at times $t \geq a$. In a next step the effective decoherence functions for finite distances, given by $\mathrm{K}^{(\chi)}(m,a,t)$ with $m > 0$, are analysed. With the approximation in equation (2.30) it is shown that these coefficients vanish up to an exponentially small contribution. In this way Eq. (3.6) simplifies to

$$\mathrm{D}_{\nu\mu}(t) = 2^{\chi-1}\, \mathrm{K}^{(1)}(0,a,t) \sum_{m=1}^{n} (\mu_m - \nu_m)^2 . \tag{3.11}$$

These results gives full insight into effective decoherence coefficients for the symmetric code $\mathcal{C}_Z^\chi$. Accordingly, the complete time evolution for these codes is determined in this way. The structure of effective decoherence coefficients remains the same for two- or three-dimensional spin arrays, but the distances have to be modified according to the positions of the logical qubits.

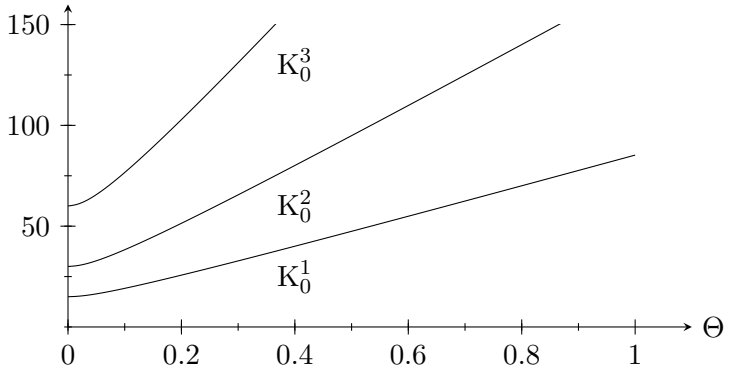

Figure 3.4: Asymptotic value of the decoherence functions $\mathrm{K}_0^\chi \equiv \mathrm{K}^{(\chi)}(0,a,\infty)$ as functions of dimensionless temperature $\Theta = Ta$ for $\chi = 1,2,3$ and cut-off $\Omega = 5 \cdot 10^3/a$.

Finally, the question arises if things improve if higher orders of encoded qubits are considered, using the codes C_Z^χ. In the high temperature regime investigating the long

time limit it is obtained that the asymptotic decoherence functions are given by

$$\mathrm{K}^{(\chi)}(0, a, \infty) = 2^{\chi-1}\,\mathrm{K}^{(1)}(0, a, \infty)\,, \tag{3.12}$$

which obviously is strongly increasing with χ. Qualitatively similar behaviour is found also at low temperatures. For a numerical analysis the non-approximated decoherence functions $\mathrm{K}^{(\chi)}(0, a, \infty)$ are chosen. The result of this analysis is plotted in Fig. 3.4. Concluding, it turns out that orders higher than one of the encoding scheme do not improve the stability of a logical qubit, but the first order of codes causes an advancement in comparison to plain qubits.

Conclusion

In this chapter the concept of quantum codes was presented. A quantum code is a subspace of the qubit system's Hilbert space. It was recapitulated that for qubits that are located at one point decoherence-free subspaces exist. These subspaces have a certain symmetry that made them invariant under the action of the interaction Hamiltonian. At a finite lattice constant the former symmetry was absent and consequently such a code ceased to be decoherence-free. Therefore, the case of finite inter-qubit distance for these subspaces was investigated. The code $\mathcal{C}_Z$ corresponding to a model without dissipation was analysed. To construct a code which was invariant under Pauli matrix Z interactions each logical qubit was encoded into two spins. Higher orders of encoding used more spins to encode a single qubit. It turned out that for small distances the code $\mathcal{C}_Z$ still led to a reduction of decoherence. Remarkable was that the effective decoherence functions for this code saturated to a finite value. This saturation definitively was a feature of a dissipationless model as no thermalisation was involved. Investigating higher orders of this code delivered no advancement in comparison to the first order.

4 A method to evaluate quantum codes

Topic of this chapter are codes which are subspaces of a given Hilbert space $\mathcal{H}_n$. A measure for the evaluation of such codes is developed. As starting point, good knowledge about the time evolution of states within the investigated code is needed. For this purpose these states are assumed to be exposed to a noise given by the operator $\mathcal{N}$. Candidates for this noise were calculated in previous chapters. For example, the noises corresponding to plain qubit registers or symmetric subspaces were derived. In each case an initially prepared state $\psi \equiv |\psi\rangle\langle\psi|$ evolves according to the given noise to the state $\mathcal{N}(|\psi\rangle\langle\psi|)$. To evaluate the agreement of $|\psi\rangle\langle\psi|$ with $\mathcal{N}(|\psi\rangle\langle\psi|)$ a measure is needed. In the case of quantum states this measure is given by the fidelity. The origin of the fidelity is found in the works of Uhlmann [Uhl76] and Jozsa [Joz94]. An introduction is given in the book of Nielsen and Chuang [NC00]. For two pure states the fidelity is just the absolute square of the overlap between these two states. This concept is generalised to work for arbitrary densities. In this chapter one of the densities remains a pure state. Therefore, the channel fidelity of ψ with respect to $\mathcal{N}$ is given by

$$F(\psi, \mathcal{N}) = \langle\psi|\,\mathcal{N}(|\psi\rangle\langle\psi|)\,|\psi\rangle\ . \tag{4.1}$$

This quantity captures how well the pure state ψ is preserved by the noise $\mathcal{N}$. In this work more than the time evolution of single states has to be evaluated, as the point of interest is the robustness of complete codes. Here, codes $\mathcal{C} \subset \mathcal{H}_n$ of dimension $k = \dim \mathcal{C}$ are investigated. For simplicity only codes that are given by a basis of computational states and noises belonging to dissipationless models are evaluated. An explicit measure for these codes is needed. Hence, the channel fidelity is extended from single states to a complete code. There are two kinds of this extension. The first one is given by the average fidelity, which is discussed in Sec. 4.1. This average fidelity is constructed by averaging the channel fidelity of every state within the desired code. The second one is the entanglement fidelity, also presented in Sec. 4.1. This quantity evaluates the fidelity of a representative pure state out of an enlarged system to determine the robustness of a given code. This pure state is a purification of the normalised projector onto the code $\mathcal{C}$. It is known e.g. by a work of Horodecki et al. [HHH99] that the entanglement fidelity in this case delivers a lower bound to the average fidelity of the code. For the large number of qubits considered in this work both fidelities essentially lead to the same results. In Sec. 4.2 it is outlined that for a dissipationless model a spin echo experiment provides the same information as the calculation of the entanglement fidelity. The mechanism of such a spin echo experiment leading to this insight is explained as well. At the end of this chapter the case of weak coupling is investigated. Approximated results that are easy to handle are derived for the entanglement fidelity.

4.1 Code fidelities

Codes $\mathcal{C}$ with n logical qubits and dimension $\dim \mathcal{C} = 2^n = k$ are considered.

The average fidelity. The performance of a chosen code $\mathcal{C}$ is determined by averaging the channel fidelity of all possible initial pure states $|\psi\rangle \in \mathcal{C}$. According to this idea the average fidelity is

$$\overline{F}(\mathcal{C},\mathcal{N}) = \frac{1}{N} \int_{\mathcal{C}} \mathrm{d}\psi \, F(\psi,\mathcal{N}), \quad N = \int_{\mathcal{C}} \mathrm{d}\psi \, 1 \,, \tag{4.2}$$

where the integral contains all pure states with respect to the unitary invariant measure. Each pure state $|\psi\rangle$ is expressed in the computational basis of the code $\mathcal{C}$, given by $\{|\nu\rangle\}_{\nu=1,\ldots,k}$, as $|\psi\rangle = \sum_{\nu=1}^{k} U_{1\nu} |\nu\rangle$ with elements $U_{1\nu}$ of a unitary $k \times k$-matrix $\mathbf{U}$. Averaging the fidelity over all possible states $|\psi\rangle$ leads to

$$\overline{F}(\mathcal{C},\mathcal{N}) = \sum_{\nu,\mu=1}^{k} \langle \nu | \mathcal{N}(|\nu\rangle\langle\mu|) |\mu\rangle \int \mathrm{d}\mu(U_{1\nu}, U_{1\mu}) \, |U_{1\nu}|^2 |U_{1\mu}|^2 \,. \tag{4.3}$$

A method to solve the occurring integral is found in the work of Pereyra and Mello [PM82]. According to this work, each column of a unitary matrix is identified with a unit vector out of a complex vectorspace. Introducing high-dimensional spherical coordinates in real space, the integral over one or more column elements is solved with the help of delta functions that respect the unit length of the given vector. This leads to

$$\int \mathrm{d}\mu(U_{1\nu}, U_{1\mu}) \, |U_{1\nu}|^2 |U_{1\mu}|^2 = \frac{1 + \delta_{\mu\nu}}{k^2} + \mathcal{O}(k^{-3}) \,. \tag{4.4}$$

This result is inserted into Eq. (4.3), such that the average fidelity is approximated by

$$\overline{F}(\mathcal{C},\mathcal{N}) = \frac{1}{k^2} \sum_{\nu,\mu=1}^{k} \langle \nu | \mathcal{N}(|\nu\rangle\langle\mu|) |\mu\rangle \, (1 + \delta_{\nu\mu}) \,. \tag{4.5}$$

For large code dimension k the term k^{-1} resulting from the δ-symbols is neglected, such that finally the sum representation of the average fidelity is

$$\overline{F}(\mathcal{C},\mathcal{N}) = \frac{1}{k^2} \sum_{\nu,\mu=1}^{k} \langle \nu | \mathcal{N}(|\nu\rangle\langle\mu|) |\mu\rangle \,. \tag{4.6}$$

The entanglement fidelity. The given code $\mathcal{C}$ is embedded into a higher-dimensional Hilbert space together with an ancillary system R, which also has the dimension k. In this case the entanglement fidelity, defined by Schumacher [Sch96], is given by

$$F_e(\mathcal{C},\mathcal{N}) = \langle \psi_{R\mathcal{C}} | \, \mathbb{1}_R \otimes \mathcal{N}(\psi_{R\mathcal{C}}) \, | \psi_{R\mathcal{C}} \rangle \,, \tag{4.7}$$

where $\psi_{R\mathcal{C}}$ is a pure state defined via $\mathrm{tr}_R\,\psi_{R\mathcal{C}} = \pi_{\mathcal{C}}$ with the normalised projection $\pi_{\mathcal{C}}$ onto $\mathcal{C}$. One possible purification fulfilling this requirement is the state

$$|\psi_{R\mathcal{C}}\rangle = \sum_{\nu=1}^{k} \frac{1}{\sqrt{k}} |\nu\rangle_R |\nu\rangle , \quad \psi_{R\mathcal{C}} = \sum_{\nu,\mu=1}^{k} \frac{1}{k} |\nu\rangle_R |\nu\rangle\langle\mu|_R \langle\mu| . \tag{4.8}$$

The noise is a linear operator which acts trivially on the ancillary system. Accordingly it acts on this purification as

$$\mathcal{N}(\psi_{R\mathcal{C}}) = \frac{1}{k} \sum_{\nu,\mu=1}^{k} |\nu\rangle_R \mathcal{N}(|\nu\rangle\langle\mu|)_R \langle\mu| . \tag{4.9}$$

This result together with the defined state $|\psi_{R\mathcal{C}}\rangle$ is inserted into the definition of the entanglement fidelity. In this way the entanglement fidelity is obtained to be

$$F_e(\mathcal{C},\mathcal{N}) = \frac{1}{k^2} \sum_{\nu,\mu=1}^{k} \langle\nu|\mathcal{N}(|\nu\rangle\langle\mu|)|\mu\rangle . \tag{4.10}$$

Note that this result is the same which was derived for the average fidelity in Eq. (4.6). Actually, there exists a strict relation between the average fidelity and the entanglement fidelity [HHH99, Nie02],

$$\overline{F}(\mathcal{C},\mathcal{N}) = \frac{kF_e(\mathcal{C},\mathcal{N}) + 1}{k+1} . \tag{4.11}$$

Hence, the entanglement fidelity of the normalised projector $\pi_{\mathcal{C}}$ gives a lower bound of the corresponding average fidelity. Obviously the entanglement fidelity converges to the average fidelity if the code size is increased. Therefore, in the scope of this work the entanglement fidelity is used to evaluate the robustness of codes.

An integral representation of the fidelity. The dissipationless n-spin-boson model is investigated for further progress. Computational states $|\nu\rangle, \nu \in \mathbb{Z}_2^n$ in this model form the code $\mathcal{C}$. Accordingly, the dimension of the selected code in this case is $k = 2^n$. In Chapter 2 the time evolution of the corresponding reduced density operator of the qubit register was described by decoherence coefficients $\mathrm{D}_{\nu\mu}(t)$. It was shown that these coefficients are defined by

$$\langle\nu|\mathcal{N}(|\nu\rangle\langle\mu|)|\mu\rangle = e^{-\mathrm{D}_{\nu\mu}(t)} . \tag{4.12}$$

An explicit calculation for the spin-boson model was presented. Finally, the decoherence coefficient turned out to be described by a combination of decoherence functions $\mathrm{K}(|\mathbf{r}|,t)$ as

$$\mathrm{D}_{\nu\mu}(t) \;=\; \sum_{m,l=1}^{n} (\mu_m - \nu_m)(\mu_l - \nu_l)\, \mathrm{K}(|\mathbf{r}_m - \mathbf{r}_l|, t) . \tag{4.13}$$

Here, the double summation runs over all lattice sites, ν_m denotes the m^{th} logical qubit of the state ν and $\mathbf{r}_m$ the location corresponding to the lattice site. According to Eq. (4.10) and Eq. (4.12) the entanglement fidelity of the code $\mathcal{C}$ is given by

$$F_e(\mathcal{C},\mathcal{N}) = \frac{1}{4^n}\sum_{\nu,\mu=1}^{k} e^{-\,\mathrm{D}_{\nu\mu}(t)}\,. \tag{4.14}$$

The decoherence coefficient in Eq. (4.13) is written in form of a vector-matrix product $\mathrm{D}_{\nu\mu}(t) = \mathbf{u}^T(\nu,\mu)\mathbf{K}\mathbf{u}(\nu,\mu)$ with vector components $\mathbf{u}_m(\nu,\mu) := (\mu_m - \nu_m)$ and matrix entries $\mathbf{K}_{ml} := \mathrm{K}(|\mathbf{r}_m - \mathbf{r}_l|, t)$. By this definition $\mathbf{K}$ is a symmetric matrix, which has a Toeplitz structure as long as a one-dimensional lattice is concerned. If the lattice is not one-dimensional the Toeplitz structure does not occur in general, but the matrix remains symmetric. The motivation at this point is to get rid of the summation over the computational states to derive a simpler expression. Introducing a new field $\mathbf{x}$ via Gaussian integrals modifies the entanglement fidelity to

$$F_e(\mathcal{C},\mathcal{N}) = \sum_{\nu,\mu\in\mathbb{Z}_2^n} \frac{1}{4^n\sqrt{\pi^n \det\mathbf{K}}} \int \mathrm{d}\mathbf{x}\, e^{-\mathbf{x}^T\mathbf{K}^{-1}\mathbf{x}+2i\mathbf{u}^T(\nu,\mu)\mathbf{x}}\,. \tag{4.15}$$

Here, the dependency on the states ν and μ is given via the variable $\mathbf{u}$ in the exponent. To proceed, the summation $\sum_{\nu,\mu} e^{2i\mathbf{u}^T\mathbf{x}}$ is investigated. This summation is by rearranging transformed to

$$\sum_{\nu,\mu\in\mathbb{Z}_2^n} e^{2i\mathbf{u}^T(\nu,\mu)\mathbf{x}} = \prod_{l=1}^{n}\sum_{\mu_l,\nu_l=0}^{1} e^{2i(\mu_l-\nu_l)x_l} = 4^n\prod_{l=1}^{n}\cos^2 x_l\,. \tag{4.16}$$

Inserting this transformation gives the integral representation of the entanglement fidelity by

$$F_e(\mathcal{C},\mathcal{N}) = \frac{1}{\sqrt{\pi^n \det\mathbf{K}}} \int \mathrm{d}\mathbf{x}\, e^{-\mathbf{x}^T\mathbf{K}^{-1}\mathbf{x}}\prod_{l=1}^{n}\cos^2 x_l\,. \tag{4.17}$$

This integral representation is used in a later section to derive some explicit expressions in the case of weak couplings.

4.2 Measurement of the fidelity

This section elaborates on the measurement of the fidelity. It is shown how the methods of Ramsey spectroscopy [Ram49] and spin echo experiments [Hah50] are connected to the entanglement fidelity.

The Bloch sphere representation. A helpful visualisation to describe a state of a two level system is given by the Bloch sphere representation. Up to a phase factor, any

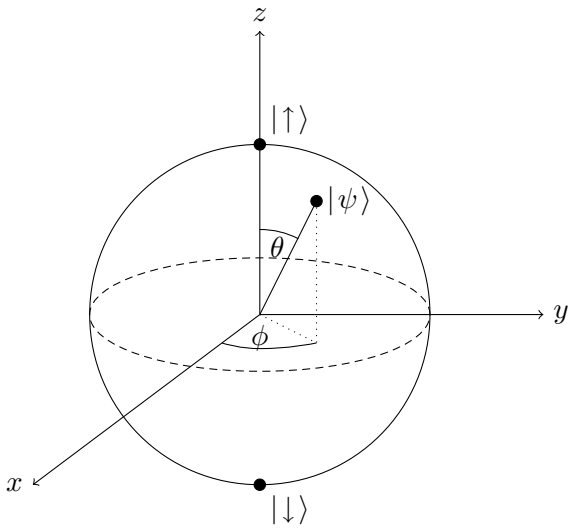

Figure 4.1: The Bloch sphere representation of a state $|\psi\rangle$ with corresponding angles θ and ϕ.

normalised pure state of a two level system can be written as

$$|\psi\rangle = \cos\frac{\theta}{2}|\uparrow\rangle + e^{i\phi}\sin\frac{\theta}{2}|\downarrow\rangle \tag{4.18}$$

with angles $0 \leq \theta < \pi$ and $0 \leq \phi < 2\pi$ as it is illustrated in Fig. 4.1. The Bloch sphere itself is described by Cartesian coordinates $x = \sin\theta\cos\phi$, $y = \sin\theta\sin\phi$ and $z = \cos\theta$.

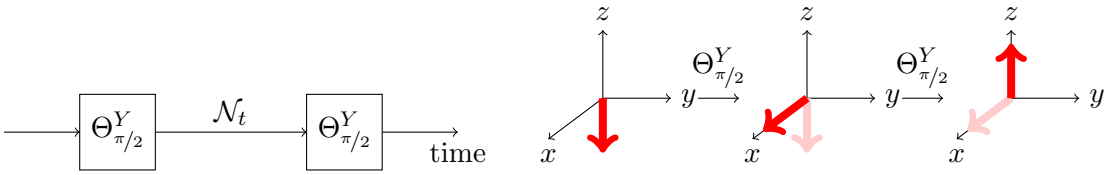

(a) (b)

Figure 4.2: (a) Impulse sequence used by Ramsey spectroscopy, having the preparation of the spin on the left side and the measurement on the right side. (b) Visualisation of a single spin during Ramsey spectroscopy, having $\mathcal{N}_t = \mathbb{1}$.

Ramsey spectroscopy in a sketch. This paragraph shall connect the presented theoretical results for the time evolution of an n-qubit register with an often used technique

in experiments. Here, only a dissipationless model is considered. Nevertheless, the following insight is also correct for a dissipative model as long as timescales far below the relaxation time of the model are concerned. First, a single spin with states $|\uparrow\rangle$ and $|\downarrow\rangle$ is considered. Beside a well working measurement device a well controlled $\Theta^Y_{\pi/2}$-pulse is needed. This pulse is given by

$$\Theta^Y_{\pi/2} = \exp\left(i\frac{\pi}{4}Y\right) = \frac{1}{\sqrt{2}}(\mathbb{1} + iY)\,, \tag{4.19}$$

and rotates an initially created state $|\downarrow\rangle$ around the Y-axis of the Bloch sphere by an amount of $\pi/2$, such that it evolves to

$$\Theta^Y_{\pi/2}\,|\downarrow\rangle = \frac{1}{\sqrt{2}}(|\downarrow\rangle + |\uparrow\rangle)\,. \tag{4.20}$$

A quantum map $I^Y_{\pi/2}$ that corresponds to this pulse and acts on density operators ρ is defined by $I^Y_{\pi/2}(\rho) = \Theta^Y_{\pi/2}\rho\Theta^{Y\dagger}_{\pi/2}$. The working mechanism of Ramsey's spectroscopy is illustrated in Fig. 4.2(b). The first picture shows the initial state on its corresponding Bloch sphere. Then, the mentioned $\Theta^Y_{\pi/2}$-pulse is applied for the first time and the resulting state on the Bloch sphere is shown. This state is the visualisation of the right-hand side of Eq. (4.20). Applying a second $\Theta^Y_{\pi/2}$-pulse directly after the first one, according to $(\Theta^Y_{\pi/2})^2 = iY$ leads to

$$(\Theta^Y_{\pi/2})^2\,|\downarrow\rangle = |\uparrow\rangle \tag{4.21}$$

which is illustrated by the third picture of Fig. 4.2(b). To get non-trivial results this procedure is repeated for different time steps t between the two pulses as illustrated in Fig. 4.2(a). During that time the system follows its non-trivial dynamics given the noise $\mathcal{N}_t$. The explicit form of the noise $\mathcal{N}_t$ can be read off in Eq. (2.8) and Eq. (2.9). Note that the occurring phase $\phi \equiv \phi_\nu - \phi_\mu$, where ν and μ form the index of the corresponding density operator, must not be neglected if a real experiment is concerned. Therefore, they are part of the equation which is derived next. Finally, to perform a real experiment the projection on $|\uparrow\rangle$ is measured for each repetition. A corresponding measurement of a density operator ρ onto the state $|\psi\rangle$ is given as $M_{|\psi\rangle} = \langle\psi|\,\rho\,|\psi\rangle$. Accordingly, the complete measurement including all pulses and the time evolution as a function of time t is

$$M_{|\uparrow\rangle} \circ I^Y_{\pi/2} \circ \mathcal{N}_t \circ I^Y_{\pi/2}(|\downarrow\rangle\langle\downarrow|) = \frac{1}{4}\sum_{\nu,\mu\in\{|\downarrow\rangle,|\uparrow\rangle\}} e^{-\mathrm{D}_{\nu\mu}(t)+i(\phi_\nu-\phi_\mu)} \tag{4.22}$$

with state and time depending phases ϕ_μ and ϕ_ν. Having in mind that the populations of a dissipationless model remain constant and the decoherence coefficients $\mathrm{D}_{\nu\mu}(t)$ are symmetric concerning ν and μ this equation simplifies to

$$M_{|\uparrow\rangle} \circ I^Y_{\pi/2} \circ \mathcal{N}_t \circ I^Y_{\pi/2}(|\downarrow\rangle\langle\downarrow|) = \frac{1}{2} + \frac{1}{2}\sum_{\nu<\mu} e^{-\mathrm{D}_{\nu\mu}(t)}\cos(\phi_\nu - \phi_\mu)\,. \tag{4.23}$$

Now this procedure is modulated to an array of n spins with initial state $|\psi_i\rangle = \otimes_i |\downarrow\rangle_i$ and final state $|\psi_f\rangle = \otimes_i |\uparrow\rangle_i$. The previously explained impulse sequence is applied to each of the spins, such that the resulting measurement as a function of the time t is

$$M_{|\psi_f\rangle} \circ I^Y_{\pi/2} \circ \mathcal{N}_t \circ I^Y_{\pi/2}(|\psi_i\rangle\langle\psi_i|) = \frac{1}{2^n} + \frac{1}{2^{2n-1}} \sum_{\nu<\mu} e^{-\mathrm{D}_{\nu\mu}(t)} \cos(\phi_\nu - \phi_\mu)\,. \tag{4.24}$$

Knowing that Rabi oscillations are caused by a coupling of a two level system to an external field the occurring phases are Rabi-like oscillations induced by the environment.

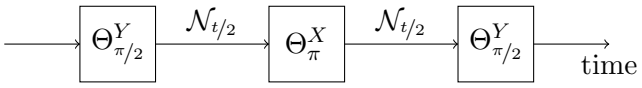

Figure 4.3: Impulse sequence used for spin echo experiments.

Connection between a spin echo experiment and the entanglement fidelity. A spin echo experiment works in the framework of the above described Ramsey spectroscopy. In addition a Θ^X_π-pulse is applied in the middle of the desired time t as illustrated in Fig. 4.3 on each of the spins. The Θ^X_π-pulse is given by

$$\Theta^X_\pi = \exp\left(i\frac{\pi}{2}X\right) = iX \quad \text{with} \quad I^X_\pi(\rho) = \Theta^X_\pi \rho \Theta^{X\dagger}_\pi\,. \tag{4.25}$$

This method is chosen to get rid of the phases which cancel due to the additional pulse. Any element of the spin system's reduced density operator $\rho_{\nu\mu}$ acquires a phase given by $\phi_\nu - \phi_\mu$ during the time $t/2$. The Θ^X_π-pulse transforms this previous element into one of a $\rho_{\mu\nu}$-type, such that the phase acquired during the remaining time is $\phi_\mu - \phi_\nu$. In this way no phase occurs in total and the measured value as function of time t is

$$M_{|\psi_f\rangle} \circ I^Y_{\pi/2} \circ \mathcal{N}_{t/2} \circ I^X_\pi \circ \mathcal{N}_{t/2} \circ I^Y_{\pi/2}(|\psi_i\rangle\langle\psi_i|) = \frac{1}{4^n} \sum_{\nu,\mu} e^{-\mathrm{D}_{\nu\mu}(t)}\,. \tag{4.26}$$

This result is identified with the sum representation of the entanglement fidelity in Eq. (4.14).

Concluding, it is shown that a spin echo experiment determines the entanglement fidelity of the complete available Hilbert space, as long as timescales below the relaxation time of the system are concerned.

4.3 The fidelity in the weak-coupling limit

The integral representation of the entanglement fidelity derived in Eq. (4.17) is closer investigated. For further progress the weak coupling limit is considered. Here, the

inverse eigenvalues of $\mathbf{K}$ become large and hence the integrand sharply peaks at the global maximum at $\mathbf{x} = 0$. In this case it is appropriate to expand the integrand as

$$e^{-\mathbf{x}^T\mathbf{K}^{-1}\mathbf{x}} \prod_{l=1}^{n} \cos^2 x_l = e^{-\mathbf{x}^T(\mathbf{K}^{-1}+\mathbb{1})\mathbf{x}+\mathcal{O}(|\mathbf{x}|^4)} \tag{4.27}$$

and to omit the $\mathcal{O}(|\mathbf{x}|^4)$ corrections. Inserting this result into Eq. (4.17) a common Gauss integral appears which leads to the weak coupling approximation

$$F_e^{\mathrm{wc}}(\mathcal{C},\mathcal{N}) = \det(\mathbb{1}+\mathbf{K})^{-1/2} \tag{4.28}$$

of the entanglement fidelity. It is quite complicated to exactly determine the range of validity of this approximation for a general $\mathbf{K}$. In the following, the range of validity is analysed by settings with restricted $\mathbf{K}$. For this purpose, two extreme regimes are investigated in different examples. The cases of independent qubits and symmetrically coupled qubits are examined. For these examples an Ohmic coupling is chosen, such that $\mathrm{K}(\mathbf{r},t) \mapsto \mathrm{K}_1(\mathbf{r},t)$, as it is pointed out in Sec. 2.1.

Example of independent qubits. The first example is a plain quantum register whose qubits are affected by identical but independent noise. Formally, this corresponds to infinite distances between the qubits, such that $\mathrm{K}_1(\mathbf{r}_l - \mathbf{r}_m, t) = 0$ for $m \neq l$. This implies a diagonal decoherence matrix with a constant diagonal,

$$\mathbf{K} = \kappa\, \mathbb{1}_n, \tag{4.29}$$

where $\kappa \equiv \mathrm{K}_1(\mathbf{0},t)$. Because of this structured matrix $\mathbf{K}$ the integral in Eq. (4.17) factorises into n one-dimensional Gaussian integrals,

$$F_e(\mathcal{C},\mathcal{N}) = \prod_{l=1}^{n} \int \frac{\mathrm{d}x_l}{\sqrt{\pi\kappa}} e^{-x_l^2/\kappa} \cos^2 x_l = \left(\frac{1+e^{-\kappa}}{2}\right)^n . \tag{4.30}$$

As expected, the entanglement fidelity of the investigated n-qubit register is exactly the n^{th} power of the entanglement fidelity of a single qubit, which would be $F_1 = (1 + e^{-\kappa})/2$. This result could have been derived also starting with the sum representation in Eq. (4.14) and direct calculation.

Example of symmetrically coupled qubits. The second example is a qubit register where all qubits are located at the same position. This ansatz results in a uniform matrix $\mathbf{K}$ with l,m-independent entries

$$\mathbf{K}_{lm} = \kappa\,, \tag{4.31}$$

where, as above, $\kappa = \mathrm{K}_1(\mathbf{0},t)$. Up to a factor $n\kappa$ the matrix $\mathbf{K}$ describes the orthogonal projection on the diagonal $\mathbf{d} = (1,\ldots,1)/\sqrt{n}$. $\mathbf{K}$ has therefore a non-degenerate

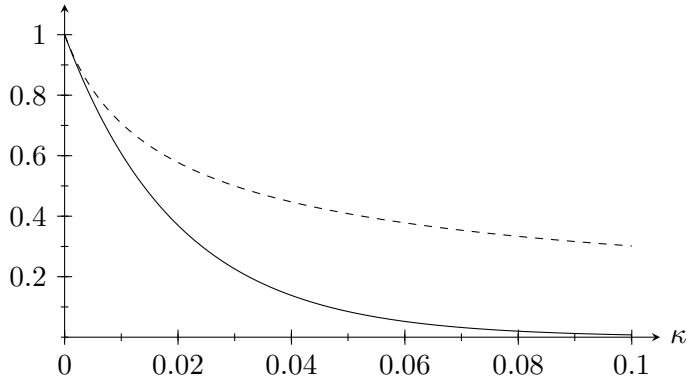

Figure 4.4: Entanglement fidelities of an 100-qubit register for independent (solid curve) and symmetrically coupled (dashed curve) qubits as a function of the decoherence parameter $\kappa = K(\mathbf{0}, t)$.

eigenvalue $n\kappa$ with an eigenvector $\mathbf{d}$, and an $(n-1)$-fold degenerated eigenvalue 0 with eigenspace $\mathbf{d}^\perp$. It follows that the integrand in Eq. (4.17) has its entire weight on the diagonal $\mathbf{d}$, as an effect of which the n-dimensional integral collapses to a one-dimensional one. In this way the entanglement fidelity results in

$$\begin{aligned} F_e(\mathcal{C},\mathcal{N}) &= \frac{1}{\sqrt{\pi n\kappa}} \int \mathrm{d}x\, e^{-x^2/n\kappa} \cos^{2n} \frac{x}{\sqrt{n}} \\ &= \frac{1}{4^n} \sum_{l=0}^{2n} \binom{2n}{l} e^{-\kappa(n-l)^2} . \end{aligned} \tag{4.32}$$

The result can be better interpreted in the limit $n \gg 1$ and $\kappa \ll 1$ (independent of n). For large n the binomial factor $4^{-n}\binom{2n}{l}$ is approximated by a Gaussian, $\exp(-(n-l)^2/n)/\sqrt{\pi n}$, and further, for small κ the sum is replaced by an integral. Then, the entanglement fidelity is given by

$$F_e(\mathcal{C},\mathcal{N}) = \frac{1}{\sqrt{1+n\kappa}}. \tag{4.33}$$

For small $n\kappa \ll 1$ almost the same entanglement fidelity is observed as in the case of independent qubits (cf. Eq. (4.30) and Fig. 4.4). A reasonable explanation for this is that in the case of $n\kappa \ll 1$ during the investigated time span with high probability only one boson has interacted with the entire n-qubit register. Concerning this regime, it is evident that any symmetry in the couplings of different qubits has no influence. However, this changes with increasing n and κ when $n\kappa \gg 1$. Here, an algebraic decay in $n\kappa$ is observed, in strong contrast to the exponential decay in $n\kappa/2$ seen before. Multi-boson processes occur with high probability and hence the symmetry in the qubit

couplings of the present model does matter. Since all qubits couple identically to the bosonic reservoir, an n-qubit state with a small total spin-z component $\sum_m Z_m$ couples much less effective to the bosonic bath than it would be the case for independent qubits. Apparently, this results in a strongly enhanced entanglement fidelity.

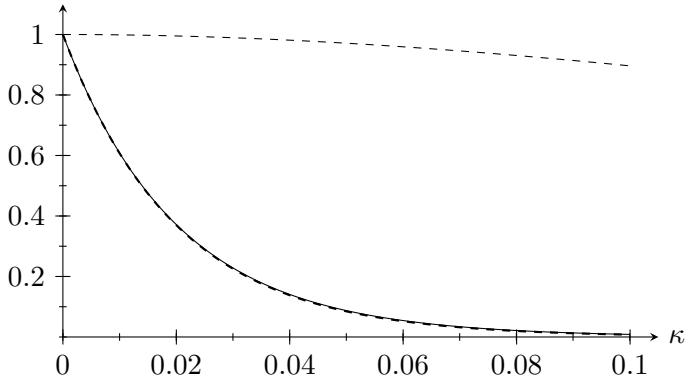

Figure 4.5: Entanglement fidelity of a 100-qubit register of independent qubits as a function of the single-qubit decoherence parameter $\kappa = K(\mathbf{0}, t)$. The exact result (thick dashed curve) and the weak coupling approximation (solid curve) agree very well in the plotted regime. The upper dashed curve shows the ratio of exact and approximate fidelity.

The validity of the weak coupling approximation. It is instructive to compare the exact entanglement fidelities for the two examples given above with the corresponding expressions in the weak coupling approximation (4.28). For the quantum register consisting of independent qubits the weak coupling expression (4.28) predicts

$$F_e^{\mathrm{wc}}(\mathcal{C}, \mathcal{N}) = (1 + \kappa)^{-n/2} \,. \tag{4.34}$$

While this is not quite the exact result (4.30), indeed a good agreement is observed for small couplings κ (cf. Fig. 4.5). To be more precise, $F_e/F_e^{\mathrm{wc}} \approx (1 - \kappa^2/8)^n$ is close to unity as long as $\kappa \ll \sqrt{8/n}$. Particularly, the weak coupling approximation holds in the regime $1/n \ll \kappa \ll \sqrt{8/n}$, where the average fidelity is already exponentially small. The weak coupling approximation works even better in the second example. The determinant of $\mathbb{1} + \mathbf{K}$ with uniform decoherence matrix $\mathbf{K}$ according to Eq. (4.31) is readily determined to be $1 + n\kappa$. This immediately results in

$$F_e^{\mathrm{wc}}(\mathcal{C}, \mathcal{N}) = \frac{1}{\sqrt{1 + n\kappa}} \,, \tag{4.35}$$

in accordance with Eq. (4.33). In both cases the weak coupling approximation is proven to be reliable at least up to coupling parameters $\kappa \sim 1/\sqrt{n}$. This strongly suggests that the approximation holds in a corresponding range of coupling parameters in cases where the distances between qubits assume finite values.

Conclusion

In this chapter a measure for the robustness of a complete quantum code against decoherence was given in form of code fidelities. First, the average fidelity was motivated as a code measure. To construct this fidelity the channel fidelity between all possible initial states of the evaluated code and their time evolved states was averaged. Then, the entanglement fidelity as lower bound for the average fidelity was introduced for practical reasons. It was shown that in the limit of large codes for a dissipationless model both quantities led to the same result. Then, a short investigation on Ramsey spectroscopy and spin echo experiments was performed. It turned out that for times, which are much smaller than the relaxation time of the given system, the measurement of a spin echo experiment delivered the entanglement fidelity. Afterwards, an integral representation of the entanglement fidelity was derived. In the case of weak coupling this result was transformed into a handy expression. The validity of this expression was motivated by two extremal examples. Accordingly, the cases of symmetrically coupled and independent qubits were investigated. These two examples covered the setting of zero and infinite inter-spin distance. Due to the validity of the derived formula in these settings it was motivated that the result also approximately worked for finite inter-spin distance.

5 Evaluation of quantum codes

In the previous chapters the entanglement fidelity turned out to be an easy to handle and well motivated measure for quantum codes. Now this measure is used to evaluate some concrete implementations of quantum codes. Formulae for the entanglement fidelity in the case of plain qubits and for the encoding in symmetric subspaces are derived in the scope of a dissipationless spin-boson model. This derivation is performed in the following way: A first result for the entanglement fidelity in a weak coupling approximation was already obtained in Eq. (4.28). Here this approximation of the entanglement fidelity is used to evaluate and compare a qubit register having either no encoding by taking the plain qubits themselves or an encoding using symmetric subspaces. The two corresponding fidelities show the expected result: there exists a critical time after which a symmetric subspace is more stable than a plain qubit register. In addition to this result it is shown how codes can be analysed in a more efficient manner. For that purpose small deviations of the entanglement fidelity from unity are discussed. This case seems to be the physically relevant one for the use of a given qubit register as quantum memory. In this case, the fidelity differs from unity only by a small quantity. Hence, this quantity is analysed in the scope of this work. It turns out that it is given by the code size times the decoherence function of a single logical qubit. The decoherence function is either the one of a single plain qubit or the rate of an effective single qubit in the case of the symmetric code.

In the second part of this chapter a generalised question is dealt with. Previous results show that symmetric subspaces outmatch plain qubits, but so far it is not ensured that they perform best. The task is to find the best code within a given setting. In the scope of this work a detailed formulation of this problem is given. Unfortunately, it is not possible to treat it in full generality. For further progress the problem has to be restricted again. Finally, the optimal encoding for a single logical qubit is investigated for the dissipationless spin-boson model. It turns out that in this case the symmetric subspace is the best available code.

5.1 Plain qubit register versus symmetric subspaces

In the last chapter a method to evaluate quantum codes was derived. Therefore, the entanglement fidelity was calculated for a model with weak coupling. Explicit expressions of the entanglement fidelity were derived for independently and symmetrically coupled qubits. These two settings correspond to an infinite and zero inter-spin distance, respectively. Consequently, the presented result of the entanglement fidelity is supposed to also hold for finite inter-spin distances. In this chapter, the entanglement fidelity is used

to evaluate a more realistic quantum register consisting of qubits arranged on a regular lattice of dimension $d = 1, 2$, and 3 with finite inter-spin distance.

5.1.1 Evaluation of the plain n-qubit register

There are $n = b^d$ qubits assumed to be located at the sites of a d-dimensional hypercubic lattice with lattice constant a and finite edge size $L = ab$. It is convenient to label the qubits by multi-indices $\mathbf{l}, \mathbf{m} \in \{1, 2, \ldots, b\}^d$. To proceed, the decoherence functions $\mathrm{K}_1(\mathbf{r}, \mathbf{t})$ are analysed. For further progress a restriction to the high temperature regime and times $t > |\mathbf{r}|$ is performed. In this regime in good approximation the decoherence function is (cf. Sec. 2)

$$\mathrm{K}_1(\mathbf{r}, \mathbf{t}) = \gamma(t - |\mathbf{r}|/2)\,, \tag{5.1}$$

where the rate $\gamma = \alpha\pi T$ is determined by the coupling strength α and the temperature T. Then, for times $t \geq \sqrt{d}L$ the time dependent decoherence matrix $\mathbf{K}$ of the register is

$$\mathbf{K}_{\mathbf{lm}} = \gamma t \left(1 - \frac{|\mathbf{r_l} - \mathbf{r_m}|}{2t}\right)\,. \tag{5.2}$$

In the limit of large times $t \gg \sqrt{d}L$ the second term yields a small $(\mathbf{l}, \mathbf{m})$-dependent correction to the leading term γt, meaning that the decoherence matrix becomes close to the uniform decoherence matrix discussed in Sec. 4.3. Neglecting the $(\mathbf{l}, \mathbf{m})$-dependent corrections, the entanglement fidelity is expected to be approximately given by

$$F_e(\mathcal{C}, \mathcal{N}) = \frac{1}{\sqrt{1 + n\gamma t}}\,. \tag{5.3}$$

This is confirmed by the data shown in Fig. 5.1. The plot of the qubit register with finite inter-spin distance seems to agree with the result of symmetrically coupled qubits up to a small amount.

5.1.2 Evaluation of symmetric subspaces

In this section the codes $\mathcal{C}_Z^\chi$ which were introduced in Sec. 3.1 are examined. The entanglement fidelity of qubit registers that are encoded in these decoherence-reduced subspaces are investigated more closely. Since effective and physical decoherence functions (cf. Eq. (3.6)) are formally identical, the representations Eq. (4.14) and Eq. (4.17) for the entanglement fidelity of a plain quantum register apply as well for the encoded register. Hence, an encoded quantum register can be analysed in the same way as before. This section is concluded with an comparison of the entanglement fidelities of plain and encoded quantum registers. To calculate the entanglement fidelity of decoherence-reduced qubits in the code $\mathcal{C}_Z^\chi$, the effective decoherence coefficients of Eq. (2.22) are inserted into Eq. (4.28). The decoherence matrix approaches very fast its saturation

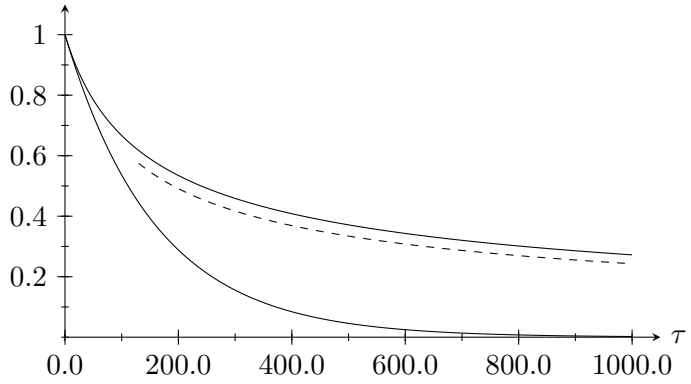

Figure 5.1: Time dependency of the entanglement fidelity for a linear quantum register (having a finite inter-spin distance) of 125 qubits (dashed curve) in comparison with the entanglement fidelity of registers consisting of 125 independently (bottom) and symmetrically (top) coupled qubits as a function of dimensionless time $\tau = t/a$. The rate is $\gamma = 10^{-4}/a$.

value $\mathbf{K} = 2^{\chi-1}\,\mathrm{K}^{(1)}(0,a,\infty)\,\mathbb{1}_n$ (cf. Eq. (3.12)). Accordingly the fidelity saturates to

$$F_e(\mathcal{C}_Z^{\chi},\mathcal{N}) = \left(\frac{1+e^{-2^{\chi-1}\gamma}}{2}\right)^n \quad \text{with} \quad \gamma \equiv \mathrm{K}^{(1)}(0,a,\infty)\ . \tag{5.4}$$

The first thing to mention is that the best derived code is $\mathcal{C}_Z^1$ and higher iterations do not deliver better results. Now it has to be decided if it is useful to take either the code $\mathcal{C}_Z^1$ or a set of plain spins to encode n logical qubits. For this purpose, a critical time t_c is calculated. At this point the saturated value of the symmetric subspaces fidelity Eq. (5.4) is larger than the fidelity of plain qubits in the weak coupling approximation given by Eq. (5.3). Under the assumption that $n\gamma a \ll 1$ it is straight forward to calculate that $t_c > 8a + \mathcal{O}\left((n\gamma a)^2\right)$. As time-regimes larger than the system size (na) are investigated the advantage of the symmetric subspaces against plain qubits emerges.

5.1.3 Small deviations of the entanglement fidelity

Now small deviations of the entanglement fidelity from unity are discussed. For that purpose a weak coupling is assumed, such that Eq. (4.28) holds for the entanglement fidelity. At the same time the entanglement fidelity is assumed to deviate by a small amount ϵ from unity. Accordingly, the fidelity is given as

$$F_e(\mathcal{C},\mathcal{N}) \equiv 1-\epsilon = \det(\mathbb{1}+\mathbf{K})^{-1/2}(1+\mathcal{O}(\mathrm{tr}\,\mathbf{K}^2))\,. \tag{5.5}$$

For further progress the logarithm is taken. Together with the well known relation $\det(\mathbb{1}+\mathbf{K}) = e^{-\operatorname{tr}\ln(\mathbb{1}+\mathbf{K})}$ this leads to

$$\ln(1-\epsilon) = -\frac{1}{2}\operatorname{tr}\ln(\mathbb{1}+\mathbf{K}) + \mathcal{O}(\operatorname{tr}\mathbf{K}^2)\,. \tag{5.6}$$

The expanded logarithm has leading order $\epsilon = \frac{1}{2}\operatorname{tr}\mathbf{K}$, and hence, since the decoherence matrix has equal diagonal elements $\mathrm{K}(0,t)$,

$$F_e(\mathcal{C},\mathcal{N}) = 1 - \frac{1}{2}n\,\mathrm{K}(0,t) + \mathcal{O}(\operatorname{tr}\mathbf{K}^2)\,. \tag{5.7}$$

Small deviations of the fidelity from unity are thus determined by the zero-distance decoherence function $\mathrm{K}(0,t)$. The decoherence function $\mathrm{K}(0,t)$ itself describes the decoherence of a single qubit. This result is valid for the plain qubit register and for the symmetric subspaces as well. In case of the symmetric subspace the rate of a plain single qubit $\mathrm{K}(0,t)$ has to be replaced by the rate of an effective qubit encoded in a symmetric subspace which is given by $\mathrm{K}^{(1)}(0,a,\infty)$. An analysis of the symmetric subspaces in comparison to plain qubits using this formalism reproduces the previous results. In addition due to the insight gained in this section it turns out that the rates corresponding to the single (effective) qubit decoherence play a dominant role for the evaluation of quantum codes.

5.2 Determination of the optimal code

In this section the investigation for the optimal code is outlined. The optimal encoding for a given quantum noise $\mathcal{N}$ which acts on a qubit register is searched for. Here, in contrast to previous chapters not only symmetric codes are examined. The aim is to maximise the entanglement fidelity by the choice of the code. The complete problem is discussed in the following . Unfortunately, it is impossible to determine the optimal code without further restrictions. Therefore, only the occurring problems are pointed out. Afterwards it is shown how this maximisation process can be performed in a n-spin-boson model without dissipation. Within this simplified model a single logical qubit is encoded. In this case it is possible to show that the optimal encoding is given by the symmetric code $\mathcal{C}_Z$.

5.2.1 General setting

The starting point is a qubit register with n qubits having a Hilbert space which is denoted by Q. For this purpose, the noise corresponding to the qubit register is given by its Kraus representation acting on density operators ρ due to Kraus operators A_i by

$$\mathcal{N}(\rho) = \sum_i A_i \rho A_i^\dagger\,. \tag{5.8}$$

The aim is to find the optimal two-dimensional code $\mathcal{C}$ within the accessible register's Hilbert space. For further illustration some notation is introduced. The space of operators on Q is denoted by $\mathcal{L}(Q)$. On this space the Hilbert-Schmidt scalar product is defined as $\langle\langle B_1|B_2\rangle\rangle = \mathrm{tr}\{B_1^\dagger B_2\}$ for operators B_1 and B_2. Back to the original problem the operator $\tilde{\mathcal{N}} = \sum_i |A_i\rangle\rangle\langle\langle A_i^\dagger|$ is defined. By Choi's theorem [Cho75] it is known that the noise $\mathcal{N}$ is completely positive if and only if $\tilde{\mathcal{N}} \geq 0$. According to this definition the entanglement fidelity of a state ρ is given by $F_e(\rho, \mathcal{N}) = \langle\langle\rho|\tilde{\mathcal{N}}|\rho\rangle\rangle$. Any state ρ within the qubit register fulfils

$$\mathrm{tr}\,\rho = 1 \iff \langle\langle\, \mathbb{1}\,|\rho\rangle\rangle = 1 \iff \langle\langle \sqrt{d}^{-1}\,\mathbb{1}\,|\rho\rangle\rangle = \frac{1}{\sqrt{d}}\,, \tag{5.9}$$

which is the normal form of a plane. In addition to this property there exists further structure in the problem which can be used to get a geometrical picture of the possible states. As the entanglement fidelity of the code $\mathcal{C}$ should be calculated, not any state but the normalised projector $\pi_\mathcal{C}$ onto $\mathcal{C}$ is needed. With the projector $P_\mathcal{C}$ onto $\mathcal{C}$ and $\pi_\mathcal{C} = P_\mathcal{C}/2$ it is easy to see that

$$\mathrm{tr}\,\pi_\mathcal{C}^2 = \frac{1}{2}\,. \tag{5.10}$$

Geometrically this corresponds to $1/\sqrt{2} = \|\pi_\mathcal{C}\|$, which is a sphere of radius $1/\sqrt{2}$. Sadly, the geometrical restrictions made so far are not sufficient to determine the optimal encoding. It would be nice to include the property that each density operator, including the projector $\pi_\mathcal{C}$ is positive into the geometrical picture, but so far this was not possible. Without any progress in this field the problem in the presented generality remains open. To give a taste of the functionality of the derived mechanism a short and simple example is given in the following.

Example of pure decoherence. This case is described by two Kraus operators $A_0 = \sqrt{p}\,\mathbb{1}$ and $A_1 = \sqrt{1-p}Z$, where p is a probability. With these Kraus operators the noise is given by

$$\tilde{\mathcal{N}} = p|\,\mathbb{1}\,\rangle\rangle\langle\langle\,\mathbb{1}\,| + (1-p)|Z\rangle\rangle\langle\langle Z|\,. \tag{5.11}$$

According to the derived formula the entanglement fidelity of a single qubit is

$$F_1 = \langle\langle\,\mathbb{1}/2|\tilde{\mathcal{N}}|\,\mathbb{1}/2\rangle\rangle = p\,. \tag{5.12}$$

This result can be compared to the case, where the noise is given by its Kraus representation. Then, it turns out that the probability p is given by $p = \frac{1+e^{-\mathrm{D}_{01}(t)}}{2}$. Accordingly, the entanglement fidelity is given by

$$F_1 = \frac{1+e^{-\mathrm{D}_{01}(t)}}{2}\,, \tag{5.13}$$

which is the expected result corresponding to previous results.

5.2.2 Dissipationless couplings

The dissipationless spin-boson model with Z-coupling is analysed. A closer investigation is needed, as the decay of qubits in the super-Ohmic case (with spectral parameter $s = 3$) possess decoherence functions and thus decoherence coefficients that saturate in time (cf. Sec. 2.2.2). In the previous section, dealing with the entanglement fidelity, it was pointed out that for small derivations the decrease of the fidelity is linear with the number of qubits and also linear with the effective decoherence function of a single qubit, neglecting effects that are second order or higher in the coupling. In the investigated super-Ohmic case this leads, as the decoherence function of a single spin also gets constant, to a saturation of the fidelity. Taking a high-dimensional qubit array with n qubits the following question arises: Can the fidelity be improved if a special sector of the complete useable Hilbert space is taken as code? This question can trivially be rephrased to another question: Can the fidelity of a single qubit be improved, if a higher-dimensional spin array with a good choice of encoding is taken? To answer this question codes of length n are investigated that encode one single logical qubit. First a simplified model is investigated. In this simplified model all inter-spin distances pairwise have the same length. Afterwards the general model of a spin chain with equidistant inter-spin distance between neighbouring spins is examined. So far only codes with computational states as codewords are considered. In a last step it is shown that more general codes do not improve the results of the computational states.

Computational states in a simplified model. In this model all qubits are assumed to have equal distance a to each other. The corresponding lattice forms a generalised high-dimensional polyhedron. Within this model only two decoherence coefficients occur. Namely the decoherence coefficient of a single qubit K_0 and the distance depending one K_a contribute. Both of this rates are assumed to be positive, K_a as a function of a has to be monotonically decreasing and fulfils $\lim_{a\to 0} \mathrm{K}_a = \mathrm{K}_0$. In this paragraph codes $\mathcal{C} = \mathrm{Span}\{|\nu\rangle, |\mu\rangle\}$, having the two computational states $|\nu\rangle$ and $|\mu\rangle$ as codewords, are investigated. Computational states have a structure given by $\otimes_{i=1}^{n} |s_i\rangle$ with $|s_i\rangle \in \{|\uparrow\rangle \equiv |0\rangle, |\downarrow\rangle \equiv |1\rangle\}$. Let the orthogonal states $|\nu\rangle = |0\rangle$ and $|\mu\rangle = |1\rangle$ be the logical zero and one, respectively. In this case the entanglement fidelity of the code $\mathcal{C}$ is determined by the decoherence coefficient $\mathrm{D}_{\nu\mu}$ as

$$F_e(\mathcal{C}) = \frac{1}{2} + \frac{1}{2} e^{-\mathrm{D}_{\nu\mu}} \,. \tag{5.14}$$

According to Chapter 2 this decoherence coefficient has the form

$$\mathrm{D}_{\nu\mu} = \sum_{i,j=1,\ldots,n} (\nu_i - \mu_i)(\nu_j - \mu_j)\, \mathrm{K}(|i-j|a) \,, \tag{5.15}$$

where, corresponding to the chosen model, the decoherence function is

$$\mathrm{K}(r) = \begin{cases} \mathrm{K}_0 & , r = 0 \\ \mathrm{K}_a & , r > 0 \end{cases} . \tag{5.16}$$

In the following the entanglement fidelity has to be maximised by the choice of the code. According to the present notation, the states ν and μ are varied. Obviously, the fidelity is maximised if the corresponding decoherence coefficient is minimised. Therefore, the decoherence coefficients are investigated more closely. It turns out that a set of basis states $|\nu\rangle$, $|\mu\rangle$ of length n with $\nu_i = \mu_i$ for a certain i has the same decoherence coefficient as the set of two basis states of length $n-1$ which is shortened by the i^{th} spin. As a shorter code is more desireable than a longer one only pairs of basis states are investigated that differ on each spin site. New variables $x_i = \nu_i - \mu_i \in \{-1, 1\}$ are introduced. Accordingly, each code of length n is described by a vector $\mathbf{x} \in \{-1, 1\}^n$. The decoherence coefficient expressed by the new variables has the form

$$\mathrm{D}_{\nu\mu} = \sum_{i=1}^{n} x_i^2 \,\mathrm{K}_0 + 2\,\mathrm{K}_a \sum_{1 \le i < j \le n} x_i x_j = n\,\mathrm{K}_0 + 2\,\mathrm{K}_a \sum_{1 \le i < j \le n} x_i x_j \,. \tag{5.17}$$

If the basis states lead to a vector $\mathbf{x}$ with k negative entries there are $k(n-k)$ negative summands in the second term of the coefficient. With $n(n-1)/2$ terms in all this leads to

$$\mathrm{D}_{\nu\mu} = n\,\mathrm{K}_0 + 2\,\mathrm{K}_a \left(\frac{n(n-1)}{2} - 2k(n-k) \right) . \tag{5.18}$$

This decoherence coefficient has three extremal points, the first one is at $k = 0$, the second one at $k = n/2$ and the third one at $k = n$. The $(k = 0)$-case and the $(k = n)$-case obviously do not lead to an improvement, but the case of $k = n/2$ leads to the decoherence coefficient

$$\mathrm{D}_{\nu\mu} = n(\mathrm{K}_0 - \mathrm{K}_a) \,. \tag{5.19}$$

This rate leads to the maximal improvement in the fidelity compared to the one of a single spin, if $n = 2$ and $\mathrm{K}_0 < 2\,\mathrm{K}_a$. In this way the minimal decoherence function is obtained to be

$$\mathrm{D}_{\min} = \begin{cases} 2(\mathrm{K}_0 - \mathrm{K}_a) & , \mathrm{K}_0 < 2\,\mathrm{K}_a \\ \mathrm{K}_0 & , \text{else} \end{cases} . \tag{5.20}$$

For the chosen model this means that, concerning computational states, the optimal code for a single qubit is constructed either by a single spin or the formerly introduced code $\mathcal{C}_Z = \mathrm{Span}\{|01\rangle, |10\rangle\}$ depending on the size of the decoherence function K_a.

A complete spin chain. A spin chain with inter-spin distance a is discussed now. The aim is to derive the optimal decoherence coefficient for computational states for this chain. The decoherence function $\mathrm{K}(r)$ is assumed to be monotonically decreasing which is motivated by the results presented in Chapter 2. For further progress Eq. (5.15) is

rewritten as

$$\mathrm{D}_{\nu\mu} = \mathbf{x}^T \mathbf{K} \mathbf{x} \tag{5.21}$$

with $\mathrm{K}_{ij} = \mathrm{K}(|i-j|a)$ and $x_i \in \{-1, 1\}$. This decoherence function $\mathrm{D}_{\nu\mu}$ has to be minimised by the code, respectively by the choice of $\mathbf{x}$, such that for a given n the minimal decoherence coefficient is given by

$$\mathrm{D}_n = \min_{\mathbf{x}\in\{-1,1\}^n} \{\mathbf{x}^T \mathbf{K} \mathbf{x}\}. \tag{5.22}$$

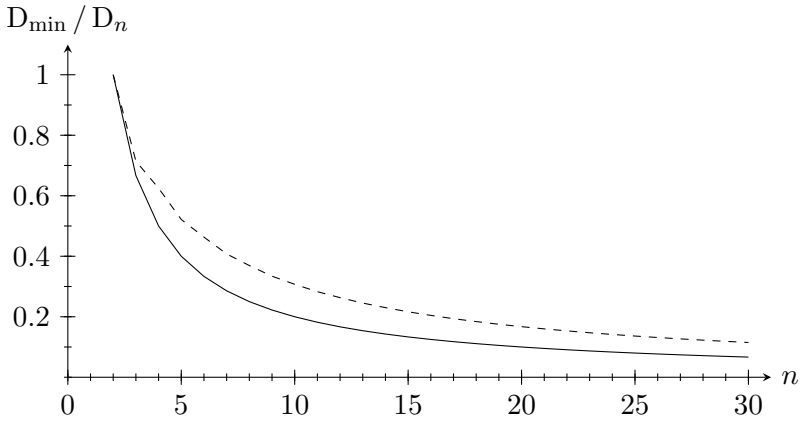

Figure 5.2: The fraction of $\mathrm{D}_{\min} / \mathrm{D}_n$ over the size n of the codes is plotted for different parameters $\kappa = r\Omega$ (and 1.000.000 iterations). The solid line corresponds to the case with $\kappa \gg 1$ and the dashed line to $\kappa = 1$.

Now the more explicit case of a spin-boson model with super-Ohmic coupling is investigated. As for large n the task to find the global minimum is still quite hard some numerics help. Finding the minimising $\mathbf{x}$ in this case can be mapped onto another problem whose solution is known. For this purpose, the original problem is mapped onto an Ising-model $\mathbf{x}$ with coupling matrix $\mathbf{K}$. The minimising $\mathbf{x}$ corresponds to the groundstate configuration of this Ising-chain. Now numerics solve the problem approximately by a simulated annealing algorithm that gives a good candidate for the groundstate. This algorithm is applied to the chosen dissipationless spin-boson model. In the limit of a large cutoff Ω of the spectral density, which is the physically relevant one in most cases, the minimal decoherence function seems to grow for larger codes. A numerical plot for the super-Ohmic case is presented in Fig. 5.2. According to these results also for a spin chain is the best encoding given by a code of size two. Furthermore, no better code than the one previously found was obtained.

General codes in the simplified model. The codes $\mathcal{C}$ of length n are defined by orthonormal basis states $|0\rangle = \sum_{i\in 2^n} \alpha_i |i\rangle$ and $|1\rangle = \sum_{i\in 2^n} \beta_i |i\rangle$ with complex coeffi-

cients $\underline{\alpha}, \underline{\beta} \in \mathbb{C}^n$. The entanglement fidelity of such a code is given by

$$F_e(\mathcal{C}) = \frac{1}{4}\sum_{i,j\in\mathcal{C}} \langle i|\,\mathcal{N}(|\,i\rangle\langle j\,|)\,|j\rangle = \frac{1}{4}\sum_{i,j\in 2^n} \left(|\alpha_i|^2 + |\beta_i|^2\right)\left(|\alpha_j|^2 + |\beta_j|^2\right) e^{-\,\mathrm{D}_{ij}}\,. \quad (5.23)$$

In principle, this fidelity has to be maximised over all possible values of $\underline{\alpha}$ and $\underline{\beta}$ to find the best code. Since $\underline{\alpha}$ and $\underline{\beta}$ are two orthonormal vectors they can be interpreted as two rows of a unitary $2^n \times 2^n$-matrix $\mathbf{U}$. Having this point of view, the problem can be reformulated to the determination of the maximum fidelity for all unitary matrices $\mathbf{U}$. As the populations in a dissipationless model remain constant due to $\mathrm{D}_{ii} = 0$, the fidelity is

$$F_e(\mathcal{C}) = \frac{1}{4}\sum_{i\in 2^n} \left(|U_{i1}|^2 + |U_{i2}|^2\right)^2 + \frac{1}{4}\sum_{i\neq j\in 2^n} \left(|U_{i1}|^2 + |U_{i2}|^2\right)\left(|U_{j1}|^2 + |U_{j2}|^2\right) e^{-\,\mathrm{D}_{ij}}\,. \quad (5.24)$$

It can be shown that an upper bound for the first term is given by

$$\sum_{i\in 2^n} \left(|U_{i1}|^2 + |U_{i2}|^2\right)^2 \leq 2\,, \quad (5.25)$$

which is proven by the following consideration. Since the sum over the absolute square of all entries for each row is equal to one, it follows $\sum_{i\in 2^n}\left(|U_{i1}|^2 + |U_{i2}|^2\right) = 2$. To derive the bound it is enough to demand that the square root of each summand in Eq. (5.25) is less or equal to one, $\forall_i : |U_{i1}|^2 + |U_{i2}|^2 \leq 1$, as in this case each of them would decrease by squaring. This last step is obvious again, as the sum over each complete row is equal to one, $\sum_j |U_{ij}|^2 = 1$ and only positively contributing terms are left out. Now the entanglement fidelity for the simplified model is

$$F_e(\mathcal{C}) \leq \epsilon + (1-\epsilon)e^{-\,\mathrm{D}_{\min}} \quad (5.26)$$

with $\epsilon = \frac{1}{4}\sum_{i\in 2^n}\left(|U_{i1}|^2 + |U_{i2}|^2\right)^2$. Using the bound of Eq. (5.25) again leads to

$$F_e(\mathcal{C}) \leq \frac{1}{2} + \frac{1}{2}e^{-\,\mathrm{D}_{\min}}\,. \quad (5.27)$$

Concluding, all codes constructed in this manner turn out to have an entanglement fidelity which is lower than the one given by the previously derived $\mathrm{D}_{\min}$. Note that generalising this method for more than one logical qubit turns out to be a hard task and could not be completed so far.

Conclusion

This chapter was divided into two parts. The first part dealt with dissipationless couplings in a spin-boson model. The case of a qubit chain with finite inter-qubit distance was investigated. The code $\mathcal{C}_Z$, which was introduced in a previous chapter, was anal-

ysed. This code respects the symmetry of the interaction Hamiltonian if all spins are located at one point to create a decoherence-free subspace. According to the present setting this symmetry was absent and the code ceased to be decoherence-free. A comparison of the code $\mathcal{C}_Z$ to another code, given by a plain qubit register, was performed. For that purpose, both codes were evaluated with help of the previously introduced code fidelity. An advantage of the code $\mathcal{C}_Z$ in comparison to the plain qubit register was revealed. This advantage emerged for times larger than the length of the chain having $c = 1$, whereas there was no advancement for very short times. The second part of this chapter dealt with the determination of the optimal encoding for a spin-boson model. Taking care of all possible kinds of noises and allowing any kind of encoding turned out to be a very difficult problem. As there was no way found to solve this problem in the scope of this work a simplified model was used. The code size was reduced to a single effective qubit and the noise was restricted to the already discussed dissipationless model. Under this restrictions the problem was solved. It turned out that the code $\mathcal{C}_Z$ with one effective qubit is best adapted to the noise.

6 Dissipative couplings

Up to now only dissipationless couplings were investigated in the scope of this work and dissipative couplings are missing. To fill this gap this chapter deals with a dissipative spin-boson model. Unfortunately, there is no way known to determine the time evolution within a dissipative spin-boson model in an analytical manner. For the present purpose a restriction to the time evolution of the reduced density operator of the spin part can be made as the dynamics of the environment is not of further interest. Thereby, the bosonic bath is assumed to start and stay in thermal equilibrium as the back action of the spin system to the bath is neglected. The time evolution of the spin system's reduced density operator is derived in form of a master equation. This master equation is of Bloch-Redfield type. Accordingly, the time derivative of the reduced density operator at a certain time is given by a Redfield super-operator which acts on the reduced density operator at the investigated time. This Redfield super-operator is determined for dissipative and dissipationless couplings. Due to an integration of the Redfield super-operator over time the time evolved reduced density operator can be calculated for given initial conditions.

The aim of this chapter is to evaluate the decoherence-reduced subspace $\mathcal{C}_{XZ}$ which was introduced in Sec. 3.1. This code was established to be decoherence-free in the case of spatial localised qubits. Here, the case of finite inter-spin distances is investigated. More precisely, a single logical qubit is encoded into a subspace given by this code. Then, this code is evaluated by its entanglement fidelity. For this purpose, the time derivative of the entanglement fidelity is determined and an approximated rate for the regime of long times obtained. In a weak coupling approximation this rate is essentially given by the calculated Redfield super-operator. This result is used to evaluate the above mentioned code. Consequently, the time derivative of the entanglement fidelity is calculated for the code $\mathcal{C}_{XZ}$ and for plain qubits as reference. Comparing these two rates reveals whether the code $\mathcal{C}_{XZ}$ or plain qubits perform better. Hence, different starting conditions for the present inter-spin distance and spin energy splitting are analysed. It turns out that the code $\mathcal{C}_{XZ}$ delivers better results than plain qubits if the product of inter-spin distance and spin energy splitting is below a critical value.

6.1 Bloch-Redfield master equation

In a first step the derivation of the Bloch-Redfield master equation is recapitulated, as it is presented in the book of Breuer and Petruccione [BP02]. Thereby, the mechanism is slightly modified concerning the Markov approximation. To contain all relevant cases, this derivation is as far as possible performed without any restriction to the interaction.

To consider the most general case a system S is coupled to a bath E via an interaction given by a Hamiltonian $\hat{H}_I$. The free Hamiltonian of the joint system SE is $\hat{H}_0$. Later on, the explicit form of the interaction Hamiltonian of the spin-boson model is inserted. To determine the dynamics of the combined system SE, the Liouville-von-Neumann equation is used. This Liouville-von-Neumann equation for the time derivative of the density operator ρ_{SE} of the total system in the interaction picture is

$$\dot{\rho}_{SE}(t) = -i\hbar^{-1}[\tilde{H}_I(t), \rho_{SE}(t)]\,. \tag{6.1}$$

Thereby, the operator $\tilde{H}_I(t)$ is the interaction Hamiltonian in the interaction picture. This operator is as usual produced via the time evolution of the free Hamiltonian $\hat{H}_0$ acting on the corresponding Schrödinger operator $\hat{H}_I$ as $\tilde{H}_I(t) = e^{i\hat{H}_0 t}\hat{H}_I e^{-i\hat{H}_0 t}$. The time evolution of the system SE is achieved by integrating $\dot{\rho}_{SE}(t)$ over time with respect to the initial conditions. Accordingly, the density operator of the combined system at time t is formally given by

$$\rho_{SE}(t) = \rho_{SE}(0) + \int_0^t \mathrm{d}s\, \dot{\rho}_{SE}(s)\,, \tag{6.2}$$

where $\rho_{SE}(0)$ is the initial state. Combining the last two equations and tracing out the degrees of freedom belonging to the bath an equation of motion for the reduced density operator ρ of the system S (in the interaction picture) reads

$$\dot{\rho}(t) = -i\hbar^{-1}\operatorname*{tr}_E[\tilde{H}_I(t), \rho_{SE}(0)] - \hbar^{-2}\int_0^t \mathrm{d}s\, \operatorname*{tr}_E[\tilde{H}_I(t), [\tilde{H}_I(s), \rho_{SE}(s)]]\,. \tag{6.3}$$

For problems dealt with in this work it can be assumed that initially $\rho_{SE}(0)$ is a product of an initial state $\rho(0)$ of the system S and a thermal bath state ρ_E. Having such a product state a short consideration reveals that $\mathrm{tr}_E[\tilde{H}_I(t)\ ,\ \rho(0)\otimes\rho_E] = 0$ holds for the interaction Hamiltonian presented in Eq. (1.7) or (1.8). To see this, the trace over the environmental degrees of freedom is written in Fock space for each mode. As the interaction Hamiltonian in each case only involves single annihilation or creation operators which do not preserve the particle number of the corresponding mode the trace over Fock states vanishes. Furtheron, the Born-Markov approximation is applied to the given setting by $\rho_{SE}(s) \overset{\text{Born}}{\to} \rho(s)\otimes\rho_E \overset{\text{Markov}}{\to} \rho(t)\otimes\rho_E$. Thereby, the Born approximation is justified for a large bath and weak coupling, such that the back-action of the system onto the bath can be neglected. Obviously, the Markov approximation is good in the limit of weak couplings as $\rho(s)$ and $\rho(t)$ do not differ to much from each other. Inserting this approximation into the previous equation results in the Bloch-Redfield master equation

$$\dot{\rho}(t) = \mathcal{R}_t(\rho(t))\,. \tag{6.4}$$

The operator $\mathcal{R}_t$ which occurs in this equation is called Redfield super-operator. According to the previous Born-Markov approximation and the negelection of the first term in Eq. (6.3) the Redfield super-operator is given by

$$\mathcal{R}_t(\rho) = -\hbar^{-2} \int_0^t \mathrm{d}s \ \mathop{\mathrm{tr}}_E[\tilde{H}_I(t), [\tilde{H}_I(s), \rho \otimes \rho_E]] \,. \tag{6.5}$$

Within this integral the parameter s is substituted by $s \mapsto t - s$ with a constant time t. This substitution transforms the Redfield super-operator to

$$\mathcal{R}_t(\rho) = -\hbar^{-2} \int_0^t \mathrm{d}s \ \mathop{\mathrm{tr}}_E[\tilde{H}_I(t), [\tilde{H}_I(t-s), \rho \otimes \rho_E]] \,. \tag{6.6}$$

For further progress this Redfield super-operator has to be determined by a closer investigation of the occurring interaction Hamiltonian. Note that the Redfield operator is explicitly time-dependent and therefore the resulting dynamics does not exhibit a semigroup structure. In this sense, the Bloch-Redfield equation Eq. (6.4) is non-Markovian, notwithstanding the fact that the Born-Markov approximation has been used to derive it. In many cases it is justified to eliminate this "deficiency" by simply extending the domain of integration in Eq. (6.6) from $[0, t]$ to $[0, \infty]$ (cf. Ref. [BP02]). However, as it has been stressed by Doll et al. [DWHK07], when dealing with a spatially extended quantum object this procedure would lead to noncausal behaviour and thus to spurious results. In Ref. [DWHK07] this problem has been circumvented by using a master equation in which causality is explicitly taken care of by step functions in the time domain that truncate acausal contributions. The resulting dynamics has been shown to approximate quite well the known exact solution.

The Redfield super-Operator for the spin-boson model. Starting point is a common interaction Hamiltonian of the form

$$\hat{H}_I = \sum_m A_m \otimes B_m \,. \tag{6.7}$$

Here, each operator A_m acts on the system only and each operator B_m exclusively acts on the environment. The index m labels existing degrees of freedom, for instance the lattice site. The free Hamiltonian $\hat{H}_S$ corresponding to the system S is assumed to have a discrete spectrum of eigenvalues ϵ which is a valid assumption for the spin-boson model. Knowing these eigenvalues for each m an operator

$$A_m(\Delta) = \sum_{\epsilon' - \epsilon = \Delta} \Pi(\epsilon) A_m \Pi(\epsilon') \tag{6.8}$$

is defined. Thereby, $\Pi(\epsilon)$ is the projector on the eigenspace belonging to the eigenvalue ϵ. It is easy to verify that following equations,

$$[\hat{H}_S, A_m(\Delta)] = -\Delta A_m(\Delta) \quad \text{and} \quad [\hat{H}_S, A_m^\dagger(\Delta)] = +\Delta A_m^\dagger(\Delta)\,, \tag{6.9}$$

hold for the previously defined operators. With the help of the Baker-Hausdorff relation and these formulae it is easy to show that

$$e^{i\hat{H}_S t/\hbar} A_m(\Delta) e^{-i\hat{H}_S t/\hbar} = e^{-i\Delta t/\hbar} A_m(\Delta) \tag{6.10a}$$

$$e^{i\hat{H}_S t/\hbar} A_m^\dagger(\Delta) e^{-i\hat{H}_S t/\hbar} = e^{i\Delta t/\hbar} A_m^\dagger(\Delta)\,. \tag{6.10b}$$

According to the definition in Eq. (6.8) it is obvious that $A_m^\dagger(\Delta) = A_m(-\Delta)$. Finally a short calculation shows

$$[\hat{H}_S, A_m^\dagger(\Delta) A_l(\Delta)] = 0\,. \tag{6.11}$$

By the definition of the operator $A_m(\Delta)$ it turns out that a complete summation over all energy levels Δ produces the initial operator A_m according to $\sum_\Delta A_m(\Delta) = \sum_\Delta A_m^\dagger(\Delta) = A_m$. Using this insight the interaction Hamiltonian can be rewritten as

$$\hat{H}_I = \sum_{m,\Delta} A_m(\Delta) \otimes B_m\,. \tag{6.12}$$

Here, this interaction Hamiltonian is given in the Schrödinger picture. For the Redfield super-operator in Eq. (6.6) this interaction Hamiltonian has to be transformed into the interaction picture. According to the transformation of the operators $A_m(\Delta)$, shown in Eq. (6.10a) and Eq. (6.10b), the interaction Hamiltonian in the interaction picture is given by

$$\tilde{H}_I(t) = \sum_{m,\Delta} e^{-i\Delta t/\hbar} A_m(\Delta) \otimes B_m(t)\,. \tag{6.13}$$

Note that during this change of the picture also the bath operators B_m are transformed to time dependent bath operators $B_m(t)$. Inserting this concrete form of an interaction Hamiltonian into Eq. (6.6) reveals that the Redfield super-operator has the form

$$\mathcal{R}_t(\rho) = \sum_{\Delta,\Delta'} \sum_{m,l} e^{i(\Delta'-\Delta)t/\hbar} \Gamma_{ml}(\Delta, t) \left(A_l(\Delta) \rho A_m^\dagger(\Delta') - A_m^\dagger(\Delta') A_l(\Delta) \rho \right) + H.c.\,, \tag{6.14}$$

where the occurring rate $\Gamma_{ml}(\Delta, t)$ is

$$\Gamma_{ml}(\Delta, t) = \hbar^{-2} \int_0^t \mathrm{d}s\, e^{i\Delta s/\hbar} \left\langle B_m^\dagger(t) B_l(t-s) \right\rangle\,. \tag{6.15}$$

If the relaxation time τ_R of the system is much smaller than the time $\tau_S = |\Delta - \Delta'|^{-1}$ the rotating wave approximation is performed. In this approximation the sum over Δ and Δ' in the operator $\mathcal{R}_t$ collapses to a single one. Hence, the Redfield super-operator is given as

$$\mathcal{R}_t(\rho) = \sum_{\Delta} \sum_{m,l} \Gamma_{ml}(\Delta, t) \left(A_l(\Delta) \rho A_m^\dagger(\Delta) - A_m^\dagger(\Delta) A_l(\Delta) \rho \right) + H.c.\,. \tag{6.16}$$

According to its definition in Eq. (6.15) the rate $\Gamma_{ml}(\Delta, t)$ turns out to be a complex quantity. For this purpose, the rate $\Gamma_{ml}(\Delta, t)$ is separated into real an imaginary part according to

$$\Gamma_{ml}(\Delta, t) = \frac{1}{2} C_{ml}(\Delta) + i S_{ml}(\Delta)\,, \tag{6.17}$$

defining the real valued rates $C_{ml}(\Delta)$ and $S_{ml}(\Delta)$. Using this decomposition the Redfield super-operator divides into real and a imaginary part,

$$\mathcal{R}_t(\rho) = -i[H_{LS}, \rho] + \mathcal{D}(\rho)\,. \tag{6.18}$$

The first term of this equation involves the Lamb shift Hamiltonian H_{LS}. This Lamb shift Hamiltonian includes the rate $S_{ml}(\Delta)$ and is given by

$$H_{LS} = \sum_{\Delta} \sum_{m,l} S_{ml} A_m^\dagger(\Delta) A_l(\Delta)\,. \tag{6.19}$$

This Hamiltonian leads to a Lamb-type renormalisation of the unperturbed energy levels induced by the system-environment coupling. Note that the Lamb shift Hamiltonian commutes with the unperturbed system Hamiltonian, $[H_S, H_{LS}] = 0$ according to Eq. (6.11). For simplification, as this term does not lead to decoherence, the contribution caused by the Lamb shift Hamiltonian is neglected in the following. The second term $\mathcal{D}$ of Eq. (6.18) is called dissipator and contains the rate $C_{ml}(\Delta)$. Accordingly, $\mathcal{D}$ is given by

$$\mathcal{D}(\rho) = \sum_{\Delta} \sum_{m,l} C_{ml}(\Delta) \left(A_l(\Delta) \rho A_m^\dagger(\Delta) - \frac{1}{2} \{ A_m^\dagger(\Delta) A_l(\Delta), \rho \} \right)\,. \tag{6.20}$$

As the first term in Eq. (6.18) is neglected, the master equation simplifies to the later on used form of

$$\mathcal{R}_t(\rho) = \mathcal{D}(\rho)\,. \tag{6.21}$$

In this way, for each setting only the dissipator $\mathcal{D}$ has to be calculated.

6.2 Dissipative couplings

Coupling via X. As the dissipationless model is solved analytically in the previous chapters the focus is on dissipative couplings in this section. A one-dimensional spin chain is investigated which is modeled by a spin-boson model. Here, a dissipative cou-

pling between spin part and bath is chosen. Therefore, the model has an interaction Hamiltonian given by Eq. (1.8), having a coupling between bath and spin system via the Pauli matrix X at each lattice site. According to this choice of the model the dissipator simplifies to

$$\mathcal{D}(\rho) = \sum_{m,l} \Bigg(C(|r_m - r_l|, \Delta) \left(d_l(\Delta)\rho u_m(\Delta) - \frac{1}{2}\{u_m(\Delta)d_l(\Delta), \rho\} \right) + C(|r_m - r_l|, -\Delta) \left(u_l(\Delta)\rho d_m(\Delta) - \frac{1}{2}\{d_m(\Delta)u_l(\Delta), \rho\} \right) \Bigg). \tag{6.22}$$

Here, the notation of $C(|r_m - r_l|, \Delta) \equiv C_{ml}(\Delta)$ for the rates is introduced. The Hilbert space of the spin at each lattice site is restricted to $\mathrm{Span}\{|0\rangle, |1\rangle\}$. The operators $d_l(\Delta)$ and $u_l(\Delta)$ are annihilation and creation operators of the l^{th} lattice site acting on this Hilbert space. Accordingly, they are given by $u_l(\Delta) = \sigma_{+,l} = X_l + iY_l$ and $d_l(\Delta) = \sigma_{-,l} = X_l - iY_l$. In the following the rates $C_{ml} = 2\Re[\Gamma_{ml}]$ are calculated. To get a physical meaning for these rates a concrete model is chosen. A dipole interaction in the form of Eq. (1.26) is assumed, such that the interaction Hamiltonian is given by $\hat{H}_I = -\mathbf{E} \cdot \underline{\mathcal{D}}$, where $\mathbf{E}$ is the quantised electric field and $\underline{\mathcal{D}}$ is the dipole operator. The bath correlator for this setting is calculated to be

$$\left\langle B_m^\dagger(t) B_l(0) \right\rangle = \frac{|\wp_{eg}|^2}{\nu} \sum_{\mathbf{k}} \frac{\hbar\omega_{\mathbf{k}}}{\epsilon_0} \left((n(\omega_{\mathbf{k}}) + 1) e^{-i\omega_{\mathbf{k}} t} + n(\omega_{\mathbf{k}}) e^{i\omega_{\mathbf{k}} t} \right) \cos(\mathbf{k} \cdot (\mathbf{r}_m - \mathbf{r}_l)), \tag{6.23}$$

where $n(\omega) = (e^{\hbar\omega/(k_{\mathrm{B}}T)} - 1)^{-1}$ is the Planck distribution of the bathmodes. This bath correlator is main ingredient for the rate Γ_{ml} (cf. Eq. (6.15)). To determine Γ_{ml} the integration in Eq. (6.15) has to be performed. In a first step the rate $\Gamma_{mm}(\Delta)$ is calculated which corresponds to the rate of a single qubit. Therefore, a Markov approximation in Eq. (6.15) is performed by letting the upper limit of the integral go to infinity, $t \to \infty$. This approximation is justified as the integrand sharply peaks around zero. As a result, the complex rate $\Gamma_{mm}(\Delta)$ is given by

$$\Gamma_{mm}(\Delta) = \frac{1}{\pi^2 \epsilon_0} \frac{|\wp_{eg}|^2}{3\hbar c^3} \int_0^\infty \mathrm{d}\omega\, \omega^3 e^{-\frac{\omega}{\Omega}} \left((n(\omega)+1) \int_0^\infty \mathrm{d}s\, e^{-i(\omega-\Delta)s} + n(\omega) \int_0^\infty \mathrm{d}s\, e^{i(\omega+\Delta)s} \right). \tag{6.24}$$

Note that at this point the result of Sec. 1.3.1 is used, where it was shown that $|g_k|^2 \sim \cos^2\theta \cos^2\varphi + \sin^2\varphi$. Now it can be used that $\int_0^\infty \mathrm{d}s\, e^{i\epsilon s} = \pi\delta(s) + iP\frac{1}{\epsilon}$, where P denotes the primal value. As $C(0, \Delta)$ is the real part of the rate $\Gamma_{mm}(\Delta)$ this immediately shows that

$$C(0, \Delta) = \gamma_0 (1 + n(\Delta)) e^{-\Delta/\Omega} \quad \text{with} \quad \gamma_0 = \frac{1}{4\pi\epsilon_0} \frac{4\Delta^3 |\wp_{eg}|^2}{3\hbar c^3}. \tag{6.25}$$

The rate γ_0 is in complete agreement with the Weisskopf-Wigner theory of spontaneous emission which is outlined in Appendix C. Accordingly, the rate that describes spontaneous and thermally induced emission processes is given by

$$C(0,\Delta) = \gamma_0(n(\Delta)+1)e^{-\Delta/\Omega}\,, \tag{6.26}$$

Thermally induced absorption processes are given by the rate

$$C(0,-\Delta) = \gamma_0 n(\Delta)e^{-\Delta/\Omega}\,. \tag{6.27}$$

It turns out that the relaxation time τ_R (often referred to as longitudinal (or spin-lattice) relaxation T_1-time) for a single spin is the inverse of the rate γ_0, $\tau_R = \gamma_0^{-1}$. It remains to calculate the distant depending rates $C(|r_m - r_l|,\Delta) \equiv C_{ml}(\Delta)$ for $m \neq l$. According to previous chapters only a factor $\sin(\omega r)/\omega r$ occurs within this rates during the continuum limit. Consequently, the distance depending rates can easily be calculated using the same mechanism as above to be

$$C(r,\pm\Delta) = C(0,\pm\Delta)\frac{\sin(\Delta r)}{\Delta r}\Theta(t-r)\,, \tag{6.28}$$

where the factor $\Theta(t-r)$ takes care of spurious effects caused by the Markov approximation. Having the rates $C(r,\pm\Delta)$, it is numerically possible to determine the time evolution of the investigated spin chain for given starting conditions. These starting conditions include the initial state of the spin chain. At each time step the change of the spin chain density operator is given by Eq. (6.4). Accordingly, the initial state can be numerically evolved in time by short discrete time steps. As similar calculations can be found in many common text books, e.g. the book of Breuer and Petruccione [BP02], such a result is not given in the scope of this work.

Coupling via X and Z. Now the most general interaction Hamiltonian presented in Eq. (1.6), having X and Z-couplings at each site, is investigated. In this case there are additional contributions to those caused by the dissipative operators $u_l(\Delta)$ and $d_l(\Delta)$ given by Z_l. Thereby, Z_l is the Pauli matrix $Z = \sigma_z$ acting on the spin at the l^{th} lattice site. The additional terms to the dissipator involve rates $C(|r_m - r_l|, 0)$ in combination with Z_l and Z_m for lattice sites m and l. Completely, the dissipator is given by

$$\begin{aligned}\mathcal{D}(\rho) = \sum_{m,l}\Bigg(& C(|r_m-r_l|,\Delta)\left(d_l(\Delta)\rho u_m(\Delta) - \frac{1}{2}\{u_m(\Delta)d_l(\Delta),\rho\}\right) \\ & + C(|r_m-r_l|,-\Delta)\left(u_l(\Delta)\rho d_m(\Delta) - \frac{1}{2}\{d_m(\Delta)u_l(\Delta),\rho\}\right) \\ & + C(|r_m-r_l|,0)\left(Z_l\rho Z_m - \frac{1}{2}\{Z_m Z_l,\rho\}\right)\Bigg)\,.\end{aligned} \tag{6.29}$$

A short calculation shows that the rates $C(|r_m - r_l|, 0)$ for $\Delta = 0$ are given by

$$C(r,0) = \frac{\alpha}{2\hbar\epsilon_0}\int_0^\infty \mathrm{d}\omega\, \omega^2 \coth\frac{\omega}{2T}\sin(\omega t)e^{-\omega/\Omega}\begin{cases} 1 & ,r=0 \\ \frac{\sin(\omega r)}{\omega r} & ,r>0 \end{cases}. \tag{6.30}$$

Just like in previous calculations the rates for vanishing distance have to be calculated on its own. This calculation for the $r = 0$ case is performed using the integral representation of the polygamma function. Thereby, the coefficient $C(0,0)$ is obtained to be

$$C(0,0) = \frac{\alpha T^3}{\hbar\epsilon_0}\Im\left[\psi^{(2)}(T/\Omega + iTt)\right] - \frac{\alpha}{\hbar\epsilon_0}\frac{t(3/\Omega^2 - t^2)}{(1/\Omega^2 + t^2)^3}. \tag{6.31}$$

The missing rate for finite $r > 0$ is, using the same technique, turns out to be given by

$$\begin{aligned} C(r,0) =& \frac{\alpha T^2}{2\hbar\epsilon_0 r}\Re\left[\psi^{(1)}(T/\Omega + iT(r-t)) - \psi^{(1)}(T/\Omega + iT(r+t))\right] \\ &+ \frac{\alpha}{4\hbar\epsilon_0 r}\left(\frac{(r-t)^2 - 1/\Omega^2)}{(1/\Omega^2 + (r-t)^2)^2} - \frac{(r+t)^2 - 1/\Omega^2)}{(1/\Omega^2 + (r+t)^2)^2}\right). \end{aligned} \tag{6.32}$$

Now the dissipator for the investigated interaction Hamiltonian is completely determined. Accordingly, all information is available which is needed to solve the time evolution for any state of the given spin chain.

Evaluation of the symmetric code. Full knowledge about the time evolution of a spin chain in the most general spin-boson model is achieved, at least on a numerical level. Having this time evolution is the main ingredient to evaluate quantum codes. In the scope of this work, the entanglement fidelity is used to evaluate the robustness of the symmetric code $\mathcal{C}_{XZ}$ (cf. Sec. 3). The entanglement fidelity was introduced in Sec. 4.1. A short calculation shows that the rates of the entanglement fidelity for the used model are given by

$$\frac{\mathrm{d}}{\mathrm{d}t}F_e(\mathcal{C},\mathcal{N}) = \sum_{i,j}\frac{1}{k^2}\left\langle i\right|\frac{\mathrm{d}}{\mathrm{d}t}\mathcal{N}\left(\sum_{a,b}|\,a\rangle\langle b\,|\right)\left|j\right\rangle \tag{6.33}$$

for any code $\mathcal{C}$. Obviously the time differentiated noise is just the Redfield super-operator, $\frac{\mathrm{d}}{\mathrm{d}t}\mathcal{N} = \mathcal{R}_t$. For further progress the case of qubits which are weakly coupled to the environment is investigated, such that the code might be a useful candidate for quantum memory. The coupling coefficients α for the X and Z-coupling are assumed to be of equal size. As long as the fidelity is close to unity, the approximation

$$\frac{\mathrm{d}}{\mathrm{d}t}F_e(\mathcal{C},\mathcal{N}) = \sum_{i,j}\frac{1}{k^2}\left\langle i\right|\mathcal{R}_t(|\,i\rangle\langle j\,|)\left|j\right\rangle \tag{6.34}$$

is performed. Within this approximation it is assumed that the Redfield super-operator does not change the value of the initial state. This leads to an asymptotic rate for the

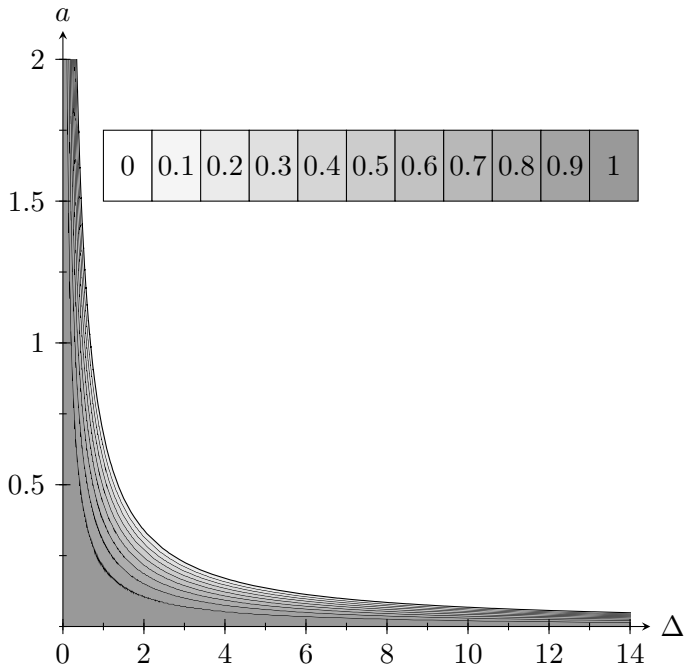

Figure 6.1: Contour plot of the ratio of the long time rates γ_1/γ_0 as function of energy Δ on the horizontal axis and inter-spin distance a on the vertical axis.

entanglement fidelity.

Now this asymptotic rate is evaluated for two different settings. First the rate of a single spin used as a qubit as reference is investigated, then the rate of an encoded qubit within the code $\mathcal{C}_{XZ}$ is looked at. Afterwards they are compared to find regimes where it is useful to use the larger code. After a short calculation the asymptotic rate of the 4-spin code $\mathcal{C}_{XZ}$ turns out to be

$$\gamma_1 = \alpha \frac{1+e^{-\Delta/T}}{1-e^{-\Delta/T}} \frac{\Delta^2}{9a} \left(18a\Delta - 9\sin(a\Delta) - 3\sin(2a\Delta) - \sin(3a\Delta)\right) e^{-\Delta/\Omega} . \tag{6.35}$$

The rate of a single spin is easily determined to be given by

$$\gamma_0 = \alpha \frac{1+e^{-\Delta/T}}{1-e^{-\Delta/T}} \frac{\Delta^3}{2} e^{-\Delta/\Omega} . \tag{6.36}$$

Fig. 6.1 shows a contour plot of the ratio γ_1/γ_0 as function of energy splitting Δ and inter spin distance a. The darker the region, the better is the code $\mathcal{C}_{XZ}$ in comparison to a plain qubit. Analysing Eq. (6.35) and (6.36) reveals that this ratio depends on a parameter p only, where p is the product of a and Δ. The corresponding graph of γ_1/γ_0 as a function of p is shown in Fig. 6.2. Within this graph a function value of less than

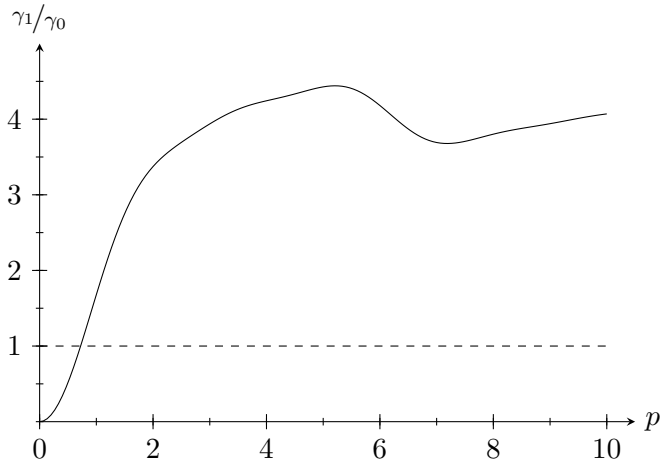

Figure 6.2: The ratio of the long time rates γ_1/γ_0 as function of the parameter $p = a\Delta$. Values lower than one indicate a range of parameters, where the fidelity of the code $\mathcal{C}_{XZ}$ dominates over the one of a single spin.

one indicates that the code $\mathcal{C}_{XZ}$ is superior to plain qubits. Concluding, there is an advantage of the code $\mathcal{C}_{XZ}$ as expected in the regime if either the inter-spin distance a is short or the energy splitting Δ is low.

Conclusion

In this chapter a spin-boson model with dissipation was considered. As for a dissipative model no analytic solution for its time evolution is known a numerical method via master equations was chosen. Therefore, a master equation of Bloch-Redfield type was derived which was determined by a Redfield super-operator. This Redfield super-operator was calculated for the given model. It turned out that this operator for weak couplings provided the opportunity to determine the entanglement fidelity in an easy way. By analysing this entanglement fidelity the evaluation of quantum codes was possible. In particular, the extension of the code $\mathcal{C}_Z$ to the code $\mathcal{C}_{XZ}$, which respects Z and X couplings, was discussed in the scope of this work. As expected, it turned out that for a regime of a small product between inter-qubit distance and qubit splitting this code was superior to a plain qubit register.

7 Quantum error correction

Quantum codes $\mathcal{C}$ out of a Hilbert space Q in combination with quantum error correction are analysed. The analysed setting is given by a noise $\mathcal{N}$ acting on the selected code. According to previous chapters this noise arises due to interactions of the qubit register with its surrounding environment. Such a set of code $\mathcal{C}$ and noise $\mathcal{N}$ is evaluated by the entanglement fidelity. Additional in this chapter, error correction on the code $\mathcal{C}$ is implemented by a recovery operator $\mathcal{R}$ which acts after the noise on the system by $\mathcal{R}\circ\mathcal{N}$. The optimal recovery operator $\mathcal{R}$ is given by the optimisation of the entanglement fidelity as $\max_{\mathcal{R}} F_e(\mathcal{C}, \mathcal{R}\circ\mathcal{N})$. Thus the recovery operator which maximises the entanglement fidelity is the one which leads to optimal error correction. Accordingly, optimal error correction in this context means that there is no additional error by the error correcting mechanism itself.

Similarly to previous chapters all investigations are based on the spin-boson model. Concerning quantum error correction, a dissipative setting is not analysed within the scope of this work but again a dissipationless model is discussed. In difference to previous chapters not only the time evolution of a qubit register is observed as the mentioned error correction is implemented. Thereby, perfect quantum error correction is assumed and faulty quantum error correction is not dealt with. Two tasks are dealt with in this chapter. First, the benefits of quantum error correction in the dissipationless spin-boson model are outlined. Second, the combinations of quantum error correction together with symmetric subspaces are investigated. Existing methods are used to evaluate quantum error correction working on a given code and its corresponding noise. Most of these methods are formulated on the basis of a quantum noise which is given by its Kraus representation. Accordingly, starting point in this chapter is the representation of the spin system's dynamics in form of the Kraus representation in Sec. 7.1. This Kraus representation is obtained by a direct diagonalisation of the noise which was already determined in Chapter 2. This diagonalisation is realised by numerical methods. Having the Kraus representation a way is developed to evaluate the code $\mathcal{C}$. In Sec. 7.2 a lower bound for the corresponding entanglement fidelity in combination with quantum error correction is derived. This lower bound provides the opportunity to compare different codes. The robustness of a randomly chosen code with error correction is compared to the decoherence-reduced subspace $\mathcal{C}_Z$ combined with quantum error correction or without any correcting mechanism. This calculation is performed in the last part of this chapter. It turns out that decoherence-reduced subspaces with error correction are slightly more effective than decoherence-reduced subspaces without error correction. Furtheron, there exist randomly chosen codes which provide with error correction much better results than any decoherence-reduced subspace.

7.1 Kraus representation

Aim of this section is to calculate the Kraus representation for the dissipationless n-spin-boson model. Accordingly, the Hilbert space of the qubit register is N-dimensional, where $N = 2^n$ with n the number of qubits. From previous chapters it is known that the time evolution of the qubit register is determined by the unitary time evolution operator U_I of the joint system given as $\rho \mapsto \mathcal{N}(\rho) = \mathrm{tr}_E\{U_I \rho \otimes \rho_E U_I^\dagger\}$, where ρ is the reduced density operator of the spin system and the noise $\mathcal{N}$ is a completely positive map. According to the Kraus theorem [KBDW83, NC00] there exists a set of operators $A_1, \ldots, A_K$ with the properties, that for all reduced density operators ρ the noise can be expressed as

$$\mathcal{N}(\rho) = \sum_{k=1}^{K} A_k \rho A_k^\dagger \quad \text{with} \quad \sum_{k=1}^{K} A_k^\dagger A_k = \mathbb{1} \; . \tag{7.1}$$

As the dissipationless model is concerned, the time evolution has an alternative representation given by $\mathcal{N}(\rho) = \sum_{i,j} e^{-\mathrm{D}_{ij}} \rho_{ij}$, which was derived in Chapter 2. Here, the summation index is given by the states $|i\rangle$ and $|j\rangle$, which are elements of the computational basis $\{|1\rangle, \ldots, |N\rangle\}$ and D_{ij} is a decoherence coefficient (cf. Eq. (2.12)). This representation of the noise is reformulated as

$$\mathcal{N}(\rho) = \sum_{i,j=1}^{N} M_{ij} P_i \rho P_j \, , \tag{7.2}$$

where $M_{ij} = e^{-\mathrm{D}_{ij}}$ and $P_i = |i\rangle\langle i|$ is the projector on the normalised state $|i\rangle$. The introduced matrix $\mathbf{M}$ is symmetric as each decoherence coefficient D_{ij} itself is already symmetric. Now the matrix $\mathbf{M}$ is diagonalised by an orthogonal transformation $\mathbf{O}$ to $\mathbf{M} = \mathbf{O}^T \mathbf{\Lambda} \mathbf{O}$, where $\mathbf{\Lambda} = \mathrm{diag}(\lambda_1, \ldots, \lambda_N)$ with real and non-negative eigenvalues. There are $K \leq N$ of these eigenvalues larger than zero, such that finally the noise is given by

$$\mathcal{N}(\rho) = \sum_{k=1}^{K} \lambda_k \left(\sum_{i=1}^{N} O_{ki} P_i \right) \rho \left(\sum_{j=1}^{N} P_j O_{jk}^T \right) \; . \tag{7.3}$$

Comparing Eq. (7.1) and the derived Eq. (7.3), the Kraus operators are identified to be

$$A_k = \sqrt{\lambda_k} \sum_{i=1}^{N} O_{ki} P_i \, . \tag{7.4}$$

It is easy to see that in this special case the Kraus operators are self-adjoined, $A_k = A_k^\dagger$. A short calculation shows that also the condition $\sum_{k=1}^{K} A_k^\dagger A_k = \mathbb{1}$ holds. The formal expression of the Kraus operators in Eq. (7.4) is used later on.

7.2 Evaluating quantum codes

Now quantum codes together with quantum error correction are analysed. In the scope of this work a dissipationless spin-boson model is taken. Codes are embedded into the Hilbert space of the corresponding spin part. In contrast to previous chapters an additional error correction is taken into account. Thereby, perfect error-correction is assumed, meaning that the correction process itself is assumed to work without any error. Formally the investigated setting starts with a spin system having a Hilbert space Q and the interacting environment with Hilbert space E. An ancillary system R as a copy of Q is connected to the joint system as illustrated in Fig. 7.1. Then, the new joint system RQE with a code $\mathcal{C} \subset Q$ and its time evolution is investigated. An initial state

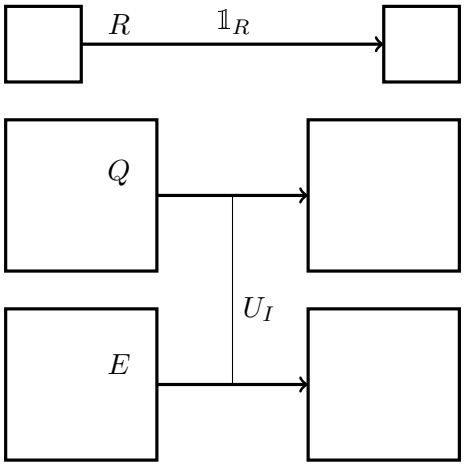

Figure 7.1: Illustration of the time evolution of the system RQE.

$|\psi\rangle_Q |\psi_E\rangle_E$ is investigated, where $|\psi\rangle \in Q$ is a state of the qubit register and $|\psi_E\rangle \in E$ is an arbitrary environment state. The dynamics on the system QE is given by the corresponding time evolution operator U_I (cf. Eq. (2.5)). According to the previously introduced Kraus operators A_i the time evolution of the initial state is obtained to be

$$U_I |\psi\rangle_Q |\psi_E\rangle_E = \sum_{i=1}^{K} A_i |\psi\rangle_Q |i\rangle_E \ . \tag{7.5}$$

Not only the system QE has to be taken into account, as also the ancillary system R is involved. Therefore, the initial state of the complete system is needed. Initially the state of the system RQ is taken to be a purification of the normalised projector onto the

desired code $\mathcal{C}$. This normalised projector $\pi_{\mathcal{C}}$ has a purification, given by

$$|\phi_{RQ}\rangle = \frac{1}{\sqrt{C}} \sum_{j=1}^{C} |j\rangle_R |j\rangle \ . \tag{7.6}$$

Here, a set of basis states of the code $\mathcal{C} = \text{Span}\{|1\rangle, \ldots, |C\rangle\}$ are chosen by $|j\rangle = \sum_{k=1}^{N} U_{jk} |k\rangle_Q$ with computational states $|k\rangle_Q$ and a unitary matrix $\mathbf{U}$. The total initial state of the system RQE is $|\phi_{RQ}\rangle |\psi_E\rangle \equiv |\psi_{RQE}\rangle$. Now the time evolution of the complete system is given by

$$\left|\psi'_{RQE}\right\rangle = (\mathbb{1}_R \otimes U_I) |\psi_{RQE}\rangle = \frac{1}{\sqrt{C}} \sum_{i=1}^{K} \sum_{m=1}^{C} |m\rangle_R \otimes A_i |m\rangle \otimes |i\rangle_E \ . \tag{7.7}$$

The corresponding density operator to this state is easily calculated to be

$$\psi'_{RQE} = \frac{1}{C} \sum_{i,j=1}^{K} \sum_{m,n=1}^{C} |m\rangle\langle n| \otimes A_i |m\rangle\langle n| A_j^\dagger \otimes |i\rangle\langle j| \ . \tag{7.8}$$

At this point full knowledge about the time evolution of the initial state ψ_{RQE} of the joint system RQE to the state ψ'_{RQE} is achieved. This result is the basis for further calculations. Schumacher and Westmoreland [SW02] delivered lower and upper bounds for the entanglement fidelity of the code $\mathcal{C}$ which were extended by Klesse [Kle07]. These bounds are given by

$$F(\rho'_{RE}, \rho_R \otimes \rho'_E) \leq F_e(\mathcal{C}, \mathcal{R} \circ \mathcal{N}) \leq \sqrt{F(\rho'_{RE}, \rho_R \otimes \rho'_E)} \,, \tag{7.9}$$

where $\mathcal{R}$ is any recovery operation. This result delivers a lower bound for the investigated code assuming optimal error correction on the one side and the best available Fidelity on the other side by simply taking the square root. Here, the fidelity between ρ'_{RE} and $\rho_R \otimes \rho'_E$ is calculated to get the desired bound. The occurring densities are calculated to be

$$\rho'_{RE} = \operatorname*{tr}_Q \psi'_{RQE} = \frac{1}{C} \sum_{i,j=1}^{K} \sum_{m,n=1}^{C} \left\langle n \middle| A_j^\dagger A_i \middle| m \right\rangle |m\rangle\langle n| \otimes |i\rangle\langle j| \ , \tag{7.10}$$

$$\rho'_E = \operatorname*{tr}_R \rho'_{RE} = \frac{1}{C} \sum_{i,j=1}^{K} \sum_{m=1}^{C} \left\langle m \middle| A_j^\dagger A_i \middle| m \right\rangle |i\rangle\langle j| \ , \tag{7.11}$$

$$\rho'_R = \rho_R = \frac{1}{C} \sum_{m=1}^{C} |m\rangle\langle m| \ , \tag{7.12}$$

by tracing out the corresponding parts of the system. With a restriction to the case of a dissipationless model the exact form of the derived Kraus representation in Eq. (7.4)

is inserted. Having these Kraus operators, a product of two of them is given by

$$A_i^\dagger A_j = \sqrt{\lambda_i \lambda_j} \sum_{l=1}^{N} O_{jl} P_l O_{li}^T \,, \tag{7.13}$$

where P_l is a projector on the computational state $|l\rangle_Q$. This result is inserted into the above standing density operators. Then, the projector P_l fishes the corresponding coefficients of the matrix $\mathbf{U}$ out of each state of the code $\mathcal{C}$ by $\langle n| P_l |m\rangle = U_{ln}^\dagger U_{ml}$. Accordingly, the density operator ρ'_{RE} is obtained to be

$$\rho'_{RE} = \frac{1}{C^2} \sum_{i,j=1}^{K} \sqrt{\lambda_i \lambda_j} \sum_{m,n=1}^{C} \sum_{l=1}^{N} O_{il} O_{jl} U_{ln}^\dagger U_{ml} \, |m\rangle\langle n| \otimes |i\rangle\langle j| \,, \tag{7.14}$$

whereas the density operator $\rho_R \otimes \rho'_E$ is given as

$$\rho_R \otimes \rho'_E = \frac{1}{C^2} \sum_{n=1}^{C} |n\rangle\langle n| \otimes \sum_{i,j=1}^{K} \sqrt{\lambda_i \lambda_j} \sum_{m=1}^{C} \sum_{l=1}^{N} O_{il} O_{jl} U_{lm}^\dagger U_{ml} \, |i\rangle\langle j| \,. \tag{7.15}$$

The fidelity of these two density operators, $F(\rho'_{RE}, \rho_R \otimes \rho'_E)$, has to be calculated to get the bounds of Eq. (7.9). In the scope of this work the fidelity is calculated by direct numerical methods, meaning that the right side of

$$F(\rho'_{RE}, \rho_R \otimes \rho'_E) = \left(\operatorname*{tr}_{R,E} \left\{ \sqrt{(\rho_R \otimes \rho'_E)^{1/2} \rho'_{RE} (\rho_R \otimes \rho'_E)^{1/2}} \right\} \right)^2 \tag{7.16}$$

is evaluated. Note that this expression is just the definition of the fidelity between the two inserted states.

7.2.1 Simplified model

In the previous section a method was shown to evaluate codes in combination with error correction for a dissipationless spin-boson model. For further progress, a simplified model of a generalised tetrahedron with n spins is chosen. Here, the distance in all decoherence functions with non-vanishing distance is set to the maximum distance, such that only two different functions, namely $\mathrm{K}(0)$ and $\mathrm{K}(r)$, occur. This model was already investigated by Klesse and Frank [KF05], but with a completely different method. The decoherence coefficient in this model is obtained to be

$$\mathrm{D}_{\nu\mu} = |\nu \oplus \mu| (\mathrm{K}(0) - \mathrm{K}(r)) + (|\nu| - |\mu|)^2 \, \mathrm{K}(r) \,, \tag{7.17}$$

where $|\cdot|$ denotes the Hamming weight, and $\oplus$ means a bitwise addition modulo 2 in $\mathbb{Z}_2^n$. As outlined in Sec. 7.1 the corresponding noise $\mathcal{N}$ and its Kraus representation is determined. Afterwards, codes $\mathcal{C}$ and their optimal quantum recovery operations $\mathcal{R}$ are analysed by evaluating their entanglement fidelity $F_e(\pi_\mathcal{C}, \mathcal{R} \circ \mathcal{N})$. Since the direct

calculation of the optimal recovery operator $\mathcal{R}$ seems unsolvable, a lower bound for the entanglement fidelity, given by Eq. (7.9), is evaluated.

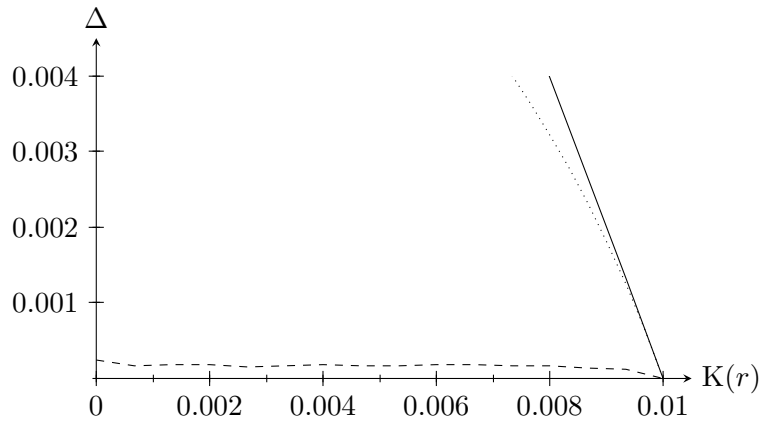

Figure 7.2: The parameter $\Delta = 1 - F_e$ is plotted as a function of the parameter $\mathrm{K}(r)$ for $\mathrm{K}(0) = 0.01$. The dashed line corresponds to the best found code of size two which is encoded into an array of four spins with additional error correction. The solid line gives Δ for a two-dimensional symmetric subspace $\mathcal{C}_Z$ without any error correction. The dotted line shows the best found code which is a subset of the four-dimensional code $\mathcal{C}_Z$ with error correction.

An optimisation for a single qubit. A lower bound for the fidelity of a single encoded qubit is searched for. The size of the spin lattice is taken to be $n = 4$. As a single qubit is encoded the dimension of the code is $C = 2$. For fixed values of $\mathrm{K}(0)$ and $\mathrm{K}(r)$ the matrix $\mathbf{M}$ and its eigensystem are determined to calculate the corresponding Kraus representation. Random codes are selected and their lower bound fidelity is calculated according to Eq. (7.16). Then, these codes are varied a little in a iterative algorithm to find a local (in code space) optimal code. This procedure is repeated for different starting codes. Sadly, the algorithm commonly leads to different optimal codes corresponding to modified starting conditions. In this way locally optimised codes are determined, each of them with a local maximised fidelity. Due to the lack of a better algorithm this result has to be evaluated. Accordingly, the code with the maximal lower bound of the entanglement fidelity gives the resulting lower bound and turns out to be the best found code. Of course, this procedure does not guarantee the locating of the global optimum. The results of this algorithm are shown in Fig. 7.2. As expected the error for the used decoherence-reduced subspace $\mathcal{C}_Z$ tends to zero as $\mathrm{K}(r) \to \mathrm{K}(0)$. This is due to the fact that for $\mathrm{K}(r) = \mathrm{K}(0)$ the qubits are located at one point. As the achieved minimal error for the codes with quantum error correction is in a wide range below the error of the decoherence-reduced subspace it clearly turns out that quantum error correction by far

outnumbers the effect of decoherence-reduced subspace.

Now error correction on a decoherence-reduced subspace formed by the code $\mathcal{C}_Z$ is investigated. In the present case the available Hilbert space is given by $\mathrm{Span}\{|0101\rangle, |0110\rangle, |1001\rangle, |1010\rangle\}$. Within this Hilbert space a two-dimensional code is selected. Then, the previous algorithm is applied to this code. An additional restriction that each varied code has to lie within the available Hilbert space is implemented into the algorithm. This algorithm is repeated several times for randomly chosen starting conditions. Again, it cannot be guaranteed to find the global optimum by this procedure. The resulting lower bound of this algorithm are also shown in Fig. 7.2. It turns out that in the examined case the investigated codes seem to be much less effective than randomly chosen codes.

Conclusion

In this chapter the possibilities of quantum error correcting codes were pointed out in the scope of a dissipationless spin-boson model. For this purpose, in a first step the Kraus representation of the quantum noise acting on the spin part of the spin-boson model was derived. Using this Kraus representation lower bounds of the entanglement fidelity were evaluated by numerical methods. It was shown that error correcting codes can easily be found which store quantum information much better than a decoherence-reduced subspace. In this way, the question dealt with in this chapter was completely answered. But, the general problem to find the optimal code even for the simplified dissipationless model was not answered satisfactorily. In this work the best code out of a number of locally optimised codes was selected. Thereby, the codes were optimised by selecting a basis which was orthogonal to the code and along all directions given by this basis better codes were looked for. According to this attempt and the high-dimensional Hilbert space, only a small amount of the possible code space around the given code was analysed. This method was chosen nevertheless as the fidelity was expressed in the form of coefficients of a computational basis and this algorithm seemed to be best suited to this form. In a first step, for this determination of the local optima a better algorithm might be invented. In a generalised setting of a normalised projector onto the code maybe a kind of gradient algorithm might be useful to find the optimal code. At this point also another fundamental problem should be mentionend: Due to the fact that optimal quantum error correction was assumed, results give a tendency but establishing quantum error correction remains a task on its own.

Conclusion

The present work contributes to a better understanding of the performance of quantum error-correcting and -avoiding methods. Conceptually this work started with general realisations of qubit registers and their time evolution in the scope of a spin-boson model. Afterwards the concept of quantum codes was introduced and a mechanism invented to evaluate them with or without error correction.

Specifically, quantum memory was analysed in the first chapters. The quantum memory was given by a qubit register and decoherence countered its stability. To illustrate different decoherence producing mechanisms several qubit constructions starting from fundamental Hamiltonians were presented. Each of these fundamental Hamiltonians was mapped onto a spin-boson model. All investigated realisations of qubits lead to a super-Ohmic coupling as a result of their three-dimensional environment given by thermal radiation. An Ohmic coupling would be expected e.g. for an effective one-dimensional environment. At this point it was possible to identify different classes of spin-boson models corresponding to different spectral densities and whether the interaction was dissipationless or involved dissipation. As a first step the time evolution of the spin part was determined within an analytical approach for a dissipationless model. These exact solutions of the spin system's dynamics for given settings are basic results of the present work. Using this knowledge about the time evolution allowed to investigate more complicated problems.

One of these problems is the encoding of quantum information into quantum codes. Quantum codes are subspaces of the Hilbert space associated to the spin part. Here, only block-type codes were investigated that encode each qubit into a couple of neighbouring spins in a regular manner. In this context, the decoherence-reduced subspaces $\mathcal{C}_Z$, $\mathcal{C}_X$ and $\mathcal{C}_{XZ}$ were introduced. These subspaces respect a certain symmetry of the interaction Hamiltonian if all spins are located at one point such that they are decoherence-free in this case. In the scope of this work a finite distance between the spins was analysed which broke the former symmetry, such that the codes ceased to be decoherence-free. A measure was needed to evaluate quantum codes. The channel fidelity between two states turned out to be the key ingredient for such a code measure. To calculate this measure the channel fidelity between each state out of the code and its time evolved state was determined and finally averaged over all possible initial code states. In this way an average code fidelity was constructed. For simplification, the entanglement fidelity was used as code measure which itself is a lower bound for the average fidelity. The derivation of easy to handle formulae for code fidelities is a fundamental result of

this work. Afterwards, the entanglement fidelity was analysed with respect to real experiments. It was shown that the measurement of a spin echo experiment corresponds to the determination of the entanglement fidelity, at least for a dissipationless interaction. For dissipative interaction this insight is only approximately correct, as long as time scales much below the relaxation time of the system are concerned. Using the derived measure the decoherence-reduced subspaces were evaluated and compared to a plain qubit register. In the case of a dissipationless coupling the decoherence-reduced subspaces turned out to have a much better fidelity than plain qubits without encoding. Trying to maintain more coherence also higher iterations of the symmetric codes were constructed and analysed. For these iterations a larger number of spins was used to encode a single qubit, but it turned out that no improvement in comparison to the first iteration could be achieved. To proceed, the case of a dissipative spin-boson model was analysed with the help of a master equation. In the case of couplings via Z and X the corresponding code $\mathcal{C}_{XZ}$ was evaluated. For that purpose, the asymptotic rate for long times of the entanglement fidelity was calculated in the regime of weak couplings. In this setting the symmetric code $\mathcal{C}_{XZ}$ was compared to a plain qubit register. It turned out that the symmetric code preserves coherence better than a plain qubit register as long as the product of inter-spin distances of the chain and the energy splitting of each spin was low.

The advantage of a certain code over a plain register does not prove that the optimal encoding is found. To fill this gap, the optimal encoding of a single qubit within a larger qubit lattice in a dissipationless model was determined. It turned out that the optimal two-dimensional encoding was given by the code $\mathcal{C}_Z$ and no better code could be found. It neither was possible to extend the derived result for a single qubit to a complete register nor to determine the optimal encoding for a dissipative coupling.

Concluding, the superiority of symmetric codes in comparison to plain qubits was shown, which is a main result of this work. Also to mention is that in the case of a dissipationless model the code $\mathcal{C}_Z$ turned out to be the best available block-type code to encode a single qubit.

In the last chapter quantum error correction was investigated within a dissipationless spin-boson model. Here, the error correction mechanism was assumed to operate perfectly to derive meaningful bounds for real error correction. For further progress not a spin chain but a generalised tetrahedron was analysed. To proceed, the Kraus representation of the dynamics of this model had to be calculated. With the help of this Kraus representation it was possible to determine bounds for the entanglement fidelity of codes within the given setting. By analysing these bounds different codes were first optimised and then compared to each other. Remarkably it turned out that randomly chosen codes reached better results than codes which were restricted to the previously introduced decoherence-reduced subspaces.

A Explicit calculations

The phase of states in an n-qubit register

The time evolution of a state within the spin-boson model was examined in Chapter 2. There, it was shown that the reduced density operator of the spin part ρ evolves in time according to $\mathcal{T}_t(\rho) = \mathcal{U}_t \circ \mathcal{N}_t(\rho)$. The contributions of $\mathcal{N}_t$ was dealt with in the scope of this work and the unitary part, given by $\mathcal{U}_t$ was neglected for several reasons. Here, some contributions to the unitary evolution operator $\mathcal{U}_t$ are closer investigated. Note that the whole problem is still analysed in the interaction picture and therefore the dynamics of the free Hamiltonian is not included into $\mathcal{U}_t$. To identify other contributions to $\mathcal{U}_t$, the complete time evolution of the spin-boson model in the interaction picture is reconsidered. As mentioned in Chapter 2 the complete time evolution is given by

$$U_I(t) = T_{\leftarrow} e^{-i\hbar^{-1}\int_0^t \mathrm{d}s\, \tilde{H}_I(s)}\,. \tag{A.1}$$

In the main part of this work, the chronological order by the operator $T_{\leftarrow}$ was neglected. Now this neglection and its consequences are considered. Solving the chronological order leads with the help of the Baker-Campell-Hausdorff formula to

$$U_I(t) = e^{-\frac{1}{2\hbar^2}\int_0^t \mathrm{d}s\, \int_0^t \mathrm{d}s'\, \Theta(s-s')[\tilde{H}_I(s),\tilde{H}_I(s')]} e^{-i\hbar^{-1}\int_0^t \tilde{H}_I(s)}\,. \tag{A.2}$$

Here, the part $e^{-\frac{1}{2\hbar^2}\int_0^t \mathrm{d}s\, \int_0^t \mathrm{d}s'\, \Theta(s-s')[\tilde{H}_I(s),\tilde{H}_I(s')]} \equiv e^{i\phi}$ leads to a phase ϕ which contributes to $\mathcal{U}_t$, the remaining part of Eq. (A.2) is dealt with in the main chapter. It has to be ensured that the phase ϕ is just a real number. For this purpose, the occurring commutator has to be determined. A short calculation reveals that this commutator is given as

$$[\tilde{H}_I(s), \tilde{H}_I(s')] = -2i\sum_{\mathbf{k}} |g_{|\mathbf{k}|}|^2 \sin(|\mathbf{k}|(s-s'))\sum_{\mathbf{m},\mathbf{n}} Z_{\mathbf{m}} Z_{\mathbf{n}} \cos(\mathbf{k}\cdot(\mathbf{r}_{\mathbf{m}} - \mathbf{r}_{\mathbf{n}}))\,. \tag{A.3}$$

By analysing this equation it is obvious that the phase ϕ is just a real number which depends on the index of the reduced density operator. The dependency on the states of the index arises due to the form of Eq. (2.10). To proceed, at this point the continuum limit of the bath modes has to be performed. Remaining integrals are solved using similarly techniques to those presented in the main chapter.

Zero distance decoherence function in the Ohmic case

In Chapter 2 the decoherence function $\mathrm{K}_1(0,t)$ for distance zero in case of Ohmic coupling was calculated. It was shown that this decoherence function is essentially given by the bath correlation function $\mathrm{C}_{-1}(w,z)$. Here, a special expression for this bath correlation function is derived. The investigated bath correlation function is by definition given as

$$\mathrm{C}_{-1}(w,z) = \int_0^\infty \mathrm{d}x\, x^{-1} e^{iwx}(1-\cos(xz))\coth\frac{x}{2}\,. \tag{A.4}$$

For further progress an additional integration is introduced by the following replacement. An elementary calculation shows that $\int_0^z \mathrm{d}s\, \sin(xs) = \frac{1-\cos(xz)}{x}$. This integration can be inserted into the previous expression. Together with some trivial steps the bath correlation function transforms to

$$\mathrm{C}_{-1}(w,z) = \frac{1}{2i}\int_0^z \mathrm{d}s \int_0^\infty \mathrm{d}x\, \frac{1}{e^x-1}\left(e^{x(1+i(w+s))} - e^{ix(w-s)} + e^{x(1+i(w+s))} - e^{ix(w-s)}\right)\,.$$

Now the integral definition of the digamma function is used to rewrite this expression as

$$\frac{1}{2i}\int_0^z \mathrm{d}s\,(\psi(-i(w-s)) - \psi(-i(w+s)) + \psi(1-i(w-s)) - \psi(1-i(w+s)))\,. \tag{A.5}$$

As the digamma function is the logarithmic derivation of the gamma function (cf. Definition. 4 in Appendix B) the bath correlation function is expressed by gamma functions,

$$\frac{1}{2i}\int_0^z \mathrm{d}s\, \frac{\mathrm{d}}{i\,\mathrm{d}s}(\ln\Gamma(i(s-w))\Gamma(1+i(s-w)) + \ln\Gamma(-i(s+w))\Gamma(1-i(s+w)))\,. \tag{A.6}$$

The well known recurrence relation for the gamma function (cf. Lemma. 11 in Appendix B) $\Gamma(z+1) = z\Gamma(z)$ is applied, such that the previous integral transforms to

$$\mathrm{C}_{-1}(w,z) = -\frac{1}{2}\int_0^z \mathrm{d}s\, \frac{\mathrm{d}}{\mathrm{d}s}\ln\Gamma^2(i(s-w))\Gamma^2(-i(s+w))(s^2-w^2)\,. \tag{A.7}$$

This integral is solved by the fundamental theorem of integration theory, resulting in

$$\mathrm{C}_{-1}(w,z) = \frac{1}{2}\ln\left(\frac{\Gamma^4(-iw)}{\Gamma^2(i(z-w))\Gamma^2(-i(z+w))}\frac{w^2}{w^2-z^2}\right)\,. \tag{A.8}$$

This is the expression for the bath correlation function which was used in Chapter 2 for further calculations.

Distance depending decoherence function in the Ohmic case

In Chapter 2 the decoherence function $\mathrm{K}_1(r,t)$ for a finite distance r in case of Ohmic coupling was derived. Here, the exact calculations for Eq. (2.29) and Eq. (2.30) are presented. Starting point is the integral representation of the decoherence function $\mathrm{K}_1(r,t)$. For a finite distance $r>0$ this representation is given by

$$\mathrm{K}_1(r,t) = \alpha \int_0^\infty \mathrm{d}\omega\, \omega^{-1}(1-\cos(\omega t))\frac{\sin(\omega r)}{\omega r}\coth\frac{\omega}{2T}\,\mathrm{cutoff}(\omega,\Omega)\,. \tag{A.9}$$

Here, the cut off is only introduced to ensure the convergence of the integral. Neither the explicit form of the cut off nor the cut-off parameter Ω will enter into the results. In a first step a new variable $x=\omega/(2T)$ is substituted. Taking care of the limit $r \gg 1/\Omega$ to negelect the cut off, the previous integral transforms to $\mathrm{K}_1(r,t) = \frac{\alpha}{2Tr}\int_0^\infty \mathrm{d}x\,\frac{1-\cos(2Ttx)}{x^2}\coth x\sin(2Trx)$. For a shorter notation the variables $\rho=2Tr$ and $\tau=2Tt$ are introduced. Using the symmetry of the integral occurring by $x\to -x$ it is easy to see that

$$\mathrm{K}_1(\rho,\tau) \;=\; \frac{\alpha}{2\rho}\int_{\mathbb{R}} \mathrm{d}x\,\frac{1-\cos(\tau x)}{x^2}\coth x\sin(\rho x)\,. \tag{A.10}$$

The further calculation is split into two parts, the first one given for times $t\le r$ and the second one for $t>r$.

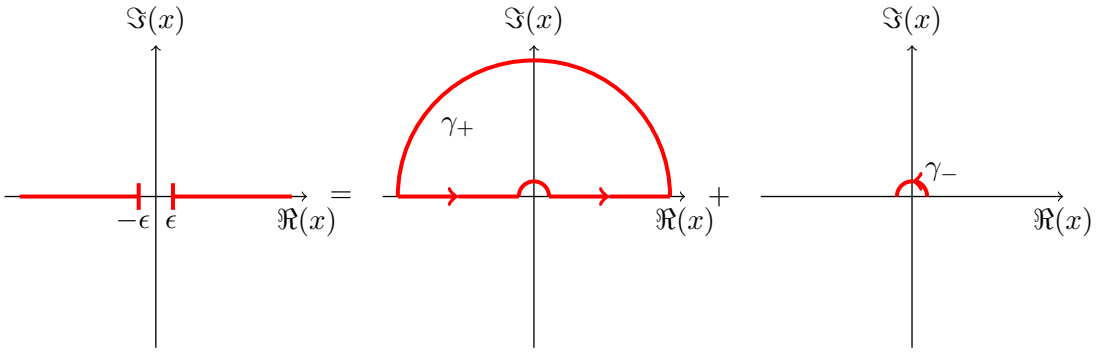

Figure A.1: This contour is used to calculate the primal value in Eq. (A.11).

Now the case of times $t\le r$ is considered. In a first step the occurring $\sin(\rho x)$ in Eq. (A.10) is replaced by $\Im[e^{i\rho x}]$. Then, the integrand is expanded over the complete complex plain. Having a complex variable $x\in\mathbb{C}$ the previous integral transforms into

$$\mathrm{K}_1(\rho,\tau) = \frac{\alpha}{2\rho}\Im\!\!\int \mathrm{d}x\,\frac{1-\cos(\tau x)}{x^2}\coth x e^{i\rho x}\,. \tag{A.11}$$

This integral is solved by the methods of contour integration with the contour (cf. Fig. A.1)

$$\not\int \equiv \lim_{\epsilon\to 0}\left(\int_{-\infty}^{-\epsilon} + \int_{\epsilon}^{\infty}\right) = \int_{\gamma_+} + \int_{\gamma_-}. \tag{A.12}$$

In the following common polylogarithms $\mathrm{Li}_s(x) = \sum_{l=1}^{\infty}\frac{x^l}{l^s}$ are needed. The mathematical positive part γ_+ of the contour is calculated to be

$$\begin{aligned}\int_{\gamma_+}\mathrm{d}x\,\frac{1-\cos(\tau x)}{x^2}\coth x e^{i\rho x} &= 2\pi i\sum_{l=1}^{\infty}\mathrm{Res}_{x=i\pi l}\left(\frac{1-\cos(\tau x)}{x^2}\coth x e^{i\rho x}\right)\\ &= 2\pi i\sum_{l=1}^{\infty}\frac{\cosh(\pi\tau l)-1}{\pi^2 l^2}e^{-\pi\rho l}\\ &= -\frac{2i}{\pi}\sum_{l=1}^{\infty}\frac{1}{l^2}\left(e^{-\pi\rho l}-\frac{1}{2}e^{-\pi(\rho-\tau)l}-\frac{1}{2}e^{-\pi(\rho+\tau)l}\right)\\ &= \frac{i}{\pi}\left(\mathrm{Li}_2\left(e^{-\pi(\rho-\tau)}\right)+\mathrm{Li}_2\left(e^{-\pi(\rho+\tau)}\right)-2\mathrm{Li}_2\left(e^{-\pi\rho}\right)\right).\end{aligned} \tag{A.13}$$

The missing negative part is $\int_{\gamma_-}\mathrm{d}x\,\frac{1-\cos(\tau x)}{x^2}\coth x e^{i\rho x} \underset{\epsilon\to 0}{=} \frac{\tau^2}{2}\int_{\gamma_-}\mathrm{d}x\,\frac{1}{x} = i\frac{\pi\tau^2}{2}$. Finally, for the case of times $t \le r$ the derived decoherence coefficient is

$$\mathrm{K}_1(r,t) = \alpha\left(\frac{\pi T t^2}{2r}+\frac{\mathrm{Li}_2\left(e^{-2\pi T(r-t)}\right)+\mathrm{Li}_2\left(e^{-2\pi T(r+t)}\right)-2\mathrm{Li}_2\left(e^{-2\pi Tr}\right)}{4\pi T r}\right). \tag{A.14}$$

This expression is used in Chapter 2 for further progress.

Now the case of times $t > r$ is examined. First the derivation of the decoherence coefficient with respect to the rescaled time τ is determined. Thereby, τ and ρ are defined as before. The investigated derivation turns out to be

$$\frac{\mathrm{d}\,\mathrm{K}_1(\rho,\tau)}{\mathrm{d}\tau} = \frac{\alpha}{2\rho}\int_{\mathbb{R}}\mathrm{d}x\,\frac{\sin(\tau x)}{x}\coth x\sin(\rho x). \tag{A.15}$$

Following the same idea as before the integrand is expanded over the complex plain. Thus, the derivation with complex variable $x \in \mathbb{C}$ is given as

$$\frac{\mathrm{d}\,\mathrm{K}_1(\rho,\tau)}{\mathrm{d}\tau} = \frac{\alpha}{2\rho}\Im\not\int\mathrm{d}x\,\frac{e^{i\tau x}}{x}\coth x\sin(\rho x). \tag{A.16}$$

Again, this integral is solved by methods of contour integration having the previously introduced contour. A short calculation reveals that the positive part of this contour is

given by

$$\int\limits_{\gamma_+} \mathrm{d}x\, \frac{e^{i\tau x}}{x} \coth x \sin(\rho x) = \frac{1}{2i} \left(\int\limits_{\gamma_+} \mathrm{d}x\, \frac{\coth x}{x} e^{ix(\tau+\rho)} - \int\limits_{\gamma_+} \mathrm{d}x\, \frac{\coth x}{x} e^{ix(\tau-\rho)} \right)$$
$$= i \ln\left(1 - e^{-\pi(\tau+\rho)}\right) - i \ln\left(1 - e^{-\pi(\tau-\rho)}\right), \tag{A.17}$$

whereas the negative contribution to the contour is given by

$$\int\limits_{\gamma_-} \mathrm{d}x\, \frac{e^{i\tau x}}{x} \coth x \sin(\rho x) \underset{\epsilon \to 0}{=} \rho \int\limits_{\gamma_-} \mathrm{d}x\, \frac{1}{x} = i\pi\rho\,. \tag{A.18}$$

By connecting these two results in the right manner the searched derivative is obtained to be

$$\frac{\mathrm{d}\,\mathrm{K}_1(\rho,\tau)}{\mathrm{d}\tau} = \frac{\alpha\pi}{2} + \frac{\alpha}{2\rho}\left(\ln\left(1 - e^{-\pi(\tau+\rho)}\right) - \ln\left(1 - e^{-\pi(\tau-\rho)}\right)\right). \tag{A.19}$$

To proceed, this derivative is integrated over the time interval from ρ to τ. This integral is given by

$$\int\limits_{\rho}^{\tau} \mathrm{d}\tilde{\tau}\, \frac{\mathrm{d}\,\mathrm{K}_1(\rho,\tilde{\tau})}{\mathrm{d}\tilde{\tau}} = \frac{\alpha\pi}{2}(\tau-\rho) + \frac{\alpha}{2\rho}\int\limits_{\rho}^{\tau} \mathrm{d}\tilde{\tau}\, \ln\left(1 - e^{-\pi(\tilde{\tau}+\rho)}\right) - \frac{\alpha}{2\rho}\int\limits_{\rho}^{\tau} \mathrm{d}\tilde{\tau}\, \ln\left(1 - e^{-\pi(\tilde{\tau}-\rho)}\right)$$
$$= \frac{\alpha\pi}{2}(\tau-\rho) + \frac{\alpha}{2\pi\rho}\left(\mathrm{Li}_2\left(e^{-\pi(\tau+\rho)}\right) - \mathrm{Li}_2\left(e^{-2\pi\rho}\right) - \mathrm{Li}_2\left(e^{-\pi(\tau-\rho)}\right) + \mathrm{Li}_2(1)\right). \tag{A.20}$$

To get the result for the decoherence coefficient in the investigated case of $t > r$, take the result of Eq. (A.14) with time equal to distance $\mathrm{K}_1(r,r)$ and add $\int_\rho^\tau \mathrm{d}\tilde{\tau}\, \frac{\mathrm{d}\,\mathrm{K}_1(\rho,\tilde{\tau})}{\mathrm{d}\tilde{\tau}}$. Taking care of the above calculated results and $\mathrm{Li}_2(1) = \zeta(3)$ the decoherence coefficient in the case of an Ohmic bath is

$$\mathrm{K}_1(r,t) = \alpha\left(\pi T\left(t - \frac{r}{2}\right) + \frac{\pi}{12Tr} + \frac{\mathrm{Li}_2\left(e^{-2\pi T(t+r)}\right) - \mathrm{Li}_2\left(e^{-2\pi T(t-r)}\right) - 2\mathrm{Li}_2\left(e^{-2\pi Tr}\right)}{4\pi Tr}\right). \tag{A.21}$$

This is the decoherence coefficient for times t which are larger than the distance r which is used in the main part of this work.

B Mathematical fundamentals

Transcendental functions

Transcendental functions occur in this work in the context of Chapter 2 where they are used to express decoherence functions. A good introduction to transcendental function is given in the book of Erdelyi et al. [EMOT53]. Here, definitions and integral representations of the used functions are given. Namely zeta functions and the whole family of gamma-, digamma- and polygamma functions are presented.

Definitions of transcendental functions

Definition 1. *For a complex variable* $s \in \mathbb{C}$ *with positive real part* $\Re[s] > 1$ *the zeta function is defined as* $\zeta_s = \sum_{n=1}^{\infty} \frac{1}{n^s}$.

Definition 2. *For a complex variable* $z \in \mathbb{C}$ *and a real variable* $s \in \mathbb{R}$ *the Hurwitz-zeta function is formally defined as* $\zeta_s(z) = \sum_{n=0}^{\infty} \frac{1}{(n+z)^s}$.

Definition 3. *For a complex variable* $z \in \mathbb{C}$ *the gamma function is defined as* $\Gamma(z) = \lim_{n\to\infty} \frac{n!n^z}{z(z+1)...(z+n)}$.

Definition 4. *The digamma function is the logarithmic derivation of the gamma function, and therefore for a complex variable* $z \in \mathbb{C}$ *given by* $\psi(z) = \frac{\mathrm{d}}{\mathrm{d}z} \ln \Gamma(z)$.

Definition 5. *The polygamma function* $\psi^{(n)}(z)$ *with complex variable* $z \in \mathbb{C}$ *is the* n^{th} *derivative of the digamma function,* $\psi^{(n)}(z) = \frac{\mathrm{d}^n}{\mathrm{d}z^n}\psi(z)$.

Integral representations of transcendental functions

Lemma 6. *For complex argument* $z \in \mathbb{C}$ *the Hurwitz-zeta function has the integral representation* $\zeta_n(z) = \frac{1}{\Gamma(n)} \int_0^{\infty} \mathrm{d}t \, \frac{t^{n-1}e^{-zt}}{1-e^{-t}}$.

Lemma 7. *For positive real part of* z, $\Re[z] > 0$, *the gamma function has the integral representation* $\Gamma(z) = \int_0^{\infty} \mathrm{d}t \, e^{-t}t^{z-1}$.

Lemma 8. *For complex argument* $z \in \mathbb{C}$ *the digamma function has the integral representation* $\psi(z) = -\gamma + \int_0^{\infty} \mathrm{d}t \, \frac{e^{-t} - e^{-zt}}{1-e^{-t}}$ *where* $\gamma = -\psi(1) = -\int_0^{\infty} \mathrm{d}t \, e^{-t} \ln(t)$.

Lemma 9. *For complex argument* $z \in \mathbb{C}$ *the integral representation of the polygamma function is* $\psi^{(n)}(z) = (-1)^{n+1} \int_0^{\infty} \mathrm{d}t \, \frac{t^n e^{-zt}}{1-e^{-t}}$ *for* $\Re(z) > 0$ *and* $n > 0$.

Recurrence relations of transcendental functions

Lemma 10. *For complex argument* $z \in \mathbb{C}$ *the recurrence relation for the Hurwitz-zeta function is* $\zeta_s(z+1) = \zeta_s(z) - \frac{1}{z^s}$.

Lemma 11. *For complex argument* $z \in \mathbb{C}$ *the recurrence relation for the gamma function is* $\Gamma(z+1) = z\Gamma(z)$. *Together with the value* $\Gamma(1) = 1$ *it is obvious that the gamma function generalises the factorial.* $n! = \Gamma(n+1)$ *holds for* $n \in \mathbb{N}$.

Lemma 12. *For complex argument* $z \in \mathbb{C}$ *the recurrence relation for the digamma function is* $\psi(z+1) = \psi(z) + \frac{1}{z}$.

Lemma 13. *For complex argument* $z \in \mathbb{C}$ *the recurrence relation for the polygamma function is* $\psi^{(n)}(z+1) = \psi^{(n)}(z) + (-1)^n n! z^{-n-1}$.

Properties of transcendental functions

Lemma 14. *The polygamma function can be expressed by the Hurwitz-zeta function as* $\psi^{(n)}(z) = (-1)^{n+1} n! \zeta_{n+1}(z)$.

Lemma 15. *For a complex variable* z, *with* $|z| \ll 1$ *the gamma function is approximated by* $\Gamma(z) = \frac{1}{z+O(z^2)}$.

Lemma 16. *For a real variable* $y \in \mathbb{R}$ *the absolute square of the gamma function fulfils* $|\Gamma(iy)|^2 = \frac{\pi}{y \sinh(\pi y)} = |\Gamma(-iy)|^2$.

Lemma 17. *With complex variables* $z, w \in \mathbb{C}$ *the digamma function satisfies* $\psi(w \pm iz) = \frac{\mathrm{d}}{\pm i \, \mathrm{d}z} \ln \Gamma(\omega \pm iz)$.

C Physical fundamentals

Harmonic oscillator

The explicit form of the states of a harmonic oscillator are needed to construct a quantum dot qubit in Section 1.3.3. For this purpose, a short introduction to the derivation of these states is presented.

Hermite polynomials

The states of the harmonic oscillator can be expressed in the form of Hermite polynomials. Thus, these Hermite polynomials are introduced.

Definition 18. *The n^{th} Hermite polynomial is defined as $H_n(z) = (-1)^n e^{z^2} \frac{\mathrm{d}^n}{\mathrm{d}z^n} e^{-z^2}$. Hence, the first Hermite polynomials are given by*

$$H_0(z) = 1, \quad H_1(z) = 2z, \quad H_2(z) = 4z^2 - 2, \quad H_3(z) = 8z^3 - 12z\,. \tag{C.1}$$

Lemma 19. *The n^{th} Hermite polynomial satisfies Hermite's differential equation, $H_n''(z) - 2xH_n'(z) + 2nH_n(z) = 0$.*

Quantum harmonic oscillator

The Hamiltonian of a harmonic oscillator with mass m and circular frequency ω_0 in one dimension is

$$\hat{H} = \frac{\hat{p}^2}{2m} + \frac{m\omega_0^2 \hat{x}^2}{2}\,, \tag{C.2}$$

where $\hat{p}$ is the momentum operator and $\hat{x}$ is the position operator. The stationary Schrödinger equation for this problem to energy E is

$$\frac{\mathrm{d}^2}{\mathrm{d}x^2}\varphi(x) = \left(\frac{m^2\omega_0^2}{\hbar^2}x^2 - \frac{2mE}{\hbar^2}\right)\varphi(x)\,. \tag{C.3}$$

To solve this differential equation the asymptotic behaviour for the limit $x \to \pm\infty$ is investigated. A first aim is to produce the first term on the right hand side by differentiating twice. The exponential ansatz

$$\varphi(x) = e^{-\beta x^2/2} f(\alpha x) \tag{C.4}$$

having a function $f(x)$ as well as free parameters α and β is chosen. Inserting this ansatz into the stationary Schrödinger equation leads to

$$\begin{aligned} e^{-\beta x^2/2}\left((\beta^2 x^2-\beta)f(\alpha x)-2\alpha\beta x f'(\alpha x)+\alpha^2 f''(\alpha x)\right) \\ =\left(\frac{m^2\omega_0^2}{\hbar^2}x^2-\frac{2mE}{\hbar^2}\right)e^{-\beta x^2/2}f(\alpha x)\,. \end{aligned} \tag{C.5}$$

The leading term on both sides vanishes if $\beta = m\omega_0/\hbar$, such that the following differential equation for the function $f(x)$ remains,

$$\alpha^2 f''(\alpha x)-2\alpha\beta x f'(\alpha x)+\left(\frac{2mE}{\hbar^2}-\beta\right)f(\alpha x)=0\,. \tag{C.6}$$

With the energies $E_n = \hbar\omega_0(n+\frac{1}{2})$ and $\alpha=\sqrt{\beta}$ for $n=0,1,2,\ldots$ this equation looks like

$$f''(\sqrt{\beta}x)-2\sqrt{\beta}x f'(\sqrt{\beta}x)+2nf(\sqrt{\beta}x)=0\,. \tag{C.7}$$

The solution of this equation for the function f is the n^{th} Hermite polynomial $H_n(\sqrt{\beta}x)$, such that the complete normalised state for $n\in\mathbb{N}_0$ of the harmonic oscillator is given by

$$\varphi_n(x)=\left(\frac{\beta}{\pi}\right)^{1/4}\frac{1}{\sqrt{2^n n!}}e^{-\beta x^2/2}H_n(\sqrt{\beta}x)\,. \tag{C.8}$$

Thus, the ground an first exited state of the harmonic oscillator are

$$\varphi_0(x)=\left(\frac{\beta}{\pi}\right)^{1/4}e^{-\beta x^2/2}\quad\text{and}\quad\varphi_1(x)=\left(\frac{\beta}{\pi}\right)^{1/4}e^{-\beta x^2/2}\sqrt{2\beta}x\,. \tag{C.9}$$

Quantisation of the electromagnetic field

The quantisation of the electromagnetic field is done in the canonical way on the basis of the Hamilton formalism similar to way presented in [Lou73]. Starting point is the vector potential $\mathbf{A}$ of the electromagnetic field. The coulomb gauge $\nabla\mathbf{A}=0$ is chosen for the vector potential. Technically this is performed by the gauge transformation $\mathbf{A}=\mathbf{A}_{\text{old}}+\frac{\nabla\chi(\mathbf{x},t)}{e}$ with gauge field $\chi(\mathbf{x},t)=\frac{e}{4\pi}\int_{\mathbb{R}^3}\mathrm{d}\mathbf{x}'\,\frac{\nabla'\mathbf{A}_{\text{old}}(\mathbf{x}',t)}{|\mathbf{x}-\mathbf{x}'|}$. This gauge field is the solution of the Poisson equation $\Delta\chi(\mathbf{x},t)=-e\nabla\mathbf{A}_{\text{old}}(\mathbf{x},t)$, which leads to the deserved condition of $\nabla\mathbf{A}=0$ for the new field. In this gauge the scalar potential $A_0=\Phi$ does not solve the wave equations but the Poisson equation

$$\Delta\Phi(\mathbf{x},t)=-\frac{\rho(\mathbf{x},t)}{\epsilon_0}\,. \tag{C.10}$$

A solution to the Poisson equation is given by

$$\Phi(\mathbf{x},t)=\frac{1}{4\pi\epsilon_0}\int\mathrm{d}\mathbf{x}'\,\frac{\rho(\mathbf{x}',t)}{|\mathbf{x}-\mathbf{x}'|}\,. \tag{C.11}$$

To proceed, the vector potential is decomposed in parallel part $\mathbf{A}_\parallel$ and transversal part $\mathbf{A}_\perp$, $\mathbf{A} = \mathbf{A}_\parallel + \mathbf{A}_\perp$. Forcing this decomposition to fulfil the requirement that $\nabla \mathbf{A}_\perp = 0$ and $\nabla \times \mathbf{A}_\parallel = 0$ leads to $\mathbf{A}_\parallel = 0$. Now an ansatz for the Hamiltondensity is performed. Thereby, the Hamiltondensity is chosen to be

$$\mathcal{H} = \mathcal{H}_{\text{em}} + \mathcal{H}_{\text{mat}} + \mathcal{H}_{\text{int}} \,, \tag{C.12}$$

where $\mathcal{H}_{\text{em}}$ is the contribution of the electromagnetic field, $\mathcal{H}_{\text{mat}}$ is the kinetic energydensity of non-relativistic particles and $\mathcal{H}_{\text{int}}$ is the interaction between matter and electromagnetic field. The Hamiltonian itself is given in the usual way as $H = \int \mathrm{d}\mathbf{x}\, \mathcal{H}$. It is known using the SI-system that

$$\mathcal{H}_{\text{em}} = \frac{\epsilon_0}{2}(\mathbf{E}^2 + c^2\mathbf{B}^2) - \rho\Phi \tag{C.13}$$

$$\mathcal{H}_{\text{int}} = -j_\mu A_\mu = -\mathbf{j}\cdot\mathbf{A}_\perp + \rho\Phi \tag{C.14}$$

The last term of $\mathcal{H}_{\text{int}}$ cancels with the last term in $\mathcal{H}_{\text{em}}$. Now the electric and magnetic fields in these equations are replaced by the vector potential according to existing connections. The magnetic field is expressed by $\mathbf{B} = \nabla \times \mathbf{A}_\perp$ and the electric field is given as $\mathbf{E} = -\nabla\Phi - \dot{\mathbf{A}}_\perp$. The decomposition of the electric field in longitudinal and transversal part is given by $\mathbf{E}_\parallel = -\nabla\Phi$ and $\mathbf{E}_\perp = -\dot{\mathbf{A}}_\perp$. To calculate the energy of the electromagnet field in H_{em} the integrals

$$\int \mathrm{d}\mathbf{x}\, \mathbf{E}_\parallel \cdot \mathbf{E}_\perp = \int \mathrm{d}\mathbf{x}\, \nabla\Phi \cdot \dot{\mathbf{A}}_\perp = \int \mathrm{d}\mathbf{x}\, [\nabla(\Phi\dot{\mathbf{A}}_\perp) - \Phi\nabla\dot{\mathbf{A}}_\perp] = 0 \tag{C.15}$$

and also

$$\int \mathrm{d}\mathbf{x}\, \mathbf{E}_\parallel \cdot \mathbf{E}_\parallel = \int \mathrm{d}\mathbf{x}\, \nabla\Phi \cdot \nabla\Phi = \int \mathrm{d}\mathbf{x}\, [\nabla(\Phi\nabla\Phi) - \Phi\Delta\Phi] = \frac{1}{\epsilon_0}\int \mathrm{d}\mathbf{x}\, \Phi\rho \tag{C.16}$$

are needed. Together with the matter interaction the Hamiltonian turns out to be

$$H_{\text{em}} + H_{\text{int}} = \frac{\epsilon_0}{2}\int \mathrm{d}\mathbf{x}\, (\mathbf{E}_\perp^2 + c^2\mathbf{B}^2) + \int \mathrm{d}\mathbf{x}\, \left(\frac{\Phi\rho}{2} - \mathbf{j}\cdot\mathbf{A}_\perp\right) . \tag{C.17}$$

The Hamiltonian describing the thermal field is extracted as

$$H_{\text{radiation}} = \frac{\epsilon_0}{2}\int \mathrm{d}\mathbf{x}\, \left(\dot{\mathbf{A}}_\perp^2 + c^2(\nabla \times \mathbf{A}_\perp)^2\right) . \tag{C.18}$$

This operator, describing thermal radiation, is used for further progress. For the completeness of this section also the full Hamiltonian of the investigated setting is derived. It is given by

$$H = \sum_j \frac{1}{2m_j}(\mathbf{p}_j - e_j\mathbf{A}_\perp(\mathbf{r}_j, t))^2 + H_{\text{radiation}} + \frac{1}{4\pi\epsilon_0}\sum_{i<j}\frac{e_i e_j}{|\mathbf{r}_i - \mathbf{r}_j|} + (\text{selfenergy}) \,. \tag{C.19}$$

Thermal radiation

For thermal radiation there is no charge density $\rho = 0$, such that the scalar potential vanishes, $\Phi = 0$. In radiation gauge there exists the relativistic Lorentz convention $\partial_\mu A_\mu = 0$, such that $\mathbf{A}_\perp$ fulfils the homogeneous wave equation $\Box \mathbf{A}_\perp = 0$. The ansatz $\mathbf{A}_l(\mathbf{x}, t) = \mathbf{u}_l(\mathbf{x}) q(t)$ is chosen with $\nabla \mathbf{u}_l = 0$ and $\mathbf{A}(\mathbf{x}, t) = \sum_l \mathbf{A}_l(\mathbf{x}, t)$. The eigenmodes $\mathbf{u}_l$ have to be orthogonal to each other, such that $\int \mathrm{d}\mathbf{x}\, \mathbf{u}_l(\mathbf{x}) \cdot \mathbf{u}_m(\mathbf{x}) = \delta_{lm}$. Using this notation the Hamiltonian of the thermal field has the form

$$H_{\text{radiation}} = \frac{\epsilon_0}{2} \sum_l (\dot{q}_l^2 + \omega_l^2 q_l^2) \,. \tag{C.20}$$

Canonical variables $Q_l = q_l \sqrt{\epsilon_0}$ and $P_l = \dot{q}_l \sqrt{\epsilon_0}$ are introduced. The quantised version of this canonical variables is $Q_l = \sqrt{\frac{\hbar}{2\omega_l}} (a_l + a_l^\dagger)$ with creation and annihilation operators $a_l^\dagger, a_l$. The vector potential with the same ansatz is given by

$$\mathbf{A}(\mathbf{x}, t) = \sum_l \mathbf{u}_l(\mathbf{x}) \sqrt{\frac{\hbar}{2\epsilon_0 \omega_l}} (a_l e^{-i\omega_l t} + a_l^\dagger e^{i\omega_l t}) \,, \tag{C.21}$$

where the Heisenberg picture is chosen. Using common impulse eigenstates with parameters $l = \mathbf{k}\lambda$ and polarisation $\lambda = 1, 2$, $\mathbf{u}_{\mathbf{k}\lambda}(\mathbf{x}) = \nu^{-1/2} e^{i\mathbf{k}\mathbf{x}} \epsilon_{\mathbf{k}\lambda}$ leads to

$$\mathbf{A}(\mathbf{x}, t) = \frac{1}{\sqrt{\nu}} \sum_{\mathbf{k},\lambda} \sqrt{\frac{\hbar}{2\epsilon_0 \omega_k}} (a_{\mathbf{k}\lambda} e^{i(\mathbf{k}\mathbf{x} - \omega_k t)} \epsilon_{\mathbf{k}\lambda} + a_{\mathbf{k}\lambda}^\dagger e^{-i(\mathbf{k}\mathbf{x} - \omega_k t)} \epsilon_{\mathbf{k}\lambda}^*) \,. \tag{C.22}$$

With the relation $\mathbf{E}_\perp(\mathbf{x}, t) = -\dot{\mathbf{A}}(\mathbf{x}, t)$ the electric field is calculated to be

$$\mathbf{E}_\perp(\mathbf{x}, t) = \frac{i}{\sqrt{\nu}} \sum_{\mathbf{k},\lambda} \sqrt{\frac{\hbar\omega_k}{2\epsilon_0}} (a_{\mathbf{k}\lambda} e^{i(\mathbf{k}\mathbf{x} - \omega_k t)} \epsilon_{\mathbf{k}\lambda} - a_{\mathbf{k}\lambda}^\dagger e^{-i(\mathbf{k}\mathbf{x} - \omega_k t)} \epsilon_{\mathbf{k}\lambda}^*) \,. \tag{C.23}$$

The magnetic field is determined, using $\mathbf{B}(\mathbf{x}, t) = \nabla \times \mathbf{A}(\mathbf{x}, t)$, as

$$\mathbf{B}(\mathbf{x}, t) = \frac{1}{c} \frac{i}{\sqrt{\nu}} \sum_{\mathbf{k},\lambda} \sqrt{\frac{\hbar\omega_k}{2\epsilon_0}} \frac{\mathbf{k}}{|\mathbf{k}|} \times (a_{\mathbf{k}\lambda} e^{i(\mathbf{k}\mathbf{x} - \omega_k t)} \epsilon_{\mathbf{k}\lambda} - a_{\mathbf{k}\lambda}^\dagger e^{-i(\mathbf{k}\mathbf{x} - \omega_k t)} \epsilon_{\mathbf{k}\lambda}^*) \,. \tag{C.24}$$

Performing the continuum limit of the modes is done by

$$\sum_{\mathbf{k},\lambda} \to \sum_\lambda \frac{\nu}{(2\pi)^3} \int_0^{2\pi} \mathrm{d}\varphi \int_0^{\pi} \mathrm{d}\theta \, \sin\theta \int_0^{\infty} \mathrm{d}k \, k^2 \,. \tag{C.25}$$

This limit is often performed in the scope of this work to derive easier expressions.

Quantum mechanics of the atom - absorption and emission

The Einstein theory of absorption and emission is outlined in this section. This introduction is performed similar to the way presented in Rodney Loudon's book [Lou73]. The basic interaction processes between electromagnetic radiation and atoms are considered. For this purpose, imagine a gas of N identical atom, each atom having a pair of bound-state energy levels E_1 and E_2, such that $\hbar\omega_0 = E_2 - E_1$. These atomic levels might be multiplets, with degeneracies g_1 and g_2, but for simplicity all other atomic levels are neglected. The number of atoms that have energies E_1 and E_2 are denoted by the level population N_1 and N_2 respectively. The probabilities per unit time of photon

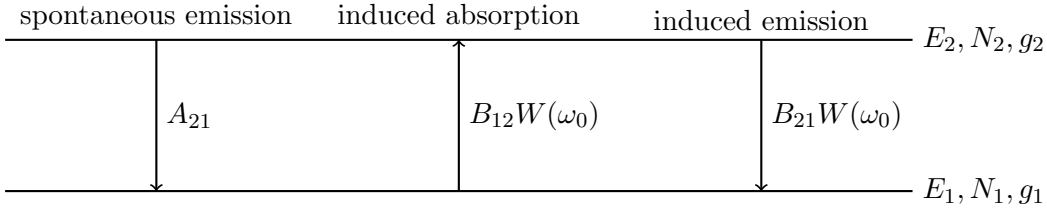

Figure C.1: The three basic kinds of radiative processes.

absorption and emission are defined as follows. For an atom in state 2 there is a finite probability A_{21} to decay spontaneous into state 1. There also is a thermally induced probability $B_{21}W(\omega_0)$, with energy density $W(\omega_0)$, that this emission takes place. On the other hand thermal activity can also lead to absorption with probability $B_{12}W(\omega_0)$. The coefficients A_{21}, B_{21} and B_{12} are called Einstein coefficients. Accordingly, the rate for the populations of the different energy levels are given by

$$\dot{N}_1(t) = -\dot{N}_2(t) = N_2 A_{21} - N_1 B_{12} W(\omega_0) + N_2 B_{21} W(\omega_0)\,. \tag{C.26}$$

In thermal equilibrium, the level populations are constant, such that $N_2 A_{21} - N_1 B_{12} W_T(\omega_0) + N_2 B_{21} W_T(\omega_0) = 0$. This equation is transformed, such that the energy density $W_T(\omega_0)$ turns out to be

$$W_T(\omega_0) = \frac{A_{21}}{(N_1/N_2)B_{12} - B_{21}}\,. \tag{C.27}$$

As the level populations N_1 and N_2 are related in thermal equilibrium by Boltzmann's distribution their quotient is given by $N_1/N_2 = g_1 \exp(-E_1/k_B T)/(g_2 \exp(-E_2/k_B T)) = (g_1/g_2)\exp(\hbar\omega_0/k_B T)$. This result is inserted into the previous equation, such that the energy density is

$$W_T(\omega_0) = \frac{A_{21}}{(g_1/g_2)\exp(\hbar\omega_0/k_B T)B_{12} - B_{21}}\,. \tag{C.28}$$

To be consistent with Planck's law, which is given by

$$W_T(\omega_0)\,\mathrm{d}\omega_0 = \frac{\hbar\omega_0^3}{\pi^2 c^3}\frac{\mathrm{d}\omega_0}{\exp(\hbar\omega_0/k_B T)-1} \tag{C.29}$$

the parameters of the chosen model are identified as

$$(g_1/g_2)B_{12} = B_{21} \quad \text{and} \quad (\hbar\omega_0^3/\pi^2 c^3)B_{21} = A_{21}\,. \tag{C.30}$$

The Einstein coefficients for atomic processes are determined within the Weisskopf-Wigner theory in the next section.

Weisskopf-Wigner theory

The Weisskopf-Wigner theory describes the spontaneous emission between two atomic levels. In the scope of this work this theory provides a rate for the spontaneous emission which can be compared to results in the chapter about dissipative couplings. Here, a presentation close to the book of Scully and Zubairy [SZ97] is chosen. Accordingly, a Hamiltonian consisting of three parts is investigated. The first part describes the atom, the second one a thermal bath and third one the interaction in between the previous parts. The interaction picture is chosen for calculations. In this picture the interaction Hamiltonian in the rotating-wave approximation is given by

$$\tilde{H}_I(t) = \hbar\sum_{\mathbf{k},\lambda} g^*_{\mathbf{k}}(\mathbf{r}_0)\sigma_+ a_{\mathbf{k},\lambda} e^{i(\omega_0-\omega_k)t} + H.c.\,, \tag{C.31}$$

where $g^*_{\mathbf{k}}(\mathbf{r}_0) = g_{\mathbf{k}} e^{i\mathbf{k}\cdot\mathbf{r}_0}$ is a coupling coefficient and $\mathbf{r}_0$ is the location of the atom.

The atom is assumed to be initially in the excited state at time $t = 0$. The initial state vector is therefore given by

$$|\,\psi(t)\rangle = c_e(t)\,|\,e,0\rangle + \sum_{\mathbf{k},\lambda} c_{g,k}(t)\,|\,g,1\rangle \tag{C.32}$$

with probability amplitudes $c_e(0) = 1$ and $c_{g,k}(0) = 0$. Here, the time dependency of the state is transferred to these probability amplitudes. The initial state is inserted into the Schrödinger equation $\left|\dot{\psi}(t)\right\rangle = \frac{1}{i\hbar}\tilde{H}_I(t)\,|\,\psi(t)\rangle$. This results in a set of equations of motion for the probability amplitudes given by

$$\dot{c}_e(t) = \frac{1}{i\hbar}\sum_{\mathbf{k},\lambda} g^*_{\mathbf{k}}(r_0) e^{i(\omega_0-\omega_k)t} c_{g,\mathbf{k}}(t) \quad \text{and} \quad \dot{c}_{g,\mathbf{k}}(t) = \frac{1}{i\hbar} g_{\mathbf{k}}(r_0) e^{-i(\omega_0-\omega_k)t} c_e(t)\,. \tag{C.33}$$

The aim is to derive an equation that involves c_e only. Hence, first the second equation

is integrated over the time interval from zero to t, such that

$$c_{g,\mathbf{k}}(t) = \frac{1}{i\hbar} g_k(r_0) \int_0^t \mathrm{d}\tau \, e^{-i(\omega_0-\omega_k)\tau} c_e(\tau) \,. \tag{C.34}$$

This result is substituted into the first equation to get a differential equation for the coefficient c_e. This differential equation is given by

$$\dot{c}_e(t) = -\sum_{\mathbf{k}} \frac{|g_{\mathbf{k}}(r_0)|^2}{\hbar^2} \int_0^t \mathrm{d}\tau \, e^{i(\omega_0-\omega_k)(t-\tau)} c_e(\tau) \,. \tag{C.35}$$

Now the continuum limit of the bath modes is performed. Accordingly, $\sum_{\mathbf{k},\lambda}$ is replaced by $\sum_\lambda \frac{\nu}{(2\pi)^3} \int_0^{2\pi} \mathrm{d}\varphi \int_0^{\pi} \mathrm{d}\theta \, \sin\theta \int_0^{\infty} \mathrm{d}k \, k^2$. For further progress the absolute square of the coupling coefficients $|g_{\mathbf{k}}(r_0)|^2$ has to be determined. In the derivation of the dipole-interaction Hamiltonian in Sec. 1.3.1 these coefficients were given as

$$|g_{\mathbf{k}}(r_0)|^2 = \frac{\hbar\omega_k}{2\epsilon_0 \nu} |\wp_{eg}|^2 (\cos^2\theta \cos^2\varphi + \sin^2\varphi) \,. \tag{C.36}$$

By inserting this result in the previous equation it takes the form of

$$\dot{c}_e(t) = -\frac{4|\wp_{eg}|^2}{(2\pi)^2 6\hbar\epsilon_0 c^3} \int_0^{\infty} \mathrm{d}\omega \, \omega^3 \int_0^t \mathrm{d}\tau \, e^{i(\omega_0-\omega)(t-\tau)} c_e(\tau) \,. \tag{C.37}$$

To continue, the border of the integration over the modes is lowered to minus infinity. This allowes to use $\int_{-\infty}^{\infty} \mathrm{d}\omega \, e^{i(\omega_0-\omega)(t-\tau)} = 2\pi\delta(t-\tau)$. By performing this the Weisskopf-Wigner approximation is applied. Thereby, a differential equation of first order having a rate γ_0 is achieved which has the form of

$$\dot{c}_e(t) = -\frac{\gamma_0}{2} c_e(t) \quad \text{and} \quad \gamma_0 = \frac{1}{4\pi\epsilon_0} \frac{4\omega_0^3 |\wp_{eg}|^2}{3\hbar c^3} \,. \tag{C.38}$$

A solution to this differential equation is given by the exponential function with $-\gamma_0 t/2$ as exponent. For the diagonal term of the system density corresponding to the excited state this means

$$\rho_{ee} \equiv |c_e(t)|^2 = e^{-\gamma_0 t} \,. \tag{C.39}$$

By comparing this result with the definition of the Einstein coefficients identifies the rate γ_0 to be given by $\gamma_0 = B_{12} W(\omega_0)$ As the energy density of a single photon is $W(\omega_0) = \hbar\omega_0^3/\pi^2 c^3$ the Einstein coefficient for induced emission is read off to be

$$B_{12} = \frac{\pi}{4\epsilon_0} \frac{4|\wp_{eg}|^2}{3\hbar^2} \,. \tag{C.40}$$

Accordingly the rate of spontaneous emission is given by

$$A_{21} = \frac{g_1}{g_2}\frac{1}{4\pi\epsilon_0}\frac{4\omega^3|\wp_{eg}|^2}{3\hbar c^3}\,. \tag{C.41}$$

The Rabi model and Bloch equations

The interaction of a two level system which is in contact to a classical field is investigated by the Rabi Model. A two level system having a ground state $|\,g\,\rangle$ and an excited state $|\,e\,\rangle$ together with a classical electric field $\mathbf{E}(t) = E_0\cos(\omega t)\mathbf{e}_x$ is considered. The interaction Hamiltonian is given via dipole interaction as

$$\tilde{H}_I(t) = -\underline{\mathcal{D}}\cdot\mathbf{E}(t) = -\wp_{eg}E_0\cos(\omega t) \tag{C.42}$$

with dipole operator $\underline{\mathcal{D}} = e\mathbf{r}$. By setting the groundstate energy to zero the Hamiltonian describing the atom $\hat{H}_S = \frac{1}{2}\hbar\omega_0 Z$ is rewritten as

$$\hat{H}_S = \hbar\omega_0\,|\,e\,\rangle\langle\,e\,|\,, \tag{C.43}$$

leading to time depending states $|\,g(t)\,\rangle = |\,g\,\rangle$ and $|\,e(t)\,\rangle = e^{-i\omega_0 t}\,|\,e\,\rangle$. As a classical field is concerned the Hamiltonian describing the field itself is zero, $\hat{H}_E = 0$, such that the full Hamiltonian has the form

$$\hat{H} = \hbar\omega_0\,|\,e\,\rangle\langle\,e\,| - \wp_{eg}E_0\cos(\omega t) \tag{C.44}$$

Let the two level system be in the state

$$|\,\psi(t)\,\rangle = c_g(t)\,|\,g\,\rangle + c_e(t)e^{-i\omega_0 t}\,|\,e\,\rangle\,, \tag{C.45}$$

with time dependent coefficients $c_g(t)$ and $c_e(t)$. Applying Schrödinger's Equation $i\hbar\partial_t\,|\,\psi(t)\,\rangle = \hat{H}\,|\,\psi(t)\,\rangle$ gives

$$i\hbar\partial_t\,|\,\psi(t)\,\rangle = i\hbar\dot{c}_g(t)\,|\,g\,\rangle + i\hbar\dot{c}_e(t)e^{-i\omega_0 t}\,|\,e\,\rangle + \hbar\omega_0 e^{-i\omega_0 t}\,|\,e\,\rangle \quad \text{and} \tag{C.46}$$

$$\hat{H}\,|\,\psi(t)\,\rangle = E_0\cos(\omega t)\wp_{eg}c_e(t)e^{-i\omega_0 t}\,|\,g\,\rangle + E_0\cos(\omega t)\wp^*_{eg}c_g(t)\,|\,e\,\rangle + \hbar\omega_0 e^{-i\omega_0 t}\,|\,e\,\rangle\,. \tag{C.47}$$

The coefficients of the ground and exited state are compared. By introducing the constant $\nu = \frac{E_0\wp_{eg}}{\hbar}$ these equations are rewritten as differential equations for the coefficients c_g and c_e. The resulting differential equations are given by

$$\dot{c}_g(t) = -i\nu\cos(\omega t)e^{-i\omega_0 t}c_e(t) \quad \text{and} \quad \dot{c}_e(t) = -i\nu^*\cos(\omega t)e^{i\omega_0 t}c_g(t)\,. \tag{C.48}$$

For further progress the initial conditions $c_g(0) = 1$ and $c_e(0) = 0$ are taken. The cosine is written by Euler's construction in the form of exponential functions. Then, the

rotating wave approximation is applied and reveals

$$\dot{c}_g(t) = 0 \quad \text{and} \quad \dot{c}_e(t) = -i\frac{\nu^*}{2}e^{-i(\omega-\omega_0)t}c_g(t)\,. \tag{C.49}$$

The detuning of the system is defined as $\Delta := \omega - \omega_0$ and describes how far the system is driven off resonance. A simple integrating of the previous equation leads to

$$c_e(t) = -i\frac{\nu^*}{\Omega_R}e^{-i\Delta t/2}\sin\left(\frac{\Omega_R t}{2}\right) \tag{C.50}$$

with the Rabi frequency $\Omega_R = \sqrt{\Delta^2 + |\nu|^2}$. Accordingly the population of the excited level shows Rabi oscillations given by $\rho_{ee}(t) = c_e(t)c_e^*(t) \sim \sin^2\left(\frac{\Omega_R t}{2}\right)$.

Bloch equations

The famous Bloch equations [Blo46] are easily obtained at this point. With $i, j \in \{g, e\}$ the system's density is $\rho_{ij} = c_i c_j^*$. It is known that the trace of a density is equal to one, $\rho_{gg} + \rho_{ee} = 1$. The time derivative of the density is given as

$$\frac{\mathrm{d}}{\mathrm{d}t}\rho_{ij} = \left(\frac{\mathrm{d}}{\mathrm{d}t}c_i\right)c_j^* + c_i\left(\frac{\mathrm{d}}{\mathrm{d}t}c_j^*\right) \tag{C.51}$$

The previously calculated coefficients are inserted, such that

$$\frac{\mathrm{d}}{\mathrm{d}t}\rho_{ee} = -i\cos(\omega t)\left(\nu^* e^{i\omega_0 t}\rho_{ge} - \nu e^{-i\omega_0 t}\rho_{eg}\right), \tag{C.52a}$$

$$\frac{\mathrm{d}}{\mathrm{d}t}\rho_{eg} = -i\cos(\omega t)\nu^* e^{i\omega_0 t}(\rho_{ee} - \rho_{gg})\,. \tag{C.52b}$$

The rotating wave approximation is applied to these equations, such that the Bloch equations are derived. These Bloch equations are therefore given by

$$\frac{\mathrm{d}}{\mathrm{d}t}\rho_{ee} = -\frac{i}{2}\left(\nu^* e^{i(\omega_0-\omega)t}\rho_{ge} - \nu e^{-i(\omega_0-\omega)t}\rho_{eg}\right), \tag{C.53a}$$

$$\frac{\mathrm{d}}{\mathrm{d}t}\rho_{eg} = -\frac{i}{2}\nu^* e^{i(\omega_0-\omega)t}(\rho_{ee} - \rho_{gg})\,. \tag{C.53b}$$

Bibliography

[Ben80] P. Benioff. The computer as a physical system: a microscopic quantum mechanical Hamiltonian model of computers as represented by Turing machines. *Journal of Statistical Physics*, 22:563–591, 1980.

[BK08] S. Borghoff and R. Klesse. Decoherence of encoded quatum registers. *Phys. Rev. A*, 77(1):012306, 2008.

[Blo46] F. Bloch. Nuclear induction. *Phys. Rev*, 70(7&8):460–474, 1946.

[BLW99] D. Bacon, D. A. Lidar, and K. B. Whaley. Robustness of decoherence-free subspaces for quantum computation. *Phys. Rev. A*, 60(3):1944–1955, 1999.

[BP02] H.-P. Breuer and F. Petruccione. *The theory of open quantum systems.* University Press, Oxford, 2002.

[BVJD98] V. Bouchiat, D. Vion, P. Joyez, and M. H. Devoret. Quantum coherence with a single Cooper pair. *Physica Script*, T76:165–170, 1998.

[Cho75] M. Choi. Completely positive linear maps on complex matrices. *Linear Algebra and Appl.*, 10:285–290, 1975.

[CNHM03] I. Chiorescu, Y. Nakamura, C. J. P. M. Harmans, and J. E. Mooij. Coherent quantum dynamics of a superconducting flux-qubit. *Science*, 299:2003, 2003.

[CS96] A. R. Calderbank and P. W. Shor. Good quantum error-correcting codes exist. *Phys. Rev. A*, 54(2):1098–1105, 1996.

[Deu85] D. Deutsch. Quantum theory, the church-turing principle and the universal quantum computer. *Proc. Roy. Soc., London*, A400:97–117, 1985.

[DG98] L.-M. Duan and G.-C. Guo. Reducing decoherence in quantum-computer memory with all quantum bits coupling to the same environment. *Phys. Rev. A*, 57(2):737–741, 1998.

[DWHK07] R. Doll, M. Wubs, P. Hänggi, and S. Kohler. Incomplete pure deephasing of N-qubit entangled W states. *Phys. Rev. B*, 76(4):045317, 2007.

[EMOT53] A. Erdelyi, W. Magnus, F. Oberhettinger, and F.G. Tricomi. *Higher transcendental functions.* McGraw-Hill Book Company, Inc., 1953.

[Fey82] R. P. Feynman. Simulating physics with computers. *International Journal of Theoretical Physics*, 21(6&7):467–488, 1982.

[Fey86] R. P. Feynman. Quantum mechanical computers. *Foundations of Physics*, 16:507–531, 1986.

[FLS65] R. P. Feynman, R. B. Leighton, and M. Sands. *The Feynman lectures on physics. 3: quantum mechanics.* Addison-Wesley, 1965.

[GJK+96] D. Giulini, E. Joos, C. Kiefer, J. Kupsch, I.-O. Stamatescu, and H. D. Zeh. *Decoherence and the appearance of a classical world in quantum theory.* Springer-Verlag, Berlin, 1996.

[Gro96] L. K. Grover. Quantum mechanics helps in searching for a needle in a haystack. *Phys. Rev. Lett.*, 79(2):325–328, 1996.

[GWO00] R. Grimm, M. Weidemuller, and Y. B. Ovchinnikov. Optical dipole traps for neutral atoms. *Molecular and Optical Physics*, 42:95, 2000.

[Hah50] E. L. Hahn. Spin echoes. *Phys. Rev*, 80(4):580–594, 1950.

[HHH99] M. Horodecki, P. Horodecki, and R. Horodecki. General teleportation channel, singlet fraction, and quasidistillation. *Phys. Rev. A*, 60(3):1888–1898, Sep 1999.

[Joz94] R. Jozsa. Fidelity for mixed quantum states. *Journal of Modern Optics*, 41:2315–2324, 1994.

[Joz97] R. Jozsa. Entanglement and quantum computation. *Geometric Issues in the Foundations of Science*, 1997.

[KBDW83] K. Kraus, A. Böhm, J. D. Dollard, and W. H. Wootters. *States, Effects, and Operations: Fundamental Notions of Quantum Theory.* Lecture Notes in Physics, Berlin Springer Verlag, 1983.

[KF05] R. Klesse and S. Frank. Quantum error correction in spatially correlated quantum noise. *Phys. Rev. Lett.*, 95(23):230503, 2005.

[Kle07] R. Klesse. A random coding based proof for the quantum coding theorem. *Open Systems and Information Dynamics*, 15:21–45, 2007.

[KLZ98] E. Knill, R. Laflamme, and W. H. Zurek. Resilent quantum computation: error models and thresholds. *Proc. Roy. Soc., London*, A454:365, 1998.

[LCW98] D.A. Lidar, I.L. Chuang, and K.B. Whaley. Decoherence free subspaces for quantum computation. *Phys. Rev. Lett.*, 81(12):2594–2597, 1998.

[LD98] D. Loss and D. P. DiVincenzo. Quantum computation with quantum dots. *Phys. Rev. A*, 57(1):120–126, 1998.

[Lou73] R. Loudon. *The quantum theory of light.* University Press, Oxford, 1973.

[Lyn95] R. Lynch. The quantum phase problem: a critical review. *Physics Reports*, 256:367–436, 1995.

[Mah81] G. D. Mahan. *Many-particle physics*. Plenum Press, New York and London, 1981.

[MSS03] Yuriy Makhlin, Gerd Schoen, and Alexander Shnirman. Dissipation in josephson qubits. *In: New Directions in Mesoscopic Physics (Towards Nanoscience), R. Fazio, V. F. Gantmakher, and Y. Imry, Kluwer, Dordrecht, 2003*, pages 197–224, 2003.

[NC00] M.A. Nielsen and I.L. Chuang. *Quantum computation and quantum information*. University Press, Cambridge, 2000.

[Nie02] M.A. Nielsen. A simple formula for the average gate fidelity of a quantum dynamical operation. *Phys. Lett. A*, 303:249–252, 2002.

[PM82] P. Pereyra and P.A. Mello. Marginal distribution of the S-matrix elements for Dyson's measure and some applications. *Journal of Physics A*, 16:237–254, 1982.

[PSE97] G.M. Palma, K.-A. Suominen, and A.K. Ekert. Quantum computers and dissipation. *Proc. Roy. Soc., London*, A452:567–584, 1997.

[Ram49] N. F. Ramsey. A new molecular beam resonance method. *Phys. Rev*, 76:996, 1949.

[RQJ02] J. H. Reina, L. Quiroga, and N. F. Johnson. Decoherence of quantum registers. *Phys. Rev. A*, 65(3):032326, 2002.

[Sch96] B. Schumacher. Sending entanglement through noisy quantum channels. *Phys. Rev. A*, 54(4):2614–2628, 1996.

[SDK+04] D. Schrader, I. Dotsenko, M. Khudaverdyan, Y. Miroshnychenko, A. Rauschenbeutel, and D. Meschede. A neutral atom quantum register. *Phys. Rev. Lett.*, 93(15):150501, 2004.

[Sho94] P. W. Shor. *Algorithms for quantum computation: discrete logarithms and factoring, in Proceedings of the 35th Annual Symposium on Foundations of Computer Science, edited by S. Goldwasser*. IEEE Computer Society, Los Alamitos, CA, 1994.

[Sho95] P. W. Shor. Scheme for reducing decoherence in quantum computer memory. *Phys. Rev. A*, 52(4):R2493–R2496, Oct 1995.

[Ste96] A. M. Steane. Error correcting codes in quantum theory. *Phys. Rev. Lett.*, 77(5):793–797, Jul 1996.

[SW02] B. Schumacher and M. D. Westmoreland. Approximate quantum error correction. *Journal of Quantum Information Processing*, 1:5–12, 2002.

[SZ97] M. 0. Scully and M. S. Zubairy. *Quantum optics.* University Press, Cambridge, 1997.

[Uhl76] A. Uhlmann. The "transition probability" in the state space of a *-algebra. *Rep. Math. Phys.*, 9:273, 1976.

[Unr94] W. G. Unruh. Maintaining coherence in quantum computers. *Phys. Rev. A*, 51(2):992–997, 1994.

[VHvB+02] L. M. K. Vandersypen, R. Hanson, L. H. Willems van Beveren, J. M. Elzerman, J. S. Greidanus, S. De Franceschi, and L. P. Kouwenhoven. Quantum computing with electron spins in quantum dots. 2002.

[Zeh70] H. D. Zeh. On the interpretation of measurement in quantum theory. *Foundations of Physics*, 1:69–76, 1970.

[ZR97] P. Zanardi and M. Rasetti. Noiseless quantum codes. *Phys. Rev. Lett.*, 79(17):3306–3309, 1997.

[Zur81] W. H. Zurek. Pointer basis of quantum apparatus: into what mixture does the wave packet collaps? *Phys. Rev. D*, 24(6):1516–1525, 1981.

[Zur03] W. H. Zurek. Decoherence, einselection, and the quantum origins of the classical. *Rev. Mod. Phys.*, 75(3):715, 2003.

Erklärung

Ich versichere, dass ich die von mir vorgelegte Dissertation selbständig angefertigt, die benutzten Quellen und Hilfsmittel vollständig angegeben und die Stellen der Arbeit – einschließlich Tabellen, Karten und Abbildungen –, die anderen Werken im Wortlaut oder dem Sinn nach entnommen sind, in jedem Einzelfall als Entlehnung kenntlich gemacht habe; dass diese Dissertation noch keiner anderen Fakultät oder Universität zur Prüfung vorgelegen hat; dass sie – abgesehen von unten angegebenen Teilpublikationen – noch nicht veröffentlicht worden ist sowie, dass ich eine solche Veröffentlichung vor Abschluss des Promotionsverfahrens nicht vornehmen werde.
Die Bestimmungen der Promotionsordnung sind mir bekannt. Die von mir vorgelegte Dissertation ist von Herrn Dr. Rochus Klesse betreut worden.

Köln, den 24. April 2009

Stefan Borghoff

Teilpublikationen:
S. Borghoff, R. Klesse, Decoherence of encoded quatum registers,
Phys. Rev. A **77**, 012306, (2008)

Danksagung

Mein besonderer Dank gilt Dr. Rochus Klesse für die Unterstüzung und Betreuung bei der Erstellung dieser Arbeit. Desweiteren Danke ich Dr. Tobias Lück, Dr. Anja Erven und Thomas Zell für Korrekturen an dieser Arbeit, sowie Jakob-Müller-Hill für zahlreiche Diskussionen.